TOWARDS EXPLAINABLE ROBOTS: DEVELOPING CONSENSUS REACHING MECHANISMS FOR CO-ROBOTS IN HAPTIC SHARED CONTROL PARADIGMS

by

Vahid Izadi

A dissertation submitted to the faculty of
The University of North Carolina at Charlotte
in partial fulfillment of the requirements
for the degree of Doctor of Philosophy in
Mechanical Engineering

Charlotte

2022

Approved by:

_____
Dr. Amirhossein Ghasemi

_____
Prof. Stuart T. Smith

_____
Prof. Scott David Kelly

_____
Dr. Artur Wolek

_____
Prof. Srinivas Akella

ABSTRACT

VAHID IZADI. Towards Explainable Robots: Developing Consensus Reaching Mechanisms for Co-Robots in Haptic Shared Control Paradigms. (Under the direction of DR. AMIRHOSSEIN GHASEMI)

Human-automation teaming (HAT) is gaining importance in military and commercial applications with autonomous vehicles because it promises to improve performance, reduce operating and designing platforms' costs, and increase adaptability to new situations. Given that both humans and automation systems are subject to misses, faults, or errors, to ensure the HAT performance in unpredictable conditions, it is critical to address the hand-off problem – how to transition control between a human driver and automation system. Current solutions for control transfer in semi-automated ground vehicles face issues such as prolonged transfer time, misinterpretations or misappropriations of responsibility, and incomplete or inaccurate understandings of the vehicle and environment state. Transitions involving such issues are often *bumpy* and implicated in safety compromises.

This dissertation focuses on addressing these issues by designing and testing an adaptive haptic shared control wherein a driver and an automation system are physically connected through a motorized steering wheel. We model the structure of the automation system like the structure of the human driver, including a higher-level intent generator and lower-level impedance controller. In the first part of this dissertation, we developed a nonlinear stochastic model predictive approach (SMPC) to determine how automation's impedance should be modulated in different interaction modes to enable the smooth and dynamic transition of control authority between humans and automation systems. The cost function in this SMPC is defined to maximize task performance and minimize the disagreement between humans and automation within different interaction modes. To solve the optimal control problem, first, we employed the polynomial chaos (PC) approach to construct a deterministic surrogate for

the stochastic MPC problem of adaptive HSC. Then, we employed the continuation generalized minimum residual (C/GMRES) solver that provides an iterative algorithm to solve the nonlinear model predictive controller. Finally, a set of numerical and experimental results are demonstrated to evaluate the performance of the proposed adaptive haptic shared control framework. The numerical results demonstrate that when the human control command is sufficient for avoiding the obstacle, the disagreement between the human and automation systems can be reduced by modulating and adopting smaller values for the impedance controller. On the other hand, when the human control command is insufficient, the automation system gains control authority by modulating and adopting larger values for the impedance controller parameters. It ensures the safety of the obstacle avoidance task. We also performed tests with processors in the loop (PIL) to show that the proposed predictive controller can compute the optimal modulation policy in real-time. The PIL results show high computational speed and numerical accuracy for the proposed method using low-cost microcontrollers. Finally, we quantified the performance of an adaptive haptic shared control through a set of human-subject studies using a fixed-base driving simulator.

We invited 27 participants to drive a simulated vehicle through a course with obstacles. For forty percent of these obstacles, the human is instructed to avoid the obstacles in a similar direction as the automation system. For the other sixty percent of the obstacles, the human driver is instructed to take an opposite direction than the automation system to avoid the obstacle. We compare the performance of the adaptive haptic shared control with two other shared control schemes named assistive haptic shared and active-safety haptic shared control schemes. The automation system weighs the error term between the steering angle and the driver's desired steering command in the Assistive mode. This mode represents a case where the automation has relatively high confidence in the driver. The automation system weighs the error term between the steering angle and the automation's desired steering command

in the Active-Safety mode. This mode represents a case where the automation has relatively low confidence in the driver. In the adaptive haptic shared control, the automation adaptively assigns different weights to the error terms based on the human impedance. Here, we used the human grip force as a proxy to estimate the human impedance on the steering wheel. We compared the performance of these three shared control schemes by analyzing five metrics, including obstacle hits and metrics related to driving maneuvers around the obstacles that were avoided. Our statistical analysis indicated that the adaptive haptic shared control paradigm supports the best overall team performance in resolving a conflict between the driver and automation system while keeping the vehicle safe.

In the second part of this dissertation, we studied the principles of convention formation in a haptic shared control framework to narrow down the many possible strategies for resolving a conflict to those that a driver might be more gravitated. To this end, we proposed a modular platform to separate partner-specific conventions from task-dependent representations and use this platform to learn various forms of conventions between a human-driver and automation system. We assumed the human and automation steering commands could be determined by optimizing a set of cost functions in this platform. For each agent, the cost function is defined as a combination of hand-coded features and vectors of weights. We argue that the hand-coded features can be selected to describe task-dependent representations. On the other hand, the weight distributions over these features can be used to determine the partner-specific conventions. Using this platform, we created a map of human-automation interaction outcomes to the space of conventions. Finally, an adaptable automation system is designed to reach a desirable shared convention using the convention map. In particular, we developed a reinforcement-learning-based model predictive controller to enable the automation system to learn complex policies and adapt its behavior accordingly. To this end, we designed an episode-based policy search us-

ing the Deep Deterministic Policy Gradients agent to determine automation's cost function's optimal weights vector distribution. We applied the proposed platform to the problem of intent negotiation for resolving a conflict. Specifically, we considered a scenario where both humans and automation detect an obstacle but choose different paths to maneuver around the obstacle. The simulation results demonstrate that the convention-based handover strategies can successfully resolve a conflict and improve the performance of the human-automation teaming.

DEDICATION

This work is dedicated first to my parents, Hossein Izadi and Akram Farahani, who provided the much-needed motivation to keep me focused on the finish line.

Secondly, to my brothers, Saeed and Masud Izadi and my sisters, Nahid and Mahnaz Izadi. Without the continual support and love they provided throughout my life, this would not have been possible.

And finally, to my loving wife and daughter, Rahele Jabari and Sida Izadi, for being my cheerleaders throughout my Ph.D. endeavor.

Thank you all

ACKNOWLEDGEMENTS

TABLE OF CONTENTS

LIST OF TABLES

LIST OF FIGURES

CHAPTER 1: Introduction

The main goal in human-robot teaming is to combine the best features of a human (e.g., perception, judgment) with the speed, accuracy, and tirelessness of automation to solve complex problems rapidly [1, 2, 3, 4, 5, 6]. However, the partnership between the human driver and the automation system can potentially present some challenges because the two types of intelligence are not symmetrical (a gap between the world as a human sees it vs. the world as modeled by the automation) [1, 6, 7]. A key factor in designing a successful human-automation team is to create a paradigm wherein both humans and automation are able to maintain their mode awareness [8, 9]. Mode awareness includes knowledge and understanding of (i) system status (active/armed/engaged/off), (iii) (changes in) system goals/intentions/targets, (ii) control modes (strategies for achieving goals), (iv) actual control inputs made by the system, and (v) problems/challenges faced by the automation or driver. A loss of mode awareness is more likely to occur in highly dynamic high-tempo circumstances, when the automation operates at very high levels of autonomy for extended periods and when system status and/or behavior changes in the absence of immediately preceding human input [10, 9]. To support mode awareness, recent research studies have been focused on four main themes: (1) development of models that capture human intent [11, 12, 13, 14, 15], (2) development of algorithms that can identify the system status (e.g., cooperative vs. uncooperative mode) [16, 17, 18, 19, 20], (3) development of interfaces that allows bi-directional communication between the two agents [21, 22, 23, 24, 25], (4) development of algorithms that support negotiation and arbitration of control authority between human and automation system [26, 27, 28, 29]. This project addresses a series of challenges associated with the fourth category and

develops new algorithms that support the intuitive exchange of control authority between a human and an automation system.

1.1 Hand-off Problem in Shared Control Paradigms

Numerous companies and academic groups are pushing to develop autonomous vehicles to free up attention for drivers and improve safety on the road. However, barriers remain to the deployment of fully autonomous vehicles, given current automation capabilities and the likelihood of encountering conditions for which the automation cannot guarantee safety. While the challenge of meeting human capabilities for sensing, perceiving, and predicting the road's environment is formidable, the hand-off problem is the main problem– how to transition control between a human driver and an automation system.

Supervisory control [30] involves delegating lower-level tasks to automation while the human operator monitors performance and stays engaged in higher-level tasks. In driving, however, a supervisory role for the driver is difficult to define, and transitions may become bumpy when necessary to re-delegate authority to the driver because the control challenge has exceeded automation capabilities. Rather than separating and delegating control responsibilities, sharing control between a driver and automation has been suggested as a more flexible authority structure that offloads portions of the driver's task yet supports rapid authority transitions when the need arises. The supposition is that by asking two agents to simultaneously perform the same task and share responsibility for performance outcomes, conditions are created that support rapid control authority transitions. A second supposition is that cooperating on the task requires less effort than performing the task alone. It is also possible that by having the humans stay "in the loop" on the primary task, they are better positioned to monitor safety and initiate a take-over when necessary. Other advantages are discussed in [31, 32, 33].

Various shared control schemes have been proposed, differing primarily according

to how control authority is transitioned between the two agents [34, 35, 36, 37]. These schemes can be categorized into two main categories: switch-based control schemes and continuous control schemes [3, 30, 38]. Switched-based, also known as Traded Control schemes [39], which involve complete, wholesale hand-offs of control authority between driver and automation can only be deployed in the absence of sudden and rapid transitions [31]. Depending on the scheme, transfers may be initiated by the human driver, by the automation system, or by a separate arbitration algorithm [37, 35, 36]. Switched-based control schemes involve issues such as a protracted-time interval required for full transfer, misinterpretation or misappropriation of responsibility (called mode errors), and incomplete understanding of the environment state (loss of situation awareness) [40, 2, 37].

To address these issues, various schemes have been proposed under which the control authority is continuously shared between humans and automation to address these shortcomings. Two main groups of these schemes are input-mixing control and haptic shared control [41, 42, 43, 44, 45, 46, 47, 48]. The main difference between these two paradigms is that haptic shared control paradigms involve a dynamic coupling between a human driver and automation through the steering wheel. In contrast, the input-mixing paradigms do not involve such a coupling. The dynamic coupling allows the driver to remain bodily in the loop, with his/her hands on a motorized steering wheel. A valuable feature of haptic shared control is that the role (e.g., leader/follower) played by each agent and the level of authority held by each agent (how much control an agent exerts) is a dynamic outcome of the interaction between the two agents and the vehicle [49, 50, 51, 52]. The feature of role and level of authority being outcomes of the interaction in haptic shared control is in sharp contrast to the control sharing paradigm of input mixing, where a third party imposes the level of authority (an agent or algorithm that assesses current threat) and potentially make the haptic shared control to be more robust to automation's misses, and faults

[41, 44, 42, 53, 34].

1.2   Haptic Shared Control

The control sharing scheme called *Haptic Shared Control* takes its inspiration from two humans cooperating on a manual task, for example, moving a piece of furniture [54, 42]. Figure 1.1 demonstrates a schematic of a haptic shared control paradigm in the context of steering control of a semi-automated vehicle. Here, three entities each impose a torque on the steering wheel: τ_H by a driver through his hands, τ_A by an automation system through a motor, and τ_V by the road through the steering linkage. The driver can be considered as a hierarchical two-level controller in which the upper-level control represents the cognitive controller, and its output, θ_H is the driver's intent. The lower level represents the human's biomechanics which its parameters z_H can vary over time (e.g., with muscle co-contraction). Similarly, the automation system can be modeled as a higher-level controller (AI) coupled with a lower-level impedance controller with the modest gain z_A [55, 56, 56, 57, 58].
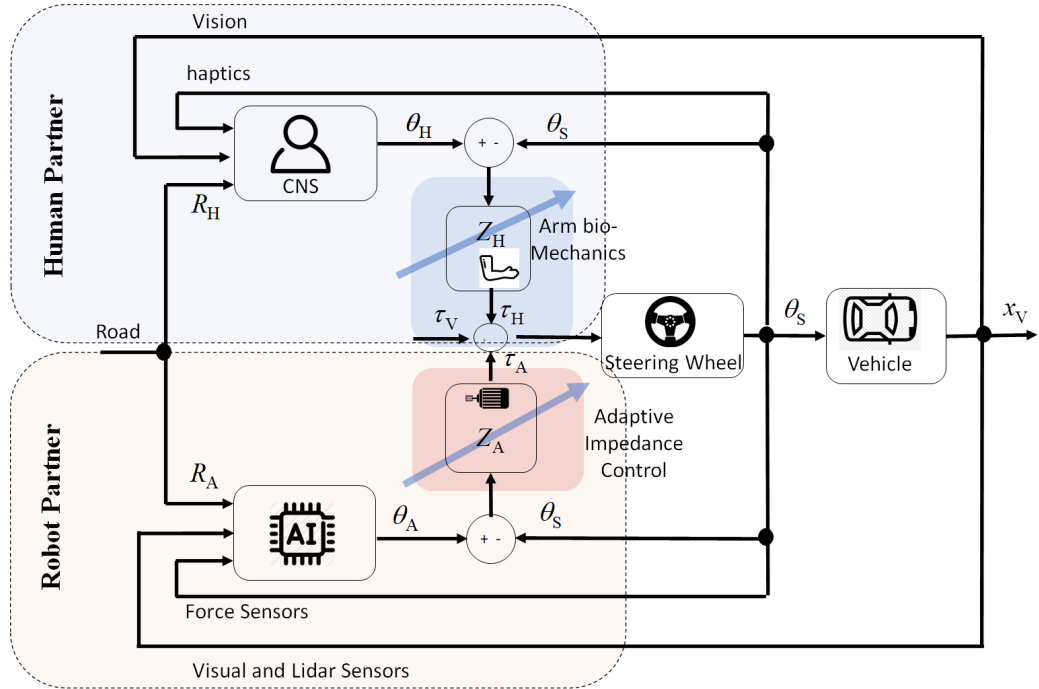
Figure 1.1: A schematic a haptic shared control paradigm

In the haptic shared control paradigm, the steering wheel's dynamics is the arbiter of authority in the haptic shared control paradigm. The human driver can increase the impedance z_H by increasing the steering grip and co-contracting the muscles to override the automation system and can reduce the impedance by decreasing the steering grip and relaxing the muscles (while keeping hands on the wheel) to yield control to the automation system. Whether active or relaxed, the human driver can monitor the actions of the automation system through haptic feedback [59, 60, 45, 61].

A majority of Haptic Shared Control designs are only concerned with human-automation cooperation at the "operational level" (or the "control level") [62, 63]. In automotive systems, cooperation at the "operational level" involves collaboratively generating a trajectory or a path using both the automation and driver inputs to determine the final steering wheel angle [62]. Although such embodiment of Haptic Shared Control still provide a smooth shift of authority during driving, they can suffer from conflicts between the driver and the automation that arise when there is a difference between the actions and intentions of the human driver and the automation system. Conflicts are undesirable as they can cause annoyance, can deteriorate driving performance, and, in worst-case scenarios, can result in accidents [64, 62].

For instance, consider a scenario when the human and automation see an obstacle but decide to maneuver around different sides of the obstacle (see Figure 1.2). If both human and automation applies the same torque but in the opposite direction on the steering wheel, they cancel out each other's input, and the vehicle would hit the obstacle. In addition, to reverse intent conflict, the other forms of conflict can be in the form of (i) one agent does not provide any control inputs (e.g., one agent doesn't detect an obstacle), (ii) too much, or too little inputs (e.g., two agents has different perceptions from the size/position of an obstacle), (iii) control inputs arrive too early or too late, and (iv) additional inputs cause conflict (e.g., disturbance feedback from the road).
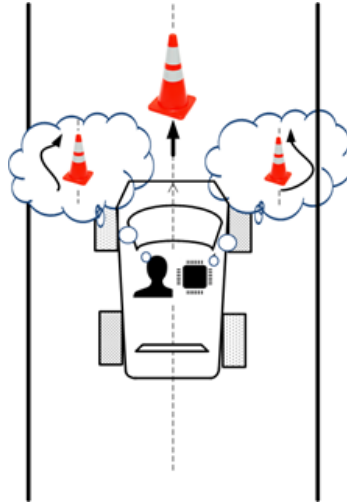
Figure 1.2: A conflict sample for the shared driving task between human driver and automation.

To resolve such a conflict, the automation can either select a lower impedance and yield the control to the human driver or adopt a higher impedance and gain the control from the human driver. However, there is a trade-off between the control authority provided to an agent (driver or automation) and the fault protection provided by the other agent [65]. For example, the protection against driver faults would be high for high impedance automation. However, the protection against automation faults may be low because the human driver can not provide sufficient torque to override the automation's commands. On the other hand, for low impedance automation, protection against driver faults provided by the automation would be low. Therefore, it seems necessary that automation should be able to adjust its impedance adaptively to have maximum protection against both human and automation errors.

To determine how the automation system shall modulate its impedance parameters, a wide range of research has been conducted [66, 29, 67, 68, 69, 50, 51, 70, 71, 72, 73, 74, 75, 76, 77, 78]. Two main streams of these approaches are non-learning-based control methodologies, wherein a set of predefined control laws is used to modulate impedance controller parameters [79, 80, 81] and learning-based control methodologies, wherein data-driven approaches are exploited for optimally varying

the impedance parameters [71, 82, 83, 75, 84]. In this dissertation, we also defined a non-learning algorithm in the context of steering control of a semi-automated vehicle. The main limitations of the non-learning-based approaches are their limited applicability because human-automation dynamics is hard-to-model and uncertain. Consider the uncertainty description in the form of a bounded set, and safe interaction is often achieved at the expense of closed-loop performance [85, 86, 87]. The learning-based approaches can be categorized into two main families of model-free and model-based approaches [88, 89, 75, 71]. The main limitation of model-free learning approaches is that these algorithms are computationally expensive to train, which often limits their application. Therefore, a promising direction is to employ model-based learning approaches [88, 89, 90, 91] to optimally modulate the automation's impedance parameters. In the future, we plan to integrate the impedance modulation algorithms developed in this dissertation with a series of learning-based approaches to further improve the performance of HAT in resolving a conflict.

1.3   Convention-based Control Transfer Mechanisms

Balancing between the driver's preference and the joint task's safety in a haptic shared control may result in several possible handover strategies that differ mainly in human and automation's shared conventions. Here, we define conventions as the shared knowledge that emerges from repeated interactions [92]. Consider a scenario when the human and automation see an obstacle but decide to maneuver around different sides of the obstacle (see Figure 1.2). There are three possible solutions to resolve such a conflict (different maneuver directions for avoiding the obstacle). Specifically, the automation can apply a lower torque and yield the control to the human driver. On the other hand, the automation can apply a higher torque and gain control from the human driver. Also, the automation can adapt its desired path and select a path similar to the human driver. Since the human driver is a non-stationary partner, it is important to study the principles of convention formation so that we

can design an adaptable automation system that can (to some extent) personalize its behavior to the human partner.

To study convention, a wide range of approaches such as the theory of mind, game theory, and pragmatic reasoning are focused on modeling the human reasoning over the partner's states and strategies based on observations of their actions and unfolding events [93, 94, 95]. The main drawback of these approaches is that they become easily computationally intractable and, therefore, can not be used to adapt automation's behavior in real-time. Recently, a few studies have proposed a platform to separate partner-specific conventions from task-dependent representations [92, 96] using a two-player Markov Decision Process (MDPs) framework. Even though the partner-specific conventions from task-dependent representations are separated, both are based on data-driven approaches. The task-dependent representation can be realized based on a mathematical model, and therefore the computational load will be decreased. This dissertation presented a framework that can be used to learn and leverage conventions in designing an adaptable automation system. Here, we model the human and automation cost function for driving a semi-automated vehicle (e.g., obstacle avoidance) as a weighted linear combination of a set of features that a human and automation care about (e.g., collision avoidance, staying on the road, or distance to the final goal). While these features can represent the task, we argue that the distribution of the weights associated with these features and how they may evolve in time can be used as a proxy to learn and leverage the conventions formed between the human driver and automation system. Additionally, defining the concept of cooperative and competitive cost functions, we create a map to characterize the outputs of human-automation interaction under different conventions. Using such a map, an adaptable automation system can be designed to change its behavior adaptive and form a desirable convention with a human driver.

An automation system should automatically learn complex policies and adjust its

behavior accordingly to adaptively form conventions. While model-predictive-base approaches are powerful tools to deal with the uncertainty and complexity of human-automation interaction, they lack the learning capability [97, 98, 99]. On the other hand, conventional end-to-end learning algorithms require significant amounts of data (hundreds or even thousands of experiments) to achieve a desired level of performance that may not be feasible. To merge the strengths of these approaches, recent efforts have been focused on combining data-driven techniques learning with the model-based controller [100]. For instance, several approaches have used RL-based methods to update the hyper-parameters of the model-predictive controller. Although there have been few works combining MPC with learning-based techniques, there seems to be no such work done for the problem in the context of convention formation to the best of our knowledge. To this end, we implement a DDPG based RL method to select appropriate weights for the automation's cost function such that the automation can adapt its desired steering policy if needed. We test the performance of our convention formation framework in the context of resolving a conflict between a human driver and automation.

1.4   Problem Statement

This dissertation focused on designing and testing an adaptive haptic shared control paradigm to shorten the control transfer time, improve interpretation and appropriation of responsibility, produce a more accurate understanding of vehicle and environment state, and reduce the human partner's cognitive load. To this end, we defined two objectives.

Aim 1: Design an Adaptive Haptic Shared Control Paradigm. To allow a smooth exchange of the control authority, we developed a predictive controller to modulate the impedance controller's parameters actively. This objective is achieved through (a) development of a model for a haptic shared control paradigm wherein the topic of role negotiation, role allocation, and intention

integration can be systematically explored on two levels of mind (intent/decision making) and motor (human biomechanics/robot's impedance control); (b) development of a set of stochastic optimal control algorithms for modulating the automation's impedance controller parameters so that the control authority can dynamically be arbitrated between the human and automation systems; (c) validation of the optimal controller for real-time implementation using a series of process-in-the-loop tests and human-subject studies.

Aim 2: Establish the Principles of Convention Formation in a Haptic Shared Control Paradigm. To improve the customizability of automation systems, the automation system must be able to narrow down its control handover strategy (from many possible strategies) to the ones that a driver may gravitate to. To this end, we created a platform that allows studying the convention formation between a human driver and utilizes this approach to determine suitable handover strategies. This objective is achieved through (a) developing a modular structure to separate partner-specific conventions from task-dependent representations and use this structure to learn and leverage different forms of conventions, (b) developing a map that connects different forms of conventions to the outputs of human-automation interaction using cooperative-competitive game theory concept, (c) designing an adaptable automation system so that a desirable shared convention can be achieved.

1.5   Thesis Structure and Outcomes

The models and algorithms developed in this dissertation bridge different fields of study, including control engineering, robotics, and cognitive science to (i) advance learning-based algorithms for intelligent robotic partners and (ii) promote human-robot teaming for performing complex tasks in a dynamic and uncertain environment.

The research presented in this dissertation is in the three-article format. Chap-

ter 2 (Paper 1) presents an adaptive haptic shared control framework wherein the automation's impedance controller parameters are modulated to enable the dynamic exchange of the control authority with a driver. This work was published in the Mechatronics journal in 2021. Chapter 3 (Paper 2) tests the performance of the adaptive haptic shared control through a series of human subject test studies. This work has been submitted to the Journal of Transportation Research Part F and is awaiting an editorial response. Finally, Chapter 4 (Paper 3) establishes a platform to study the principles of convention formation in a haptic shared control framework. This work has been submitted to the Journal of Autonomous Robots and is awaiting an editorial response. In addition to the three mentioned journal papers, seven conference papers are published in this Ph.D. research which are:

1- Game-Theoretic Intent Negotiation in a Haptic Shared Control Paradigm, 2021 American Control Conference (ACC)

2- Adaptive Impedance Control for the Haptic Shared Driving Task Based on Nonlinear MPC, 2020 Dynamic Systems and Control Conference

3- Towards explainable co-robots: Developing confidence-based shared control paradigms, 2020 Dynamic Systems and Control Conference

4- Modeling cooperative human-automation interactions in Haptic Shared Control Framework, 2020 SAE Technical Paper

5- Negotiating the Steering Control Authority within Haptic Shared Control Framework, 2020 SAE Technical Paper

6- Impedance Modulation for Negotiating Control Authority in a Haptic Shared Control Paradigm, 2020 American Control Conference (ACC)

7- Determination of Roles and Interaction Modes in a Haptic Shared Control Framework, 2019 Dynamic Systems and Control Conference

REFERENCES

[1] Jessie YC Chen and Michael J Barnes. Human–agent teaming for multirobot control: A review of human factors issues. *IEEE Transactions on Human-Machine Systems*, 44(1):13–29, 2014.

[2] Raja Parasuraman and Victor Riley. Humans and automation: Use, misuse, disuse, abuse. *Human factors*, 39(2):230–253, 1997.

[3] Calder Phillips-Grafflin, Halit Bener Suay, Jim Mainprice, Nicholas Alunni, Daniel Lofaro, Dmitry Berenson, Sonia Chernova, Robert W Lindeman, and Paul Oh. From autonomy to cooperative traded control of humanoid manipulation tasks with unreliable communication. *Journal of Intelligent & Robotic Systems*, 82(3):341–361, 2016.

[4] Jessie YC Chen, Michael J Barnes, Julia L Wright, Kimberly Stowers, and Shan G Lakhmani. Situation awareness-based agent transparency for human-autonomy teaming effectiveness. In *Micro-and nanotechnology sensors, systems, and applications IX*, volume 10194, page 101941V. International Society for Optics and Photonics, 2017.

[5] Kyle J Behymer and Brian P McKenna. Creating and evaluating human-machine teams in context. In *Human Performance in Automated and Autonomous Systems*, pages 121–138. CRC Press, 2019.

[6] Michael Barnes, Linda R Elliott, Julia Wright, Angelique Scharine, and Jessie Chen. Human-robot interaction design research: From teleoperations to human-

agent teaming. Technical report, CCDC Army Research Laboratory Aberdeen Proving Ground United States, 2019.

[7] Maya Indira Ganesh. The ironies of autonomy. *Humanities and Social Sciences Communications*, 7(1):1–10, 2020.

[8] Jill L Drury, Jean Scholtz, and Holly A Yanco. Awareness in human-robot interactions. In *SMC'03 Conference Proceedings. 2003 IEEE International Conference on Systems, Man and Cybernetics. Conference Theme-System Security and Assurance (Cat. No. 03CH37483)*, volume 1, pages 912–918. IEEE, 2003.

[9] Nadine B Sarter. Multimodal information presentation: Design guidance and research challenges. *International journal of industrial ergonomics*, 36(5):439–445, 2006.

[10] Nadine B Sarter, David D Woods, and Charles E Billings. Automation surprises. *Handbook of human factors and ergonomics*, 2:1926–1943, 1997.

[11] Luka Peternel, Nikos Tsagarakis, Darwin Caldwell, and Arash Ajoudani. Robot adaptation to human physical fatigue in human–robot co-manipulation. *Autonomous Robots*, 42(5):1011–1021, 2018.

[12] Samuel Au, Max Berniker, and Hugh Herr. Powered ankle-foot prosthesis to assist level-ground and stair-descent gaits. *Neural Networks*, 21(4):654–666, 2008.

[13] Eric C Townsend, Erich A Mielke, David Wingate, and Marc D Killpack. Estimating human intent for physical human-robot co-manipulation. *arXiv preprint arXiv:1705.10851*, 2017.

[14] Bo Yu, R Brent Gillespie, James S Freudenberg, and Jeffrey A Cook. Identi-

fication of human feedforward control in grasp and twist tasks. In *American Control Conference (ACC), 2014*, pages 2833–2838. IEEE, 2014.

[15] David J. Cole. Neuromuscular dynamics and steering feel. Technical report, Proc. Steering Tech, 2008.

[16] Zheng Wang, Angelika Peer, and Martin Buss. An hmm approach to realistic haptic human-robot interaction. In *World Haptics 2009-Third Joint EuroHaptics conference and Symposium on Haptic Interfaces for Virtual Environment and Teleoperator Systems*, pages 374–379. IEEE, 2009.

[17] Oliver C Schrempf, Uwe D Hanebeck, Andreas J Schmid, and Heinz Worn. A novel approach to proactive human-robot cooperation. In *ROMAN 2005. IEEE International Workshop on Robot and Human Interactive Communication, 2005.*, pages 555–560. IEEE, 2005.

[18] Don Joven Agravante, Andrea Cherubini, Antoine Bussy, Pierre Gergondet, and Abderrahmane Kheddar. Collaborative human-humanoid carrying using vision and haptic sensing. In *2014 IEEE international conference on robotics and automation (ICRA)*, pages 607–612. IEEE, 2014.

[19] Cigil Ece Madan, Ayse Kucukyilmaz, Tevfik Metin Sezgin, and Cagatay Basdogan. Recognition of haptic interaction patterns in dyadic joint object manipulation. *IEEE Transactions on Haptics*, 8(1):54–66, 2014.

[20] Ayse Kucukyilmaz and Illimar Issak. Online identification of interaction behaviors from haptic data during collaborative object transfer. *IEEE Robotics and Automation Letters*, 5(1):96–102, 2019.

[21] Greg A Jamieson and Kim J Vicente. Designing effective human-automation-plant interfaces: A control-theoretic perspective. *Human Factors*, 47(1):12–34, 2005.

[22] Keehoon Kim and J Edward Colgate. Haptic feedback enhances grip force control of semg-controlled prosthetic hands in targeted reinnervation amputees. *IEEE Transactions on Neural Systems and Rehabilitation Engineering*, 20(6):798–805, 2012.

[23] Fabrizio Sergi, Dino Accoto, Domenico Campolo, and Eugenio Guglielmelli. Forearm orientation guidance with a vibrotactile feedback bracelet: On the directionality of tactile motor communication. In *2008 2nd IEEE RAS & EMBS International Conference on Biomedical Robotics and Biomechatronics*, pages 433–438. IEEE, 2008.

[24] Ryan Christiansen, Jose Luis Contreras-Vidal, R Brent Gillespie, Patricia A Shewokis, and Marcia K O'Malley. Vibrotactile feedback of pose error enhances myoelectric control of a prosthetic hand. In *2013 World Haptics Conference (WHC)*, pages 531–536. IEEE, 2013.

[25] P. Boehm, A.H. Ghasemi, S. O'Modhrain, P. Jayakumar, and R.B. Gillespie. Architectures for Shared Control of Vehicle Steering. In *IFAC - Human and Machine Symposium*, 2016.

[26] S Ozgur Oguz, Ayse Kucukyilmaz, Tevfik Metin Sezgin, and Cagatay Basdogan. Haptic negotiation and role exchange for collaboration in virtual environments. In *Haptics Symposium, 2010 IEEE*, pages 371–378. IEEE, 2010.

[27] S Ozgur Oguz, Ayse Kucukyilmaz, Tevfik Metin Sezgin, and Cagatay Basdogan. Supporting negotiation behavior with haptics-enabled human-computer interfaces. *IEEE transactions on haptics*, 5(3):274–284, 2012.

[28] Nikolay Stefanov, Angelika Peer, and Martin Buss. Online intention recognition for computer-assisted teleoperation. In *Robotics and Automation (ICRA), 2010 IEEE International Conference on*, pages 5334–5339. IEEE, 2010.

[29] Nikolay Stefanov, Angelika Peer, and Martin Buss. Role determination in human-human interaction. In *EuroHaptics conference, 2009 and Symposium on Haptic Interfaces for Virtual Environment and Teleoperator Systems. World Haptics 2009. Third Joint*, pages 51–56. IEEE, 2009.

[30] Thomas B Sheridan and W Verplank. *Human and Computer Control of Undersea Teleoperators (Man-Machine Systems Lab Report)*. 1978.

[31] David A Abbink, Tom Carlson, Mark Mulder, Joost CF de Winter, Farzad Aminravan, Tricia L Gibo, and Erwin R Boer. A topology of shared control systemsfinding common ground in diversity. *IEEE Transactions on Human-Machine Systems*, (99):1–17, 2018.

[32] David A Abbink and Max Mulder. Exploring the dimensions of haptic feedback support in manual control. *Journal of Computing and Information Science in Engineering*, 9(1), 2009.

[33] S. M. Petermeijer, D. A. Abbink, M. Mulder, and J. C. F. de Winter. IEEE Transactions on Haptics. *The Effect of Haptic Support Systems on Driver Performance: A Literature Survey*, 8:467–479, 2015.

[34] Akshay Bhardwaj, Amir H Ghasemi, Yingshi Zheng, Huckleberry Febbo, Paramsothy Jayakumar, Tulga Ersal, Jeffrey L Stein, and R Brent Gillespie. Whos the boss? arbitrating control authority between a human driver and automation system. *Transportation Research Part F: Traffic Psychology and Behaviour*, 68:144–160, 2020.

[35] Arie P van den Beukel, Mascha C van der Voort, and Arthur O Eger. Towards a framework for testing drivers' interaction with partially automated driving. In *2015 IEEE 18th International Conference on Intelligent Transportation Systems*, pages 1902–1907. IEEE, 2015.

[36] Joon Woo Son, Myoung Ouk Park, et al. Situation awareness and transitions in highly automated driving a framework and mini-review. *Journal of Ergonomics*, 2017.

[37] Zhenji Lu, Riender Happee, Christopher DD Cabrall, Miltos Kyriakidis, and Joost CF de Winter. Human factors of transitions in automated driving: A general framework and literature survey. *Transportation Research Part F: Traffic Psychology and Behaviour*, 43:183–198, 2016.

[38] Amir H Ghasemi, Paramsothy Jayakumar, and R Brent Gillespie. Shared control architectures for vehicle steering. *Cognition, Technology & Work*, pages 1–11, 2019.

[39] Jim Mainprice, Calder Phillips-Grafflin, Halit Bener Suay, Nicholas Alunni, Daniel Lofaro, Dmitry Berenson, Sonia Chernova, Robert W Lindeman, and Paul Oh. From autonomy to cooperative traded control of humanoid manipulation tasks with unreliable communication: System design and lessons learned. In *2014 IEEE/RSJ International Conference on Intelligent Robots and Systems*, pages 3767–3774. IEEE, 2014.

[40] Frank Flemisch, Matthias Heesen, Tobias Hesse, Johann Kelsch, Anna Schieben, and Johannes Beller. Towards a dynamic balance between humans and automation: Authority, ability, responsibility and control in shared and cooperative control situations. *Cognition, Technology and Work*, 14(1):3–18, 2012.

[41] A.H. Ghasemi, Paramsothy Jayakumar, and R. Brent Gillespie. Shared Control Architectures for Vehicle Steering. *Cognition, Technology & Work Special Issue "Shared and cooperative control"*, page submitted., 2017.

[42] D.A. Abbink and M. Mulder. Neuromuscular analysis as a guideline in designing shared control. *Advances in Haptics*, pages 499–517, 2010.

[43] Marcia K. O'Malley, Abhishek Gupta, Matthew Gen, and Yanfang Li. Shared Control in Haptic Systems for Performance Enhancement and Training. *Journal of Dynamic Systems, Measurement, and Control*, 128(1):75, 2006.

[44] J Anderson, S Walker, and K Iagnemma. Experimental performance analysis of a constraint-based navigation framework. *Transactions on Systems, Man, and Cybernetics–Part A: Systems and Humans*, pages 1–10, 2014.

[45] Ryota Nishimura, Takahiro Wada, and Seiji Sugiyama. Haptic shared control in steering operation based on cooperative status between a driver and a driver assistance system. *Journal of Human-Robot Interaction*, 4(3):19–37, 2015.

[46] Justin Storms, Kevin Chen, and Dawn Tilbury. A shared control method for obstacle avoidance with mobile robots and its interaction with communication delay. *The International Journal of Robotics Research*, 36(5-7):820–839, 2017.

[47] S. M. Petermeijer, D. a. Abbink, and J. C. F. de Winter. Should Drivers be Operating Within an Automation-Free Bandwidth? Evaluating Haptic Steering Support Systems With Different Levels of Authority. *Human Factors: The Journal of the Human Factors and Ergonomics Society*, 57(1):5–20, 2014.

[48] Stephen M Erlien. *Shared vehicle control using safe driving envelopes for obstacle avoidance and stability*. PhD thesis, Stanford University, 2015.

[49] Ayse Kucukyilmaz et al. *Haptic role allocation and intention negotiation in human-robot collaboration*. PhD thesis, Koç University, 2013.

[50] Raphaela Groten, Daniela Feth, Harriet Goshy, Angelika Peer, David A Kenny, and Martin Buss. Experimental analysis of dominance in haptic collaboration.

In *Robot and Human Interactive Communication, 2009. RO-MAN 2009. The 18th IEEE International Symposium on*, pages 723–729. IEEE, 2009.

[51] Raphaela Groten, Daniela Feth, Roberta L Klatzky, and Angelika Peer. The role of haptic feedback for the integration of intentions in shared task execution. *IEEE Transactions on Haptics*, 6(1):94–105, 2013.

[52] Wei Bi, Xiaoyu Wu, Yueyue Liu, and Zhijun Li. Role adaptation and force, impedance learning for physical human-robot interaction. In *2019 IEEE 4th International Conference on Advanced Robotics and Mechatronics (ICARM)*, pages 111–117. IEEE, 2019.

[53] Vahid Izadi and Amir H Ghasemi. Modulation of control authority in adaptive haptic shared control paradigms. *Mechatronics*, 78:102598, 2021.

[54] Paul G. Griffiths and R. Brent Gillespie. Sharing Control Between Humans and Automation Using Haptic Interface: Primary and Secondary Task Performance Benefits. *Human Factors: The Journal of the Human Factors and Ergonomics Society*, 47(3):574–590, oct 2005.

[55] Vahid Izadi, Akshay Bhardwaj, and Amir H Ghasemi. Impedance modulation for negotiating control authority in a haptic shared control paradigm. In *2020 American Control Conference (ACC)*, pages 2478–2483. IEEE, 2020.

[56] Amir H Ghasemi, Mishel Johns, Benjamin Garber, Paul Boehm, Paramsothy Jayakumar, Wendy Ju, and R Brent Gillespie. Role negotiation in a haptic shared control framework. In *Adjunct Proceedings of the 8th International Conference on Automotive User Interfaces and Interactive Vehicular Applications*, pages 179–184. ACM, 2016.

[57] Vahid Izadi, Arjun Yeravdekar, and Amirhossein Ghasemi. Determination of roles and interaction modes in a haptic shared control framework. In *ASME*

2019 Dynamic Systems and Control Conference. American Society of Mechanical Engineers Digital Collection, 2019.

[58] Vahid Izadi, Amir H Ghasemi, and Pouria Karimi Shahri. Negotiating the steering control authority within haptic shared control framework. Technical report, SAE Technical Paper, 2020.

[59] David A Abbink, Mark Mulder, and Erwin R Boer. Haptic shared control: smoothly shifting control authority? *Cognition, Technology & Work*, 14(1):19–28, 2012.

[60] F. Mars, D. Mathieu, and Jean-Michel Hoc. Analysis of human-machine cooperation when driving with different degrees of haptic shared control. *IEEE Transactions on Haptics*, 1412(c):1–1, 2014.

[61] Franck Mars and Philippe Chevrel. Modelling human control of steering for the design of advanced driver assistance systems. *Annual Reviews in Control*, 44:292–302, 2017.

[62] Chunshi Guo, Chouki Sentouh, Jean-Baptiste Haué, and Jean-Christophe Popieul. Driver–vehicle cooperation: a hierarchical cooperative control architecture for automated driving systems. *Cognition, Technology & Work*, pages 1–14, 2019.

[63] Frank Flemisch, David Abbink, Makoto Itoh, Marie-Pierre Pacaux-Lemoine, and Gina Weßel. Shared control is the sharp end of cooperation: Towards a common framework of joint action, shared control and human machine cooperation. *IFAC-PapersOnLine*, 49(19):72–77, 2016.

[64] Makoto Itoh, Frank Flemisch, and David Abbink. A hierarchical framework to analyze shared control conflicts between human and machine. *IFAC-PapersOnLine*, 49(19):96–101, 2016.

[65] Akshay Bhardwaj, Yidu Lu, Selina Pan, Nadine Sarter, and R Brent Gillespie. Comparing coupled and decoupled steering interface designs for emergency obstacle evasion. *IEEE Access*, 9:116857–116868, 2021.

[66] K.B. Reed and M.A. Peshkin. Physical Collaboration of Human-Human and Human-Robot Teams. *IEEE Transactions on Haptics*, 1(2):108–120, jul 2008.

[67] Ingrid Pettersson and Wendy Ju. Design techniques for exploring automotive interaction in the drive towards automation. In *Proceedings of the 2017 conference on designing interactive systems*, pages 147–160, 2017.

[68] Brian Ka-Jun Mok, David Sirkin, Srinath Sibi, David Bryan Miller, and Wendy Ju. Understanding driver-automated vehicle interactions through wizard of oz design improvisation. 2015.

[69] Aaron Steinfeld, Odest Chadwicke Jenkins, and Brian Scassellati. The oz of wizard: simulating the human for interaction research. In *Proceedings of the 4th ACM/IEEE international conference on Human robot interaction*, pages 101–108, 2009.

[70] Mojtaba Sharifi, Saeed Behzadipour, and Gholamreza Vossoughi. Nonlinear model reference adaptive impedance control for human–robot interactions. *Control Engineering Practice*, 32:9–27, 2014.

[71] Loris Roveda, Jeyhoon Maskani, Paolo Franceschi, Arash Abdi, Francesco Braghin, Lorenzo Molinari Tosatti, and Nicola Pedrocchi. Model-based reinforcement learning variable impedance control for human-robot collaboration. *Journal of Intelligent & Robotic Systems*, 100(2):417–433, 2020.

[72] Misaki Hanafusa and Jun Ishikawa. Human-adaptive impedance control using recurrent neural network for stability recovery in human-robot cooperation. In

2020 IEEE 16th International Workshop on Advanced Motion Control (AMC), pages 265–272. IEEE, 2020.

[73] Mojtaba Sharifi, Saeed Behzadipour, and GR Vossoughi. Model reference adaptive impedance control in cartesian coordinates for physical human–robot interaction. *Advanced Robotics*, 28(19):1277–1290, 2014.

[74] Zhijun Li, Junqiang Liu, Zhicong Huang, Yan Peng, Huayan Pu, and Liang Ding. Adaptive impedance control of human–robot cooperation using reinforcement learning. *IEEE Transactions on Industrial Electronics*, 64(10):8013–8022, 2017.

[75] Bakur Alqaudi, Hamidreza Modares, Isura Ranatunga, Shaikh M Tousif, Frank L Lewis, and Dan O Popa. Model reference adaptive impedance control for physical human-robot interaction. *Control Theory and Technology*, 14(1):68–82, 2016.

[76] Said G Khan, Guido Herrmann, Mubarak Al Grafi, Tony Pipe, and Chris Melhuish. Compliance control and human–robot interaction: Part 1survey. *International journal of humanoid robotics*, 11(03):1430001, 2014.

[77] Chenguang Yang, Chao Zeng, Cheng Fang, Wei He, and Zhijun Li. A dmps-based framework for robot learning and generalization of human-like variable impedance skills. *IEEE/ASME Transactions on Mechatronics*, 23(3):1193–1203, 2018.

[78] Peidong Liang, Chenguang Yang, Ning Wang, Zhijun Li, Ruifeng Li, and Etienne Burdet. Implementation and test of human-operated and human-like adaptive impedance controls on baxter robot. In *conference towards autonomous robotic systems*, pages 109–119. Springer, 2014.

[79] Sugeeth Gopinathan, Pouya Mohammadi, and Jochen J Steil. Improved human-robot interaction: a manipulability based approach. In *ICRA 2018 Workshop on Ergonomic Physical Human-Robot Collaboration*, 2018.

[80] Waldez Gomes and Fernando Lizarralde. Role adaptive admittance controller for human-robot co-manipulation. In *Congresso Brasileiro de Automática-CBA*, volume 1, 2019.

[81] Isura Ranatunga, Frank L Lewis, Dan O Popa, and Shaikh M Tousif. Adaptive admittance control for human–robot interaction using model reference design and adaptive inverse filtering. *IEEE Transactions on Control Systems Technology*, 25(1):278–285, 2016.

[82] Jonas Buchli, Evangelos Theodorou, Freek Stulp, and Stefan Schaal. Variable impedance control a reinforcement learning approach. *Robotics: Science and Systems VI*, 153, 2011.

[83] Fotios Dimeas and Nikos Aspragathos. Reinforcement learning of variable admittance control for human-robot co-manipulation. In *2015 IEEE/RSJ International Conference on Intelligent Robots and Systems (IROS)*, pages 1011–1016. IEEE, 2015.

[84] Hamidreza Modares, Isura Ranatunga, Frank L Lewis, and Dan O Popa. Optimized assistive human–robot interaction using reinforcement learning. *IEEE transactions on cybernetics*, 46(3):655–667, 2015.

[85] Angelo Domenico Bonzanini, David B Graves, and Ali Mesbah. Learning-based stochastic model predictive control for reference tracking under state-dependent uncertainty: An application to cold atmospheric plasmas. *IEEE Transactions on Control Systems Technology*, Under Review, 2020.

[86] Angelo D Bonzanini, Joel A Paulson, and Ali Mesbah. Safe learning-based model predictive control under state-and input-dependent uncertainty using scenario trees. In *2020 59th IEEE Conference on Decision and Control (CDC)*, pages 2448–2454. IEEE, 2020.

[87] Angelo D Bonzanini, Joel A Paulson, Georgios Makrygiorgos, and Ali Mesbah. Fast approximate learning-based multistage nonlinear model predictive control using gaussian processes and deep neural networks. *Computers & Chemical Engineering*, 145:107174, 2021.

[88] Marc Deisenroth and Carl E Rasmussen. Pilco: A model-based and data-efficient approach to policy search. In *Proceedings of the 28th International Conference on machine learning (ICML-11)*, pages 465–472. Citeseer, 2011.

[89] Kurtland Chua, Roberto Calandra, Rowan McAllister, and Sergey Levine. Deep reinforcement learning in a handful of trials using probabilistic dynamics models. *arXiv preprint arXiv:1805.12114*, 2018.

[90] Chris J Ostafew, Angela P Schoellig, and Timothy D Barfoot. Learning-based nonlinear model predictive control to improve vision-based mobile robot path-tracking in challenging outdoor environments. In *Proceedings of the IEEE International Conference on Robotics and Automation*, pages 4029–4036, 2014.

[91] Bojan Likar and Juš Kocijan. Predictive control of a gas–liquid separation plant based on a Gaussian process model. *Computers & Chemical Engineering*, 31(3):142–152, 2007.

[92] Andy Shih, Arjun Sawhney, Jovana Kondic, Stefano Ermon, and Dorsa Sadigh. On the critical role of conventions in adaptive human-ai collaboration. *arXiv preprint arXiv:2104.02871*, 2021.

[93] Herbert A Simon. The information-processing theory of mind. *American Psychologist*, 50(7):507, 1995.

[94] Neil Rabinowitz, Frank Perbet, Francis Song, Chiyuan Zhang, SM Ali Eslami, and Matthew Botvinick. Machine theory of mind. In *International conference on machine learning*, pages 4218–4227. PMLR, 2018.

[95] Adam Lerer and Alexander Peysakhovich. Learning existing social conventions via observationally augmented self-play. In *Proceedings of the 2019 AAAI/ACM Conference on AI, Ethics, and Society*, pages 107–114, 2019.

[96] Andy Shih, Stefano Ermon, and Dorsa Sadigh. Conditional imitation learning for multi-agent games. *arXiv preprint arXiv:2201.01448*, 2022.

[97] Joel A Paulson, Georgios Makrygiorgos, and Ali Mesbah. Adversarially robust bayesian optimization for efficient auto-tuning of generic control structures under uncertainty. *AIChE Journal*, page e17591, 2021.

[98] Qiugang Lu, Ranjeet Kumar, and Victor M Zavala. Mpc controller tuning using bayesian optimization techniques. *arXiv preprint arXiv:2009.14175*, 2020.

[99] Zihang Lu and Wendy Lou. Bayesian approaches to variable selection: a comparative study from practical perspectives. *The International Journal of Biostatistics*, 2021.

[100] Baha Zarrouki, Verena Klös, Nikolas Heppner, Simon Schwan, Robert Ritschel, and Rick Voßwinkel. Weights-varying mpc for autonomous vehicle guidance: a deep reinforcement learning approach. In *2021 European Control Conference (ECC)*, pages 119–125. IEEE, 2021.

CHAPTER 2: (PAPER 1) Modulation of Control Authority in Adaptive Haptic

Shared Control Paradigms

2.1   Introduction

Haptic Shared Control is a shared control paradigm wherein humans interact with co-robot through a physical object [16, 6]. Haptic shared control paradigms have a wide range of applications, from transformative technologies in which a fully autonomous system is not yet accessible/feasible (e.g., service robots, semi-autonomous vehicles, smart manufacturing) to applications where human-robot interactions are inevitable or even desirable (e.g., rehabilitative devices, care robots, and educational robots) [1, 3, 5, 9, 17, 18, 15, 16, 48, 6, 22]. In a haptic shared control paradigm, both humans and co-robots can simultaneously exert their control inputs, and by virtue of haptic feedback continuously, monitors each other's actions. With recent advances in artificial intelligence and robotics, conflicts may arise in which an automation system can make decisions different from the human partner's. For instance, in steering a vehicle, there might be cases where both humans and automation detect an obstacle but select different trajectories to avoid it [6].

While human teams can be exceptionally efficient at resolving conflicts using shared mental models, the ability of co-robots for negotiating and resolving conflicts is significantly underdeveloped. To enable a co-robot to resolve a conflict, a series of challenges shall be addressed. First, a model that can capture the human's intent shall be developed [39, 4, 47, 52, 12]. Second, algorithms that can identify the current interaction mode shall be developed [49, 40, 2, 28, 27]. Third, algorithms that support arbitration of control authority shall be created [32, 33, 45, 44]. Finally, interfaces that allows bi-directional communication between the human and co-robot shall be

made [23, 26, 41, 11, 8].

This paper's focuses on the third technical challenge. In particular, we consider the co-robot with a similar structure to the human partner with a two-level hierarchical control structure. The higher-level controller generates the co-robot desired reference (intent), determines the current interaction mode, and estimates the human's intent. The lower level is an impedance controller generating the required torque signals. In this paper, we focus on the design of this lower-level controller. While the fundamental approaches and models proposed in this research can be applied to a wide range of physical human-robot systems, we select semi-automated vehicles' steering control as a setup for exploring the proposed study. We consider a scenario where the human and the automation system detect an obstacle and negotiate on controlling the steering wheel so that the obstacle can be avoided safely. To this end, the simulations involve four interaction modes addressing the cooperation status (cooperative and uncooperative) and the desired direction of the control transfer (active safety and assistive).

To determine how the automation system's impedance controller parameters should be dynamically modulated so that a smooth transition of control authority can occur, a cost function is designed to maximize task performance and minimize the disagreement between the human and the co-robot. We utilize a stochastic nonlinear model-predictive control approach to solve the optimal control problem. To obtain a tractable form of the cost function, the generalized polynomial chaos (PC) scheme is utilized to formulate the deterministic surrogate of the stochastic MPC with probabilistic constraints. In the PC method, the implicit mappings among the uncertain parameters (i.e., human arm's biomechanics) and the states are replaced with explicit functions in the form of a sequence of orthogonal polynomials, whose coefficient can be calculated from the expansion coefficients [30, 37]. We then employed the continuation generalized minimum residual (C/GMRES) solver that provides an iterative

algorithm to solve the tractable nonlinear model predictive controller [31, 43, 36, 34]. In this method, first, the optimal control problem is discretized over the horizon. A differential equation is then obtained by using the continuation method to update the sequence of control inputs [34]. Since the differential equation involves a large linear equation, the GMRES method [25] is employed to solve the linear equation. It is shown that the C/GMRES requires much less computational expenses than other iterative methods such as Newton's method. Moreover, C/GMRES involves no line search, which is also significantly different from standard optimization methods [35]. To evaluate the proposed methods' computational complexity, a set of PIL tests are conducted using two low-cost microcontrollers (STM32F4and ATmega2560). These processors provide direct access to the CPU's hardware resources to implement the proposed algorithm without involving the time management for handling the serial port for the data communication between the target board and the host computer. The comparative studies in the real-time PIL testbed show high accuracy with appropriate computation time in the STM32F4 Discovery target board.

In summary, the contributions of this paper are (i) development of a model for a haptic shared control paradigm wherein the topic of role negotiation, role allocation, and intention integration can be systematically explored in two levels of mind (intent/decision making) and motor (human biomechanics/robot's impedance control); (ii) development of a set of stochastic optimal control algorithms for modulating the automation's impedance controller parameters so that the control authority can dynamically be arbitrated between the human and automation systems; (iii) validation of the optimal controller for real-time implementation using a series of process-in-the-loop tests.

The outline of this paper is as follows. In section 2.2, we model the adaptive haptic shared control paradigm, and the equations of motions are derived. In section 2.3, the problem of modulation of control authority is presented as an optimal control problem.

To demonstrate the proposed approach's effectiveness, a set of numerical simulations are illustrated in Section 4. The PIL results on the low-cost microcontrollers are presented in Section 5, which shows the proposed method's implementation ability in real-time execution. Section 6 consists of the conclusions and the future directions for this research.

2.2 Adaptive Haptic Shared Control Framework

Figure 2.1 shows a schematic of an adaptive haptic shared control paradigm. Three entities each impose a torque on the steering wheel: a driver through his hands, an automation system through a motor, and the road through the steering linkage.

We model the human and automation system with a similar structure. In particular, we model the driver as a hierarchical two-level controller. The upper-level control represents the cognitive controller, and its output, θ_H, represents the drivers intent. The lower-level represent the human's biomechanics, Z_H, and is considered back-drivable [9]. To indicate that driver's biomechanic parameters vary with changes in grip on the steering wheel, use of one hand or two, muscle co-contraction, or posture changes, we have drawn an arrow through human Z_H.

Similarly, the automation system is modeled as a higher-level controller (AI) coupled with a lower-level impedance controller. The automation system is also considered to be back-drivable, and the gains of the impedance controller, Z_A, are designed to be modest rather than infinite. In other words, the automation is not intended to behave as an ideal torque source; instead, the automation imposes its command torque τ_A through an impedance Z_A that is approximately matched to the human impedance Z_H.

Furthermore, the reference signals R_H and R_A represent the goals of the driver and the automation system, respectively. It should be noted that these goals may not necessarily be the same, which is when the negotiation of control authority becomes essential. To generate algorithms that support the negotiation and dynamic transfer
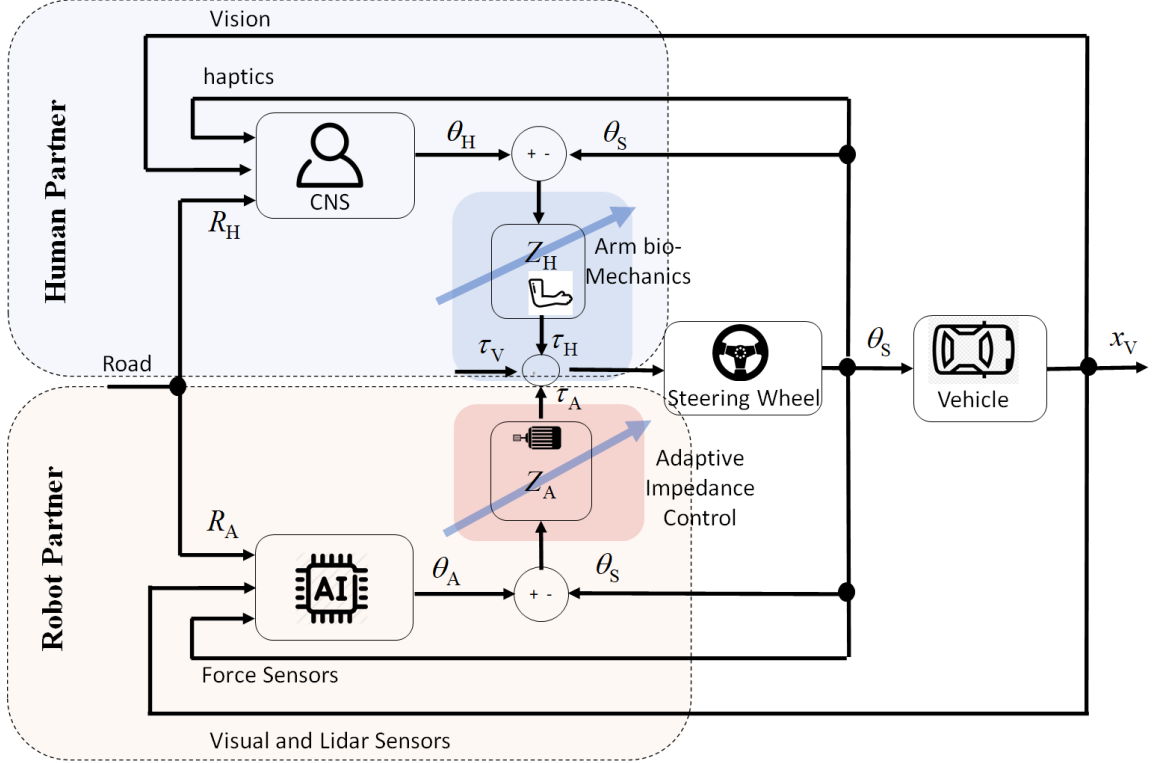
Figure 2.1: A general model of control sharing between driver and automation.

of the control authority between the human and co-robot, the robot can adjust its behavior at a higher level (changing intent) as well as at the lower level (changing Z_A). Specifically, from the model presented in Figure 2.1, it follows that the steering angle θ_S is not only a function of the humans intent θ_H, automations intent θ_A, and the road feedback torque τ_V, but also its a function of human arm's biomechanics Z_H as well as the gains of the impedance controller Z_A [7]. The crux of this paper lies in the design of a back-drivable impedance Z_A such that it enhances the negotiation and transfer of control authority between the human and automation system. To this end, we present the equations of motion of the lower-level of the adaptive haptic shared control framework shown in Figure 2.2.

2.2.1 Equations of Motion

Figure 2.2-A shows a free body diagram of an adaptive haptic shared control paradigm consisting of a driver, a steering wheel, a steering shaft, and an automation

system. Figure 2.2-A demonstrates a simplified model of a driver arms' bio-mechanics in the form of a mass-spring-damper system connected to a motion source representing the driver's intent, θ_H. The steering wheel is modeled as a disk with a rotational inertia of J_{SW}. A differential torque sensor is modeled as a rotational spring with stiffness K_T and connected to the steering wheel and steering shaft. The steering shaft is also considered as a rotational bar with the inertia of J_S that is connected to the steering wheel on the left side, to the rack and pinion on the right side, and the automation system through a timing belt with a mechanical advantage of r_S/r_M. The block diagram of the lower-level of the adaptive haptic shared control is also shown in Figure 2.2-B. In this block diagram, signals of θ_H, θ_A, and τ_V are considered as exogenous signals; signals of differential torque τ_T and the steering shaft angle θ_S can be measured by the on-board sensors.
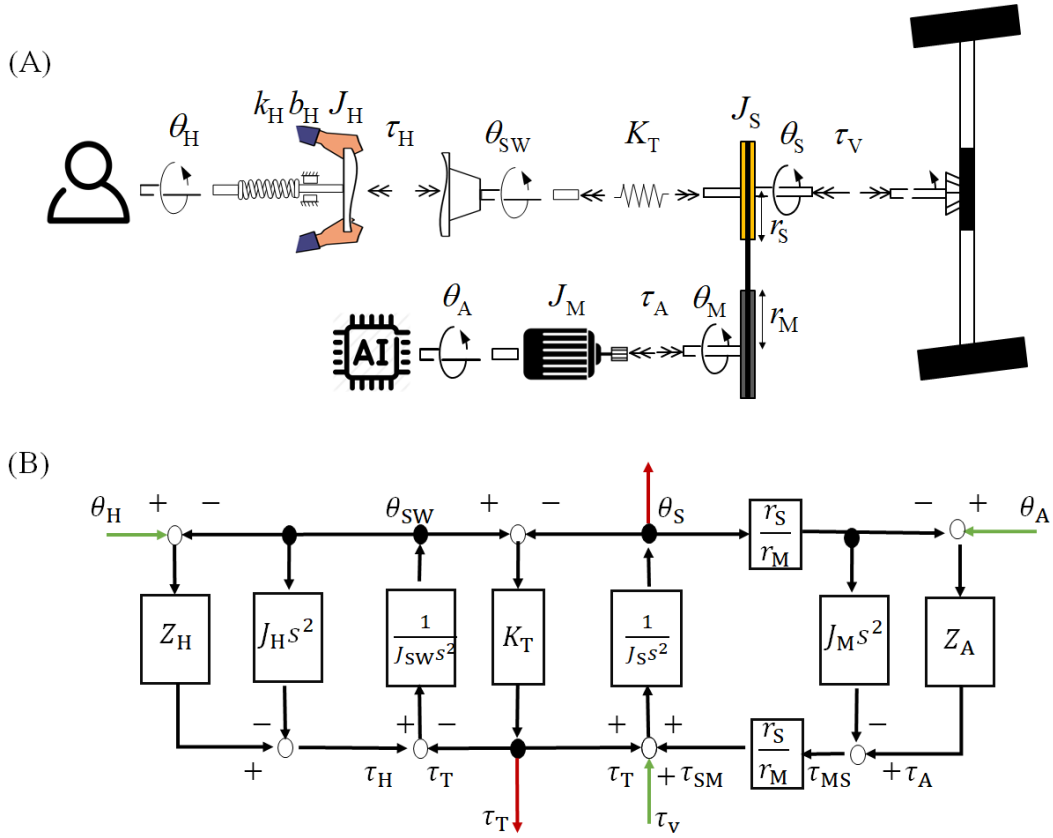
Figure 2.2: (A) Free body diagram of a haptic shared steering control, (B) A block diagram is laid out to highlight the interaction ports between subsystems. [9]

It follows from Figure 2.2 that the equations of motion for the steering wheel, steering column and the motor can be expressed as

$$J_{\text{SW}}\ddot{\theta}_{\text{SW}} = \tau_{\text{H}} - \tau_{\text{T}} \tag{2.1a}$$

$$J_{\text{S}}\ddot{\theta}_{\text{S}} = \tau_{\text{T}} + \tau_{\text{V}} + \tau_{\text{SM}} \tag{2.1b}$$

$$J_{\text{M}}\ddot{\theta}_{\text{M}} = \tau_{\text{A}} - \tau_{\text{MS}} \tag{2.1c}$$

where τ_{SM} and τ_{MS} represent the internal torque imposed by the timing belt. It should be noted that the kinematic and kinetic constraints imposed by the timing belt are $r_{\text{M}}\theta_{\text{M}} = r_{\text{S}}\theta_{\text{S}}$ and $r_{\text{M}}\tau_{\text{SM}} = r_{\text{S}}\tau_{\text{MS}}$.

Modeling the driver as a spring-mass-damper with a proximal motion source $\theta_{\text{H}}(t)$, the torque applied by the human is [18]

$$\tau_{\text{H}} = -J_{\text{H}}\ddot{\theta}_{\text{SW}} + B_{\text{H}}(\dot{\theta}_{\text{H}} - \dot{\theta}_{\text{SW}}) + K_{\text{H}}(\theta_{\text{H}} - \theta_{\text{SW}}) \tag{2.2a}$$

where J_{H}, B_{H}, and K_{H} are the inertia, damping and stiffness of the driver's arm. Similarly, considering an impedance controller in the lower-level of the automation system, the toque generated by the motor can be presented as

$$\begin{aligned} \tau_{\text{A}} &= B_{\text{A}}(\dot{\theta}_{\text{A}} - \dot{\theta}_{\text{M}}) + K_{\text{A}}(\theta_{\text{A}} - \theta_{\text{M}}) \\ &= B_{\text{A}}(\dot{\theta}_{\text{A}} - \frac{r_{\text{S}}}{r_{\text{M}}}\dot{\theta}_{\text{s}}) + K_{\text{A}}(\theta_{\text{A}} - \frac{r_{\text{S}}}{r_{\text{M}}}\theta_{\text{S}}) \end{aligned} \tag{2.2b}$$

where K_{A}, B_{A} represent the gains of the impedance controller. Furthermore, it follows from Figure 2.2 that the torque measured by the torque sensor can be expressed as

$$\tau_{\text{T}} = K_{\text{T}}(\theta_{\text{SW}} - \theta_{\text{S}}) \tag{2.2c}$$

It follows from Eq. (2.2a) that human's torque is not only a function of human's

intent θ_H but also the biomechanic parameters Z_H. By modulating these parameters, the human can either yield or retain the control authority. Similarly, algorithms can be developed to give the automation the ability to either yield authority or retain authority as a function of driver behavior and sensed threats to safety. To present how human's bio-mechanics and the automation's impedance controller parameters may evolve in time, we introduce the following simple but generic dynamic models as

$$\dot{Z}_H(t) = \alpha_H Z_H(t) + \beta_H \Gamma_H(t) + \varrho(t) \tag{2.3a}$$

$$\dot{Z}_A(t) = \alpha_A Z_A(t) + \beta_A \Gamma_A(t) \tag{2.3b}$$

where $Z_H = [B_H \ K_H]^T$, $Z_A = [B_A \ K_A]^T$, and $\Gamma_H = [\Gamma_{bH}(t) \ \Gamma_{kH}(t)]^T$ is the humans control action for modulating his impedance Z_H, $\Gamma_A = [\Gamma_{bA}(t) \ \Gamma_{kA}(t)]^T$ is the automations control input for modulating its impedance Z_A, and $\varrho(t) = [\varrho_{bH}(t) \ \varrho_{kH}(t)]^T$ reflects the uncertainty associated with measurement and model of Z_H. Furthermore,

$$\alpha_H = \begin{bmatrix} \alpha_{bH} & 0 \\ 0 & \alpha_{kH} \end{bmatrix}, \quad \beta_H = \begin{bmatrix} \beta_{bH} & 0 \\ 0 & \beta_{kH} \end{bmatrix}$$

$$\alpha_A = \begin{bmatrix} \alpha_{bA} & 0 \\ 0 & \alpha_{kA} \end{bmatrix}, \quad \beta_A = \begin{bmatrix} \beta_{bA} & 0 \\ 0 & \beta_{kA} \end{bmatrix} \tag{2.4}$$

where $\{\alpha_{bH}, \alpha_{kH}, \alpha_{bA}, \alpha_{kA}, \beta_{bH}, \beta_{kH}, \beta_{bA}, \beta_{kA}\}$ are constant parameters. The details of this model is given in [21]

In this paper, we only assumed the uncertainty in estimation of human's bio-mechanics Z_H and didn't consider the uncertainty in estimation of human's intent θ_H.

Ideally, to determine an optimal behavior for the automation system, optimization should be performed over all control signals of the automation system, including (i.e., θ_A, Γ_A). However, this paper's focus is to determine Γ_A as a means for allocating

the level of authority between the driver and the automation system. By combining Eqs. (2.1a-2.3b), the dynamics interaction between human and automation system in the lower-level of the adaptive haptic shared control framework can be expressed as following stochastic model:

$$\dot{x}(t) = x(t) + f\left(x(t), w(t)\right) + Bu(t) + G\varrho(t) \tag{2.5a}$$

$$y(t) = h\left(x(t)\right) + \varsigma(t) \tag{2.5b}$$

where $x = [\theta_{\mathrm{SW}} \ \dot{\theta}_{\mathrm{SW}} \ \theta_{\mathrm{S}} \ \dot{\theta}_{\mathrm{S}} \ B_{\mathrm{H}} \ K_{\mathrm{H}} \ B_{\mathrm{A}} \ K_{\mathrm{A}}]^{\mathrm{T}}$, are the state of the system; $u = [\Gamma_{\mathrm{bA}}(t) \ \Gamma_{\mathrm{kA}}(t)]^{\mathrm{T}}$ are the control commands, and $w = [\Gamma_{\mathrm{bH}}(t) \ \Gamma_{\mathrm{kH}}(t) \ \theta_{\mathrm{H}} \ \theta_{\mathrm{A}} \ \tau_{\mathrm{V}}]^{\mathrm{T}}$ are the exogenous signals, $y = [\theta_{\mathrm{S}} \ \dot{\theta}_{\mathrm{S}} \ \tau_{\mathrm{T}} \ K_{\mathrm{H}} \ B_{\mathrm{H}} \ K_{\mathrm{A}} \ B_{\mathrm{A}}]^{\mathrm{T}}$ are measured variables, ς denotes the measurement's noise, and G models the effects of ϱ on the system state, and

$$f\left(x, w\right) =$$

$$
\begin{bmatrix}
\dot{\theta}_{\mathrm{SW}} \\
\dfrac{B_{\mathrm{H}}\left(\dot{\theta}_{\mathrm{H}} - \dot{\theta}_{\mathrm{SW}}\right) + K_{\mathrm{H}}(\theta_{\mathrm{H}} - \theta_{\mathrm{SW}}) - K_{\mathrm{T}}(\theta_{\mathrm{SW}} - \theta_{\mathrm{S}})}{J_{\mathrm{SW}} + J_{\mathrm{H}}} \\
\dot{\theta}_{\mathrm{S}} \\
\dfrac{\frac{r_{\mathrm{S}}}{r_{\mathrm{M}}} B_{\mathrm{A}}\left(\dot{\theta}_{\mathrm{A}} - \frac{r_{\mathrm{S}}}{r_{\mathrm{M}}}\dot{\theta}_{\mathrm{S}}\right) + \frac{r_{\mathrm{S}}}{r_{\mathrm{M}}} K_{\mathrm{A}}\left(\theta_{\mathrm{A}} - \frac{r_{\mathrm{S}}}{r_{\mathrm{M}}}\theta_{\mathrm{S}}\right) + K_{\mathrm{T}}(\theta_{\mathrm{SW}} - \theta_{\mathrm{S}}) + \tau_{\mathrm{v}}}{J_{\mathrm{S}} + \left(\frac{r_{\mathrm{S}}}{r_{\mathrm{M}}}\right)^{2} J_{\mathrm{M}}} \\
\alpha_{\mathrm{bH}} B_{\mathrm{H}} + \beta_{\mathrm{bH}} \Gamma_{\mathrm{bH}} \\
\alpha_{\mathrm{kH}} K_{\mathrm{H}} + \beta_{\mathrm{kH}} \Gamma_{\mathrm{kH}} \\
\alpha_{\mathrm{bA}} B_{\mathrm{A}} \\
\alpha_{\mathrm{kA}} K_{\mathrm{A}}
\end{bmatrix}, \tag{2.6a}
$$

$$
B = \begin{bmatrix} 0 & 0 & 0 & 0 & 0 & 0 & \beta_{\mathrm{bA}} & 0 \\ 0 & 0 & 0 & 0 & 0 & 0 & 0 & \beta_{\mathrm{kA}} \end{bmatrix}^{T} \tag{2.6b}
$$

$$
G = \begin{bmatrix} 0 & 0 & 0 & 0 & 1 & 0 & 0 & 0 \\ 0 & 0 & 0 & 0 & 0 & 1 & 0 & 0 \end{bmatrix}^{T} \tag{2.6c}
$$

It should be noted that in this paper, we assume all the measured variables y are accessible. In practice, θ_S can be measured using the encoder attached to the steering column, τ_T can be measured using the differential torques indicating the difference between θ_{SW} and θ_S, K_H and B_H can be estimated using various techniques such as identification techniques discussed in [53, 51] and K_A and B_A are design parameters and directly can be calculated.

2.3   Impedance Modulation Controller Design

In this section, we present a predictive controller for modulating the automation's impedance controller parameters. For the steering control problem, we define a non-linear cost function in the form of

$$
\begin{aligned}
\min_{\Gamma_A} J(t) &= \mathbb{E}\Big\{ \varphi\left(x, w\right) + \int_t^{t+t_h} \mathcal{L}\left(x, w, u\right) d\varsigma \Big\} \\
&= \mathbb{E}\Big\{ \int_t^{t+t_h} \{\|\theta_H - \theta_S\|_{w_1} + \|\theta_A - \theta_S\|_{w_2} + \|\tau_T\|_{w_3}\} d\varsigma \Big\}
\end{aligned}
\tag{2.7}
$$

where t_h is the defined horizon for the model predictive controller, w_1, w_2 and w_3 are weights matrices, $\varphi\left(x, w\right)$ is the terminal cost value which is considered zero. The first term of the cost function over the finite horizon (integration part) aims to minimize the error between the human's intent and the steering angle. Similarly, the second term of the cost function over the finite horizon is defined to minimize the tracking error between the automation's desired angle (automation's intent) and the steering angle. Since the human's and automation's intent may not necessarily be the same, which is when the negotiation of control authority becomes important, the third term of the cost function over the finite horizon is defined to minimize the disagreement between a driver and the automation system.

In this paper, we assume that both ϱ and ς to be sequences of independent and identically distributed (i.i.d.) variables with known probability distributions p_ϱ and

p_ς, respectively. In particular, $\mathbb{E}[\varrho\varrho^{\mathrm{T}}] = Q_\varrho$, $\mathbb{E}[\varsigma\varsigma^{\mathrm{T}}] = Q_\varsigma$, and $\mathbb{E}[\varrho\varsigma^{\mathrm{T}}] = 0$. Let define, the bar symbol $|\bar{\ }|$ on a variable as the expected value (e.g., $\bar{\theta}_{\mathrm{S}} = \mathbb{E}\{\theta_{\mathrm{S}}\}$). Then, the cost function (2.7) can be expressed as

$$\min_{\Gamma_{\mathrm{A}}} J(t) = \varphi(x, w) + \int_t^{t+t_h} \mathcal{L}(x, w, u)\, d\varsigma$$
$$= \int_t^{t+t_h} \{\|\theta_{\mathrm{H}} - \bar{\theta}_{\mathrm{S}}\|_{\hat{w}_1} + \|\theta_{\mathrm{A}} - \bar{\theta}_{\mathrm{S}}\|_{\hat{w}_2} + \|\bar{\tau}_{\mathrm{T}}\|_{\hat{w}_3}\}\, d\varsigma \qquad (2.8)$$

where $\hat{w}_1 = Q_\varsigma w_1$, $\hat{w}_2 = Q_\varsigma w_2$, and $\hat{w}_3 = Q_\varsigma w_3$.

We define two sets of constraints for the nonlinear cost function J to ensure the non-negative values for the impedance controller's parameters. In particular the expectation form of the inequality constraints are:

$$C_1(t) : \left\{ s_1^2 - \bar{B}_{\mathrm{A}}(t) = 0,\ \mathbb{E}\left\{-B_{\mathrm{A}}(t)\right\} \leqslant 0 \right\} \qquad (2.9a)$$

$$C_2(t) : \left\{ s_2^2 - \bar{K}_{\mathrm{A}}(t) = 0,\ \mathbb{E}\left\{-K_{\mathrm{A}}(t)\right\} \leqslant 0 \right\} \qquad (2.9b)$$

Alternatively, constraints in (2.9a) and (2.9b) can be defined as chance constraints. Specifically,

$$C_1(t) : \left\{ \mathbb{P}\left[-B_{\mathrm{A}}^{(k)} \leqslant 0\right] \geqslant \mho_{C_1} \right\} \qquad (2.10a)$$

$$C_2(t) : \left\{ \mathbb{P}\left[-K_{\mathrm{A}}^{(k)} \leqslant 0\right] \geqslant \mho_{C_2} \right\} \qquad (2.10b)$$

where $\mho_{C_1} \in (0,\ 1)$ and $\mho_{C_2} \in (0,\ 1)$ denote the lower bound of the desired joint probability that the state constraints should satisfy.

To solve the nonlinear cost function described in Eq. 2.7, we discretize the equation of the dynamics system using the forward Euler method. Specifically,

$$x^{(k+1)} = x^{(k)} + T_{\mathrm{s}} f\left(x^{(k)}, w^{(k)}\right) + T_{\mathrm{s}} B u^{(k)} + T_{\mathrm{s}} G \varrho^k \qquad (2.11)$$

where T_{s} is the size of the time-step, k is the number of time-step (considered as the current time-step), $x^{(k)}$, $w^{(k)}$ and $u^{(k)}$ are equal to $x(t = T_{\mathrm{s}}k)$, $w(t = T_{\mathrm{s}}k)$ and $u(t = T_{\mathrm{s}}k)$, respectively. It should be noted that that higher order discretizations can be employed at the expense of the computational complexity.

Assuming that the system states can be measured at all times, the finite-horizon stochastic MPC (SMPC) problem with probabilistic constraints C_1 and C_2 and cost function J can be stated in discretized mode as follows:

$$\min_{\Gamma_{\mathrm{A}}} J^{(k)} = \sum_{j=1}^{N_{\mathrm{p}}} T_{\mathrm{s}}\{\|\theta_{\mathrm{H}}^{(k+j)} - \bar{\theta}_{\mathrm{S}}^{(k+j)}\|_{\hat{w}_1} + \|\theta_{\mathrm{A}}^{(k+j)} - \bar{\theta}_{\mathrm{S}}^{(k+j)}\|_{\hat{w}_2}$$

$$+ \|\bar{\tau}_{\mathrm{T}}^{(k+j)}\|_{\hat{w}_3}\}$$

$$\text{s.t. :} \quad \begin{cases} x^{(k+1)} = x^{(k)} + T_{\mathrm{s}}\left(f\left(x^{(k)}, w^{(k)}\right) + Bu^{(k)} + G\varrho^k\right) \\ \\ C_1^{(k)} : \{\mathbb{P}\left[-B_{\mathrm{A}}^{(k)} \leqslant 0\right] \geqslant \mho_{C_1}\} \\ \\ C_2^{(k)} : \{\mathbb{P}\left[-K_{\mathrm{A}}^{(k)} \leqslant 0\right] \geqslant \mho_{C_2}\} \end{cases} \tag{2.12}$$

The closed-loop MPC problem (2.12) is not solvable directly due to the infinite dimensional nature of the control policy Γ_{A}. A tractable approximation to (2.12) can be derived using polynomial chaos (PC) expansion method [50, 37]. Using PC expansion, the stochastic function $\psi(\varrho) = f(x, w) + G\varrho$ can be approximated with a finite second-order moments. [14, 30]. In particular,

$$\psi(\varrho) = f(x, w) + G\varrho \approx \sum_{j=0}^{L_{\mathrm{pc}}-1} \varpi_j \Phi_{\varpi_j}(\varrho) = \eta^{\mathrm{T}}\Lambda(\varrho) \tag{2.13a}$$

$$\Lambda(\varrho) = \left[\Phi_{\varpi_0}, \ \Phi_{\varpi_1}, \cdots, \ \Phi_{\varpi_{L_{\mathrm{pc}}-1}}\right]^{\mathrm{T}} \tag{2.13b}$$

$$\eta_j = \left[\varpi_0, \ \varpi_1, \cdots, \ \varpi_{L_{\mathrm{pc}}-1}\right]^{\mathrm{T}} \tag{2.13c}$$

where ϖ_j indicates the expansion coefficients and $\Phi_{\varpi_j}(\varrho) = \prod_{i=1}^{n} \Phi_{\varpi_{i,j}}(\varrho_i)$ denotes the multivariate polynomials with $\Phi_{\varpi_{i,j}}$ being univariate polynomials in ϱ_i of degree $\varpi_{i,j}$. The total number L_{pc} depends on the number of the number of uncertain parameters and the order of expansion ($L_{pc} = \frac{(n+m)!}{n!m!}$). In this paper, the measurement noises ϱ on the human bio-mechanic parameters B_H and K_H are assumed to have Gaussian distribution in the form of ($\frac{1}{2\pi}\exp\left(-\sigma_i^2/2\right), i \in \{H, B\}$). Therefore, the Hermite polynomials can be utilized to approximate nonlinear dynamics (2.5b). Specifically, the multivariate polynomials with the Gaussian distribution of ϱ becomes $\Lambda(\sigma_i) = [1, \ \sigma_i, \ \sigma_i^2 - 1, \ \sigma_i^3 - 3\sigma_i, \sigma_i^4 - 6\sigma_i^2 + 3, \cdots]$ and the expansion coefficients ϖ_j at each time state can be calculated based on the pseudo-spectral approach [42]. The details of PC expansion method can be found in [13]. By employing PC expansion, the deterministic surrogate for the stochastic MPC problem (2.12) can be expressed as follow:

$$\min_{\Gamma_A} J^{(k)} = \sum_{j=1}^{N_P} T_s \{ \|\theta_H^{(k+j)} - \bar{\theta}_S^{(k+j)}\|_{\hat{w}_1} + \|\theta_A^{(k+j)} - \bar{\theta}_S^{(k+j)}\|_{\hat{w}_2} $$

$$+ \|\bar{\tau}_T^{(k+j)}\|_{\hat{w}_3} \}$$

$$\text{s.t.} : \begin{cases} \bar{x}^{(k+1)} = \bar{x}^{(k)} + T_s \left(\left(\eta^{(k)}\right)^T \Lambda\left(\varrho^{(k)}\right) + Bu^{(k)} \right) \\ \\ C_1^{(k)} : -\sqrt{\frac{\mho_{C_1}}{1-\mho_{C_1}}} \ \text{Var}[B_A^{(k)}] - \bar{B}_A^{(k)} + s_1 = 0 \\ \\ C_2^{(k)} : -\sqrt{\frac{\mho_{C_2}}{1-\mho_{C_2}}} \ \text{Var}[K_A^{(k)}] - \bar{K}_A^{(k)} + s_2 = 0 \end{cases} \qquad (2.14)$$

where s_1 and s_2 are slack variables and Var[.] represent the variable's variance. By using the non-negative slack variables in Eq. (2.14), the inequality constraints will be transformed to the equality constraints [46].

Next, let H denote the Hamiltonian defined by

$$
\begin{aligned}
H\left(\bar{x}^{(k)}, w^{(k)}, u^{(k)}, \lambda^{(k)}, \mu^{(k)}\right) = \\
T_{\mathrm{s}}\left(\|\theta_{\mathrm{H}}^{(k)} - \bar{\theta}_{\mathrm{S}}^{(k)}\|_{\hat{w}_1} + \|\theta_{\mathrm{A}}^{(k)} - \bar{\theta}_{\mathrm{S}}^{(k)}\|_{\hat{w}_2} + \|\bar{\tau}_{\mathrm{T}}^{(k)}\|_{\hat{w}_3}\right) \\
+ \lambda^{(k)}\left(\bar{x}^{(k)} - \bar{x}^{(k+1)} + T_{\mathrm{s}}\left(\left(\eta^{(k)}\right)^T \Lambda\left(\varrho^{(k)}\right) + Bu^{(k)}\right)\right) \\
+ \mu^{(k)}\left(\left[C_1^{(k)}, C_2^{(k)}\right]^{\mathrm{T}}\right)
\end{aligned}
\tag{2.15a}
$$

where

$$
\lambda^{(k)} = \left[\lambda_{\theta_{\mathrm{S}}}^{(k)} \quad \lambda_{\dot{\theta}_{\mathrm{S}}}^{(k)} \quad \lambda_{\theta_{\mathrm{SW}}}^{(k)} \quad \lambda_{\dot{\theta}_{\mathrm{SW}}}^{(k)} \quad \lambda_{\Gamma_{\mathrm{bH}}}^{(k)} \quad \lambda_{\Gamma_{\mathrm{kH}}}^{(k)} \quad \lambda_{\Gamma_{\mathrm{bA}}}^{(k)} \quad \lambda_{\Gamma_{\mathrm{kA}}}^{(k)}\right]
\tag{2.15b}
$$

$$
\mu^{(k)} = \left[\mu_{C_1}^{(k)} \quad \mu_{C_2}^{(k)}\right]
\tag{2.15c}
$$

where λ and μ are costate vector and Lagrange multiplier vector respectively. The necessary conditions for optimality are obtained by the calculus of variations [10]. We discretize the conditions by dividing the horizon into N_{p} steps. The discretized Karush-Kuhn-Tucker (KKT) necessary conditions are given as follows:

$$
\bar{x}^{*(k+1)} = \bar{x}^{*(k)} + T_{\mathrm{s}}\left(\left(\eta^{*(k)}\right)^T \Lambda\left(\varrho^{(k)}\right) + Bu^{*(k)}\right)
\tag{2.16a}
$$

$$
\bar{x}^{*(0)} = \bar{x}^{(0)}
\tag{2.16b}
$$

$$
\lambda^{*(k)} = \lambda^{*(k+1)} + T_{\mathrm{s}}\frac{\partial H^{\mathrm{T}}\left(\bar{x}^{*(k)}, w^{(k)}, u^{*(k)}, \lambda^{*(k)}, \mu^{*(k)}\right)}{\partial \bar{x}}
\tag{2.16c}
$$

$$
\lambda^{*(k+N_{\mathrm{p}})} = 0
\tag{2.16d}
$$

$$
\frac{\partial H^{\mathrm{T}}\left(\bar{x}^{*(k)}, w^{(k)}, u^{*(k)}, \lambda^{*(k)}, \mu^{*(k)}\right)}{\partial u} = 0
\tag{2.16e}
$$

$$
\begin{bmatrix} C_1^{(k)} \\ C_2^{(k)} \end{bmatrix} = \begin{bmatrix} 0 \\ 0 \end{bmatrix}
\tag{2.16f}
$$

By employing forward recursion, for $j = 1, \cdots, N_{\mathrm{p}}$, the state variables $\bar{x}^{*(k+j)}$,

can be defined using equations (2.16a) and (2.16b). Furthermore, by employing back recursion from the final condition to the present time-step ($j = N_{\mathrm{p}}, N_{\mathrm{p}} - 1, \cdots, 1$) the co-states $\lambda^{*(k+j)}$ can be determined using (2.16c) and (2.16d). Finally, by plugging $\bar{x}^{*(k+j)}$ and $\lambda^{*(k+j)}$ into equations (2.16e) and (2.16f), a KKT vector $F(X, U, t)$ for N_p horizon can be defined, where

$$
F = \begin{bmatrix}
\dfrac{\partial H^{\mathrm{T}}\left(\bar{x}^{*(k)}, w^{(k)}, u^{*(k)}, \lambda^{*(k)}, \mu^{*(k)}\right)}{\partial u} \\[2em]
C_1^{(k)} \\[2em]
C_2^{(k)} \\
\vdots \\
\dfrac{\partial H^{\mathrm{T}}\left(\bar{x}^{*(k+N_{\mathrm{c}})}, w^{(k+N_{\mathrm{c}})}, u^{*(k+N_{\mathrm{c}})}, \lambda^{*(k+N_{\mathrm{c}})}, \mu^{*(k+N_{\mathrm{c}})}\right)}{\partial u} \\[2em]
C_1^{(k+N_{\mathrm{c}})} \\[2em]
C_2^{(k+N_{\mathrm{c}})} \\
\vdots \\
\dfrac{\partial H^{\mathrm{T}}\left(\bar{x}^{*(k+N_{\mathrm{p}})}, w^{(k+N_{\mathrm{p}})}, u^{*(k+N_{\mathrm{p}})}, \lambda^{*(k+N_{\mathrm{p}})}, \mu^{*(k+N_{\mathrm{p}})}\right)}{\partial u} \\[2em]
C_1^{(k+N_{\mathrm{p}})} \\[2em]
C_2^{(k+N_{\mathrm{p}})}
\end{bmatrix}
\tag{2.17a}
$$

where

$$
X = \left[\bar{x}^{(k)}, w^{(k)}, \bar{x}^{(k+1)}, w^{(k+1)}, ..., \bar{x}^{(k+N_{\mathrm{p}})}, w^{(k+N_{\mathrm{p}})}\right]^{\mathrm{T}}
\tag{2.17b}
$$

$$
U = \left[u^{(k)}, \mu^{(k)}, \cdots, u^{(k+N_{\mathrm{c}})}, \mu^{(k+N_{\mathrm{c}})}, \cdots, u^{(k+N_{\mathrm{c}})}, \mu^{(k+N_{\mathrm{p}})}\right]^{\mathrm{T}}
\tag{2.17c}
$$

where N_c is the number of the control horizon steps. Note that for $N_c \leq j \leq N_p$, $u^{k+j} = u^{k+N_c}$. By solving a nonlinear algebraic equation $F(X, U, t) = 0$, an optimal optimal points can be determined and the optimal control command can be determined by

$$u^{(k)} = P_0 U \tag{2.18}$$

where P_0 is a projection matrix and can be defined as

$$P_0 = \begin{bmatrix} 1 & 0 & 0 & \cdots & 0 & 0 & 0 \\ 0 & 1 & 0 & \cdots & 0 & 0 & 0 \end{bmatrix}_{2 \times 12N_p}. \tag{2.19}$$

2.3.1 Continuation method

To solve $F(X, U, t) = 0$ with respect to the unknown vector U, for each time-step, the C/GMRES method is employed [35]. In C/GMRES method, instead of solving $F(X, U, t) = 0$, we select the proper initial value $U(0)$ and take the time derivative of Eq. (2.17a) into account. Specifically, we define

$$\dot{F}(X, U, t) = A_s F(X, U, t) \tag{2.20}$$

where A_s is a stable matrix (i.e. with negative eigenvalues). Differentiating the left side of Eq. (2.20) yields

$$F_U(X, U, T)\dot{U} = A_s F(X, U, t) - F_X(X, U, t)\dot{X} - F_t(X, U, t) \tag{2.21}$$

If F_U is non singular, we can obtain the differential equation for $\dot{U}$ as

$$\dot{U} = F_U^{-1}\left(A_s F(X, U, t) - F_X(X, U, T)\dot{X} - F_t(X, U, T)\right) \tag{2.22}$$

2.3.2   Forward difference GMRES method

The calculation of Jacobians F_X, F_U and $\dot{F}$ is computationally expensive. Instead to solve Eq. (2.22), we employed the forward-difference approximation to eliminate the calculation of the Jacobians. To this end, using the concept of forward difference, we approximate the products of Jacobians and some $L \in \mathbb{R}^{11 \times N_\mathrm{P}}$, $M \in \mathbb{R}^{12 \times N_\mathrm{P}}$, and $\omega \in \mathbb{R}$ and replaced it to Eq. (2.22) which results in:

$$D_\mathrm{h}F\left(X, U, t : 0, \dot{U}, 0\right) = b\left(X, \dot{X}, U, t\right) \tag{2.23a}$$

where

$$b\left(X, \dot{X}, U, t\right) = A_\mathrm{s}F\left(X, U, t\right) - D_\mathrm{h}F\left(X, U, t : \dot{X}, 0, 1\right) \tag{2.23b}$$

$$D_\mathrm{h}F\left(X, U, t : L, M, \omega\right) = \frac{F\left(X + hL, U + hM, t + h\omega\right) - F\left(X, U, t\right)}{h} \tag{2.23c}$$

where h is a positive real number, $D_\mathrm{h}F\left(X, U, t : L, M, \omega\right)$ stands for the concept of forward difference for F. It should be noted that there is main difference between forward-difference approximation and finite-difference approximation with regards to computational expenses. The forward difference approximation of the products of the Jacobians and vectors can be calculated with only an additional evaluation of the function, which requires notably less computational burden than approximation of the Jacobians themselves. Since Eq. (2.23a) is a linear equation with respect to $\dot{U}$, we applied the forward difference GMRES method to solve it [25]. The details of this method is described in Algorithm 1.

2.3.3   Combination of continuation and GMRES

$\dot{U}$ is the output of the forward-difference GMRES algorithm, and integration of this value results in U for the current time step. For a sampling time $\triangle t$ and integer value ℓ, Algorithm 2 shows the required steps of the continuation/GMRES method

---

Algorithm 1: Forward-Difference GMRES[35]

Result: $\dot{U} := \text{FDGMRES}\left(X, \dot{X}, U, U_{\text{int}}, h, \mathcal{I}_{\max}\right)$

$\hat{r} := b\left(X, \dot{X}, U, t\right) - D_{\text{h}}F\left(X + h\dot{X}, U, t + h : 0, U_{\text{int}}, 0\right)$;

$v_1 := \hat{r}/\|\hat{r}\|,\ \rho := \|\hat{r}\|,\ \zeta := \rho,\ \mathcal{I} = 0$;

while $\mathcal{I} < \mathcal{I}_{\max}$ **do**

$\quad \mathcal{I} := \mathcal{I} + 1;$

$\quad v_{\mathcal{I}+1} := D_{\text{h}}F\left(X + h\dot{X}, U, t + h : 0, v_{\mathcal{I}}, 0\right);$

$\quad$ **for** $j = 1, 2, \ldots, \mathcal{I}$ **do**

$\quad\quad h_{j,\mathcal{I}} := v_{\mathcal{I}+1}^{\text{T}} v_j$;

$\quad\quad v_{\mathcal{I}+1} := v_{\mathcal{I}+1} - h_{j,\mathcal{I}} v_j$

$\quad$ **end**

$\quad h_{\mathcal{I}+1,\mathcal{I}} := \|v_{\mathcal{I}+1}\|;$

$\quad v_{\mathcal{I}+1} := v_{\mathcal{I}+1}/\|v_{\mathcal{I}+1}\|;$

$\quad$ **for** $e_1 = [1, 0, \ldots, 0] \in \mathbb{R}^{\mathcal{I}+1}$ **&&** $H_{\mathcal{I}} = (h_{i,j}) \in \mathbb{R}^{\mathcal{I}+1 \times \mathcal{I}}$ **do**

$\quad\quad$ Minimize $\|\zeta e_1 - H_{\mathcal{I}}\mathcal{Y}^{\mathcal{I}}\|$ with LS method to determine $\mathcal{Y} \in \mathbb{R}^{\mathcal{I}}$

$\quad$ **end**

$\quad \rho := \|\zeta e_1 - H_{\mathcal{I}}\mathcal{Y}^{\mathcal{I}}\|;$

end

$\dot{U} := \dot{U} + V_{\mathcal{I}}\mathcal{Y}^{\mathcal{I}}$ where $V_{\mathcal{I}} = [v_1, v_2, \cdots, v_{\mathcal{I}}] \in \mathbb{R}^{12 \times N_{\text{p}} \times \mathcal{I}}$.

---

for nonlinear model predictive control.

It should be noted that the C/GMRES is an iterative method that solves Eq.(2.17a) with respect to $\dot{U}$ only once at each sampling time and therefore, requires much less computational expenses than other iterative methods such as Newtons method. Moreover, C/GMRES involves no line search, which is also a significant difference from standard optimization methods [35]. The C/GMRES method's flowchart is depicted in Fig. (2.3), which demonstrates the solving procedure for each time steps in the numerical executions. The problem construction step till $U, \dot{U}_0$ initialization will be executed one time in the algorithm, which leads to a reduced computational load in the solver. The rest of the algorithm is running till the termination condition is satisfied. The termination condition in the numerical simulation is the simulation run time, and in the PIL implementations, it is set as the maximum number of control loop execution.

Algorithm 2: Continuation/GMRES [35]

Result: $U := \text{CntFDGMRES}\left(X, \dot{X}, \dot{U}, t, \triangle t, \delta\right)$

(1) $t := 0, \; \ell := 0;$
(2) Select small value $\delta > 0;$
(3) Find $U(0)$ for satisfying $\|F\left(X(0), U(0), 0\right)\| \leqslant \delta$;
(4) In $t' \in [t, t + \triangle t)$ set $u(t') := P_0 U(\ell \triangle t);$
At time $t + \triangle t$ by considering measured states $x(t + \triangle t)$ set
$\triangle x_\ell = x_\ell(t + \triangle t) - x_\ell(t);$
(5) $U_{\text{int}} = U_{t_0}, \; U_{\text{int}} = \dot{U}((\ell - 1) \triangle t);$
(6) $\dot{U}(\ell \triangle t) := \text{FDGMRES}(X, \triangle x_\ell / \triangle t, U, U_{\text{int}}, h, \mathcal{I}_{\text{max}});$
(7) Set $U\left((\ell + 1) \triangle t\right) = U\left(\ell \triangle t\right) + \triangle t \, \dot{U}\left(\ell \triangle t\right)$
(8) Set $t := t + \triangle t, \; \ell := \ell + 1$ and go back to line (4)
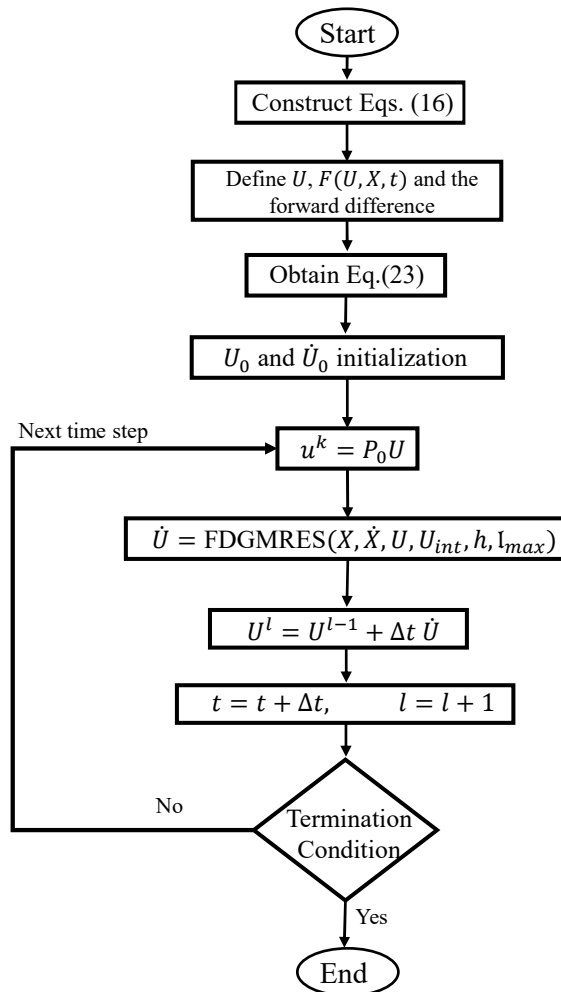
Figure 2.3: C/GMRES method's flowchart

Figure 2.4 shows the control architecture of the closed loop. The higher-level control consists of four main sections: interaction mode determination that define the appropriate form of the cost function as well as the appropriate weights of each term in the cost function [27, 29, 24], human's biomechanics identification that identifies the current state of Z_H [53, 51, 20], human's intent detection that determines θ_H [39, 4, 47] and automation system's motion planning that determine θ_A [19]. The outputs of the higher-level controller are fed to the automation's lower-level control to determine the optimal Z_A. By modulating the automation's impedance controller gains, the control authority dynamically exchanges between the human and automation, and subsequently θ_S follows the intents of humans or automation.
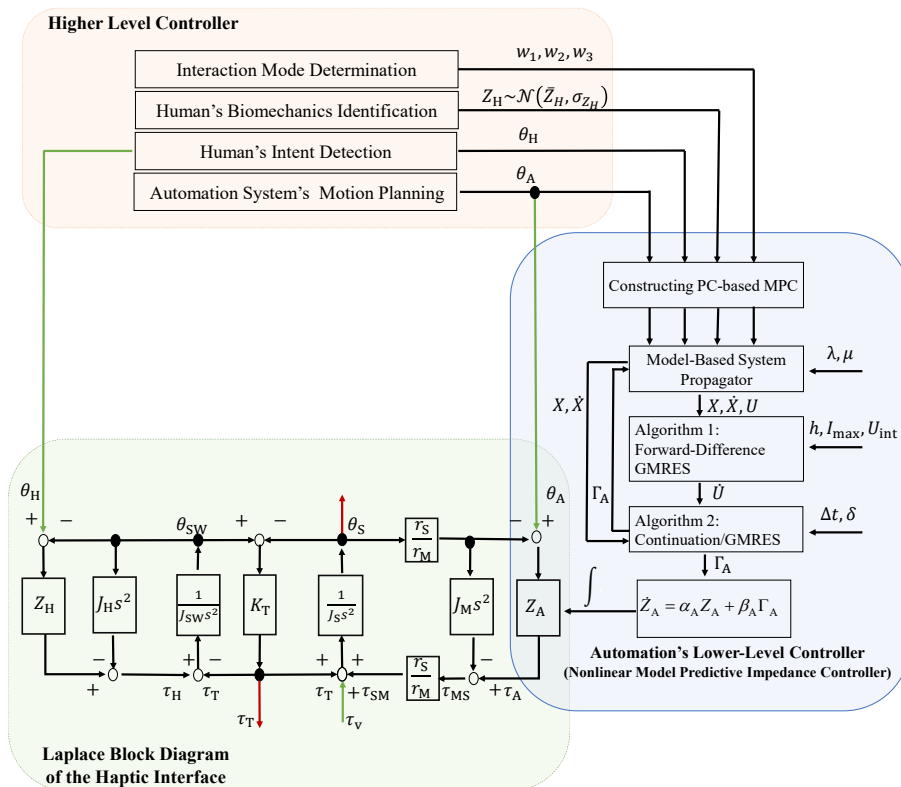
Figure 2.4: The detailed block diagram of the adaptive haptic shared control paradigm including the higher level controller, the automation's lower-level controller and Laplace block diagram of the haptic interface.

2.4   Simulation Studies and Discussions

In this section, we present a series of simulation studies demonstrating the effectiveness of the proposed controller in transferring the control authority between the driver and the automation system. The following simulations consider a scenario where the human and the automation system detect an obstacle and negotiate on controlling the steering wheel so that the obstacle can be avoided safely. To this end, the simulations involve two conditions when the control authority shifts from the human to the automation system (active safety mode), as well as when the control authority shifts from the automation system to human (assistive mode). Also, we included two other conditions where the human and automation are in cooperative and uncooperative mode. In cooperative mode, the human and automation intents detect the obstacle and decide to avoid the obstacle by maneuvering in the same direction (same intent signs $\text{sgn}(\theta_\text{H}) = \text{sgn}(\theta_\text{A})$). In uncooperative mode, humans and automation's detect the obstacle but their intents have opposite signs ($\text{sgn}(\theta_\text{H}) = -\text{sgn}(\theta_\text{A})$). In this paper, the driver's intent is expressed by the following curve

$$
\theta_\text{H} = \begin{cases} 0 & t < T_1 \\[2mm] \frac{W}{2}\cos(\frac{\pi}{T_2}t - \frac{T_{1,2}}{T_2}\pi) + \frac{W}{2} & T_1 < t < T_{1,2} \\[2mm] W & T_{1,2} < t < T_{1,2,3} \\[2mm] \frac{W}{2}\cos(\frac{\pi}{T_2}t - \frac{T_{1,2,3}}{T_2}\pi) + \frac{W}{2} & T_{1,2,3} < t < T_{1,2,3} + T_2 \\[2mm] 0 & T_{1,2,3} + T_2 < t \end{cases} \tag{2.24}
$$

$$
T_{1,2} = T_1 + T_2, \qquad T_{1,2,3} = T_1 + T_2 + T_3
$$

where $T_1 = 1$ sec, $T_2 = 5$ sec, $T_3 = 2$ sec and $W = 1$ rad are selected for the following examples. Note that in the following examples to illustrate the results clearly, we select $|\theta_\text{A}| = 0.9|\theta_\text{H}|$. We also assume no feedback from the road and consider $\tau_\text{V} = 0$

in the following examples.

Additionally, in the following simulations, we select the mean values of human arms' bio-mechanics as either $\bar{Z}_H = [0.5 \ 1]^T$ representing a case when the human control command is sufficient or $\bar{Z}_H = [0.1 \ 0.1]^T$ describing a situation when the driver's control command is insufficient. These values are selected based on a set of simulation studies. To consider the role of uncertainity in the estimation of the human's bio-mechanics parameters, K_H and B_H are generated using a series of random parameter vectors generated from the Gaussian pdfs [38]. Specifically, the human's bio-mechanics variance value $(\sigma_{B_H}, \ \sigma_{K_H})$ in random parameter vectors has maximum $(0.05, \ 0.1)$ to define the performance range of the adaptive impedance controller. The additive disturbances ϱ have a Gaussian distribution $\varrho \sim \mathcal{N}(0, \ Q_\sigma)$ with zero mean and covariance matrix $Q_\sigma = diag[0.01, \ 0.001, \ 0.005, \ 0.05, \ 0.02, 0, \ 0]$. The numerical values for the other parameters in the simulation studies are demonstrated in table 2.1.

When the human's control command is sufficient (high Z_H), the automation system shall be designed to yield the control authority to the human operator. Specifically, we select the weights of the cost function to be $w_1 = 0.2, w_2 = 0$ and $w_3 = 0.8$. With selecting these weights for the cost function, the automation system acts in an assisitive mode [6]. On the other hand, when the human's control command is insufficient (low Z_H), the automation system is designed to ensure the safety of the task by avoiding the obstacle. In particular, we select the weights of the cost function to be $w_1 = 0, w_2 = 0.8$ and $w_3 = 0.2$. With choosing these weights for the cost function, the automation system acts in the active safety mode [6].

Figure 2.5 demonstrates the problem of control authority negotiation in un-cooperative mode. Specifically, the interaction between the human and automation system in the adaptive haptic shared control paradigm is compared with the interaction in non-adaptive haptic shared control wherein the parameters of the automation's impedance

Table 2.1: Numerical values for the system parameters in the simulation

Parameters	Variables	Interaction Modes		Unit
		Active safety	Assistive	
Activation coefficient of k_A	β_{k_A}	1	0.1	-
Activation coefficient of b_A	β_{b_A}	1	0.1	-
Memory coefficient of k_A	α_{k_A}	-1		-
Memory coefficient of b_A	α_{k_A}	-1		-
Mean value of driver arm's stiffness	$\bar{\kappa}_H$	0.1	1	-
Mean value of driver arm's damping	$\bar{B}_H$	0.1	0.5	-
Driver arm's inertia	J_H	1×10^{-3}		Kg.m^2
Steering wheel inertia	J_{SW}	1×10^{-2}		Kg.m^2
Steering column inertia	J_S	1×10^{-2}		Kg.m^2
Motor's inertia	J_M	1×10^{-3}		Kg.m^2
Torque sensor stiffness	K_T	1000		N.m/rad
Timing belt mechanical advantage	r_S/r_M	1		-
Prediction horizon	N_p	10		-
Control horizon	N_c	10		-
The sample time	T_S	1×10^{-2}		Sec
Maximum index	$\mathcal{I}_{\max}$	12		-
KKT vector norm range	δ	5×10^{-2}		-

controller are invariant. The first row shows the human's intent θ_H, the automation's intent θ_A, and the steering angle θ_S. The second row shows the human's torque τ_H, the automation system's torque τ_A, and the torque measured by the torque sensor τ_T. The third and fourth row shows the parameters of the damping and stiffness of the human arm and automation's impedance controller, respectively. In this example, we select the human's biomechanics mean value to be $\bar{Z}_\mathrm{H} = [0.5\ 1]^\mathrm{T}$. Since with $\bar{Z}_\mathrm{H} = [0.5\ 1]^\mathrm{T}$, the human's control command is sufficient to maneuver the steering angle safely, we select the weights of the cost function such that the automation acts in an assistive mode [6] (i.e., $w_1 = 0.2, w_2 = 0$ and $w_3 = 0.8$). In a non-adaptive haptic shared control paradigm, the automation's impedance controller parameters are selected to be the same as the mean value of the driver's biomechanics ($\bar{Z}_\mathrm{H} = Z_\mathrm{A}$). It follows from Figure 2.5-A and 2.5-B that in the non-adaptive haptic shared control paradigm when humans and automation are in the uncooperative mode, their control commands are opposite and cancel out each other ($\tau_\mathrm{A} \approx -\tau_\mathrm{H}$); and therefore, the steering angle is almost zero ($\bar{\theta}_\mathrm{S} \approx 0$). On the other hand, it follows from Figures 2.5-C and 2.5-D that in the adaptive haptic shared control paradigm, the automation' impedance controller parameters Z_A are reduced to minimize the disagreement τ_T. It follows from Figure 2.5-B that the disagreement between humans and automation is effectively smaller than the non-adaptive haptic shared control paradigm. Furthermore, since the human's adopted impedance is sufficient, the steering angle θ_S command follows the human's intent θ_H.

Figure 2.6 also demonstrates the interaction between the driver and the automation system in the un-cooperative mode in non-adaptive and adaptive haptic shared control paradigms. In this example, we selected the human's biomechanics to be $\bar{Z}_\mathrm{H} = [0.1\ 0.1]^\mathrm{T}$. Since with $\bar{Z}_\mathrm{H} = [0.1\ 0.1]^\mathrm{T}$, the human's control command is insufficient to maneuver the steering angle safely, we select the weights of the cost function such that the automation acts in an active safety mode [6] (i.e., $w_1 = 0, w_2 = 0.8$ and $w_3 = 0.2$).
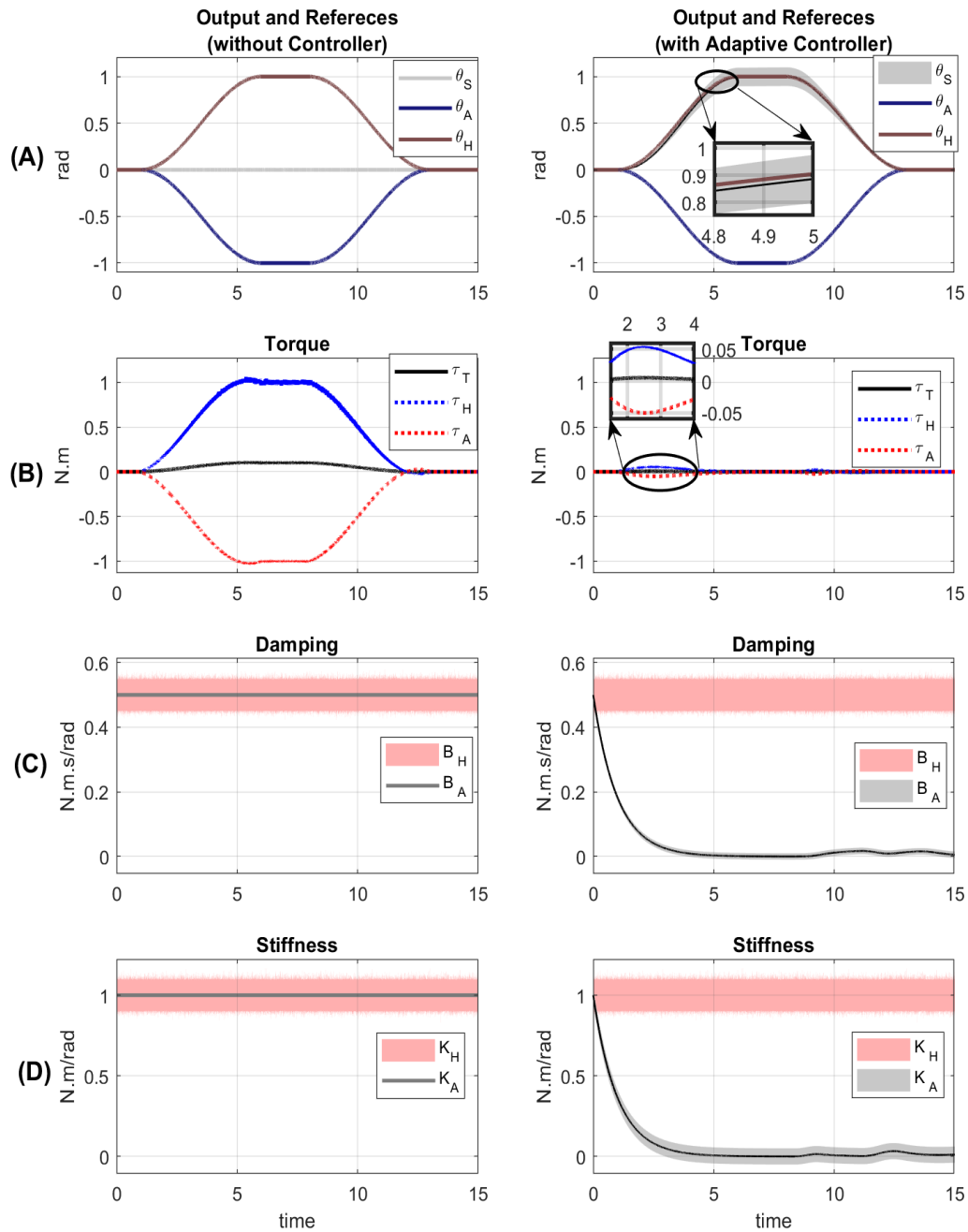
Figure 2.5: The outputs of the driver and automation system interaction within non-adaptive and adaptive haptic shared control paradigms are compared. (A) driver intent (red), autonomous system intent (blue) and steering column angle (black) (B) Measured torque (black), human torque (red) and automation torque (blue) (C) Damping coefficients of the agents (D) Stiffness coefficients of the agents. The automation system act as assistive in an uncooperative mode in the adaptive haptic shared control paradigm. By reducing the automation's impedance controller gains, the automation system reduces the disagreement between the human and automation system. The shaded bands for θ_S, K_A, and B_A represent the 95% confidence intervals.

Similar to the previous example, we assumed the automation system has an estimation of the human's biomechanics, and since the human adopted a lower impedance, the automation re-gain the control authority from the human driver. Also, similar to the previous example, in the non-adaptive paradigm, the automation's impedance controller parameters are selected to be the same as the driver, and therefore, the control commands of the human τ_H and automation system τ_A are opposite and cancel out each other (see Figure 2.6-A). On the other hand, it follows from the Figures 2.6-C and 2.6-D that in the adaptive haptic shared control paradigm, the automation system's impedance controller parameters Z_A is increased to ensure the desired performance (e.g., avoiding an obstacle in the middle of the road). Since the automation's impedance control parameters are increased, the disagreement τ_T between the two agents is also increased (See Figure 2.6-B). Furthermore, since Z_A is bigger than Z_H, the steering angle θ_S is closer to the automation's intent θ_A (see Figure 2.6-A).

Figure 2.7 demonstrates the interaction between the driver and the automation system in the cooperative mode. In this example, we select the human's biomechanics to be $\bar{Z}_\mathrm{H} = [0.5\ 1]^\mathrm{T}$. Since the human's control command is sufficient to maneuver the steering wheel safely, we select the weights of the cost function as $w_1 = 0.2, w_2 = 0$, and $w_3 = 0.8$. With choosing these weights for the cost function, the automation system acts in an assistive mode [6]. In a non-adaptive haptic shared control paradigm, the automation's impedance controller parameters are selected to be the same as the driver ($Z_\mathrm{A} = \bar{Z}_\mathrm{H}$). Although the torques of the driver τ_H and the automation system τ_A in cooperative mode are much smaller than torques in the uncooperative mode, it follows from the Figures 2.7-B that by modulating the automation' impedance controller parameters Z_A the disagreement τ_T even decreased more.

Figure 2.8 also demonstrates the interaction between the driver and the automation system in non-adaptive and adaptive haptic shared control paradigms in the coopera-
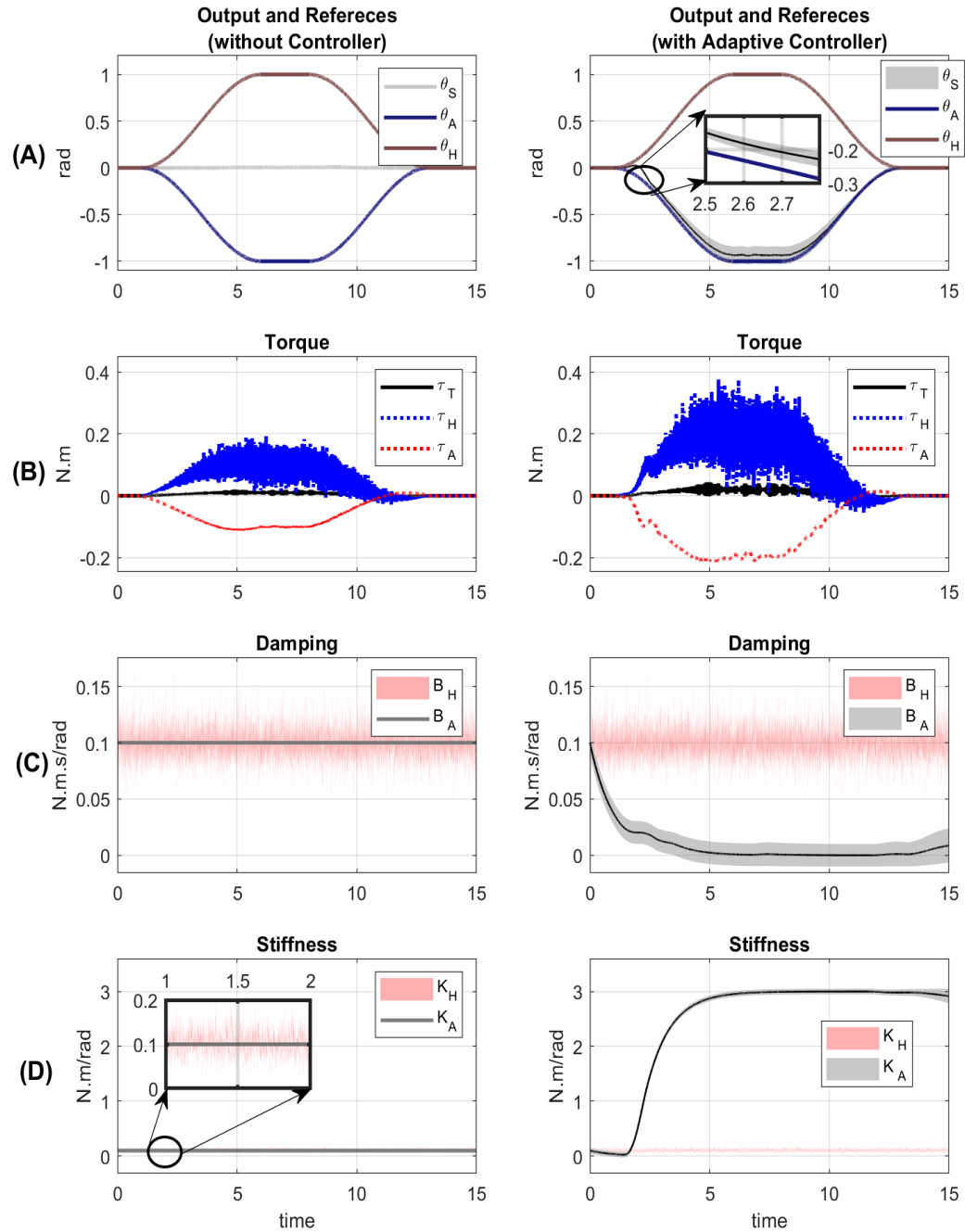
Figure 2.6: The outputs of the driver and automation system interaction within non-adaptive and adaptive haptic shared control paradigms are compared. (A) driver intent (red), autonomous system intent (blue) and steering column angle (black) (B) Measured torque (black), human torque (red) and automation torque (blue) (C) Damping coefficients of the agents (D) Stiffness coefficients of the agents. The automation system act as assistive in an uncooperative mode in the adaptive haptic shared control paradigm. The automation system provides enough control input for obstacle avoidance by increasing the automation's impedance controller gains. The shaded bands for θ_S, K_A, and B_A represent the 95% confidence intervals.
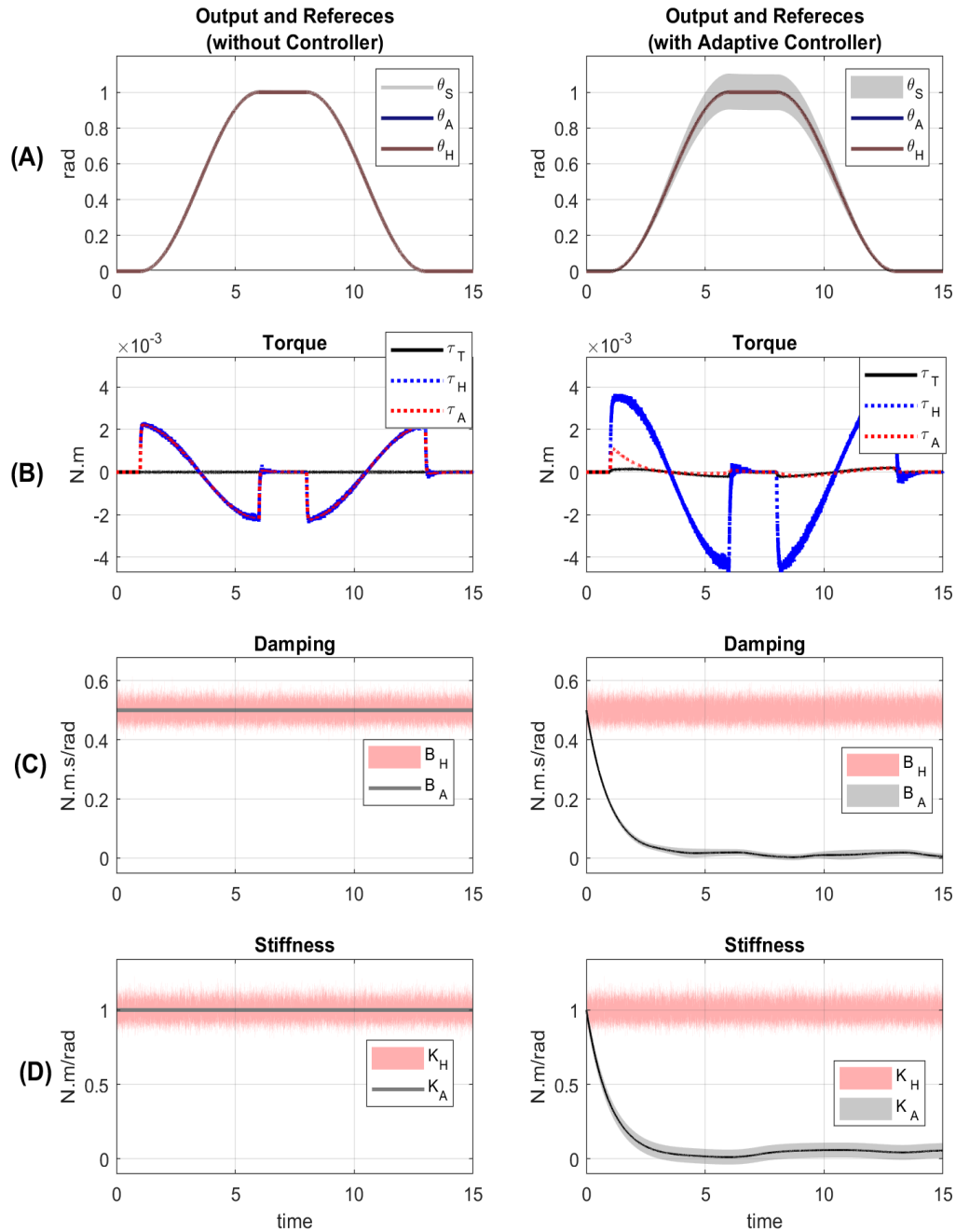
Figure 2.7: The outputs of the driver and automation system interaction within non-adaptive and adaptive haptic shared control paradigms are compared. (A) driver intent (red), autonomous system intent (blue) and steering column angle (black) (B) Measured torque (black), human torque (red) and automation torque (blue) (C) Damping coefficients of the agents (D) Stiffness coefficients of the agents. The automation system act as assistive in a cooperative mode in the adaptive haptic shared control paradigm. By reducing the automation's impedance controller gains, the automation system reduces the disagreement between the human and automation system. The shaded bands for θ_S, K_A, and B_A represent the 95% confidence intervals.

tive mode. In this example, we select the human's biomechanics to be $\bar{Z}_H = [0.1\ 0.1]^T$. Since the human's control command is insufficient to maneuver the steering wheel safely, we select the weights of the cost function to be $w_1 = 0, w_2 = 0.8$, and $w_3 = 0.2$. With choosing these weights for the cost function, the automation system acts in the active safety mode [6]. It follows from the Figures 2.8-C and 2.8-D that in the adaptive haptic shared control paradigm, the automation' impedance controller parameters Z_A are increased to ensure the desired performance (e.g., providing the required control inputs).

Considering no uncertainty in Z_H (i.e., $Z_H = \bar{Z}_H$), Figure 2.9 shows a scenario wherein all the four interaction modes are integrated into one unified framework. The sequence of these interaction modes is cooperative-active safety, uncooperative assistive, uncooperative-active safety, and cooperative-auto pilot mode. It follows from Figure 2.9 that initially, the human and automation system are in cooperative mode; however, the human's torque input is insufficient (low Z_H). The automation system increases its impedance to provide the required control command. In the next mode, the human and robot are in the uncooperative mode; however, the human's torque input is sufficient (high Z_H). The automation system reduces its impedance to minimize the disagreement with the driver. In the third mode, the human and robot are in the uncooperative mode; however, the human's torque input is insufficient (low Z_H). The automation system again increases its impedance to ensure safety at the expense of fighting with the driver (high τ_T). Finally, the human and robot are again in the cooperative mode in the fourth mode; however, the human's torque input is sufficient (high Z_H). The automation system reduces its impedance and yields the control authority to the driver. It follows from Figure 2.9 that in the proposed adaptive haptic shared paradigm, by recognizing the interaction mode, the appropriate set of weights for the cost function can be determined and automation can continuously adjust its impedance controller parameters such that not only the
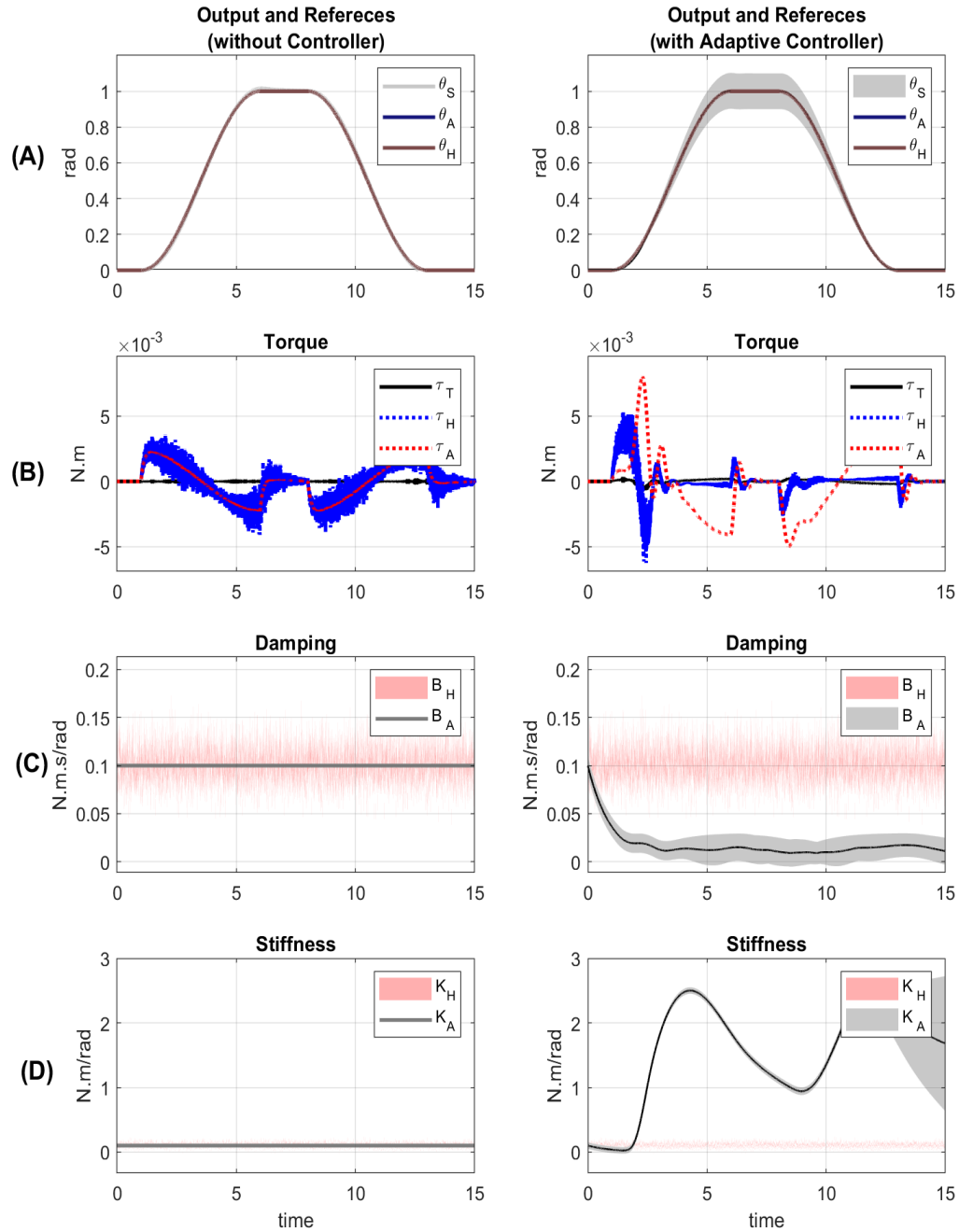
Figure 2.8: The outputs of the driver and automation system interaction within non-adaptive and adaptive haptic shared control paradigms are compared. (A) driver intent (red), autonomous system intent (blue) and steering column angle (black) (B) Measured torque (black), human torque (red) and automation torque (blue) (C) Damping coefficients of the agents (D) Stiffness coefficients of the agents. The automation system act as active safety in a cooperative mode in the adaptive haptic shared control paradigm. By increasing the automation's impedance controller gains, the automation system provides enough control input for obstacle avoidance. The shaded bands for θ_S, K_A, and B_A represent the 95% confidence intervals.

safety is ensured, but also the customizability feature of the automation system is improved.

2.5   PIL implementation

To validate the modulation algorithms developed in this paper in a human-in-the-loop setup, it is necessary to make sure the nonlinear model predictive algorithms can be solved in real-time. As a first step towards this goal, we performed a series of tests with a processor in the loop (PIL) using a set of low-cost microcontrollers.

The processor in the loop (PIL) is a test method with a compiled code that describes a controller running in an external microprocessor or processor. The deterministic plant model runs on a remote simulator. Both subsystems, controller and plant, are linked by a communication link or data transfer port. A PIL platform is developed for the proposed impedance modulation approach and illustrated in Fig. 2.10-(A). In PIL simulations, subsystems run in separate processing platforms, which intercross input and output data through a communication mean.

In PIL architecture, we select the ATMega2560 and STM32F4 discovery board to be the target boards for implementation purposes. The PIL test-bed block diagram is illustrated in Fig. (2.10). As illustrated in Fig. (2.10-B), the target board contains three main subroutines. The port decoder subroutine extracts the host computer's received data for the nonlinear MPC. The NLMPC subroutine, based on the current value of the state/co-state vector and the unknown vector on the previous time step, propagates the system to form the $F_{\mathrm{L,A}}(X_{\mathrm{LL}}, U_{\mathrm{LL}}, t)$. Then the optimal value of the unknown vector from the C/GMRES method will be defined and based on (2.18), the control signal u_{LL} will be fed to the packet generator subroutine. The communication between the target board and the Simulink environment is performed over a serial port connection by 115200 bps. The host and target modules' synchronization procedure is based on the control loop execution on the target board. Arduino Mega's processor is an ATmega2560 microcontroller, and its CPU clock is 16 MHz, while the STM32F4
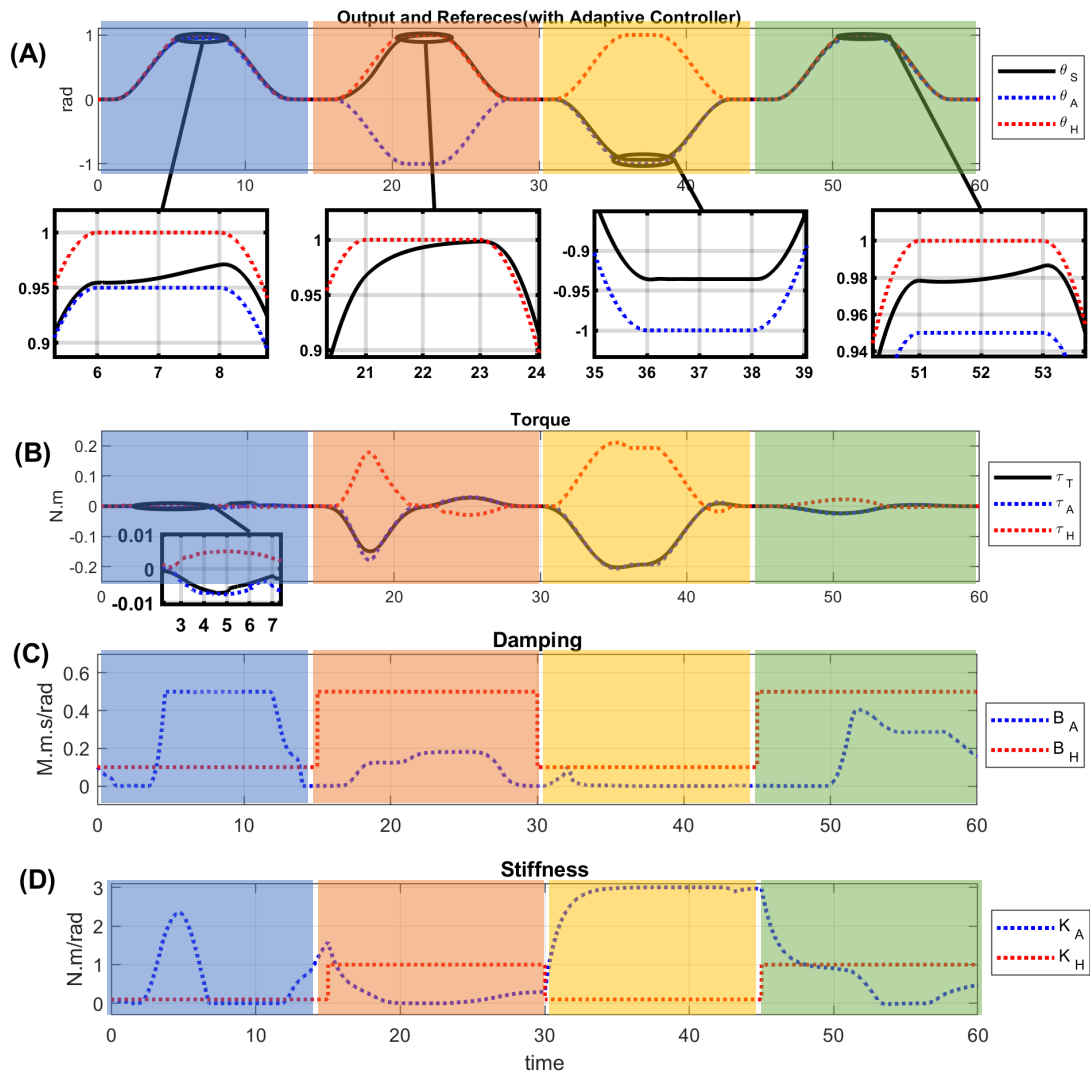
Figure 2.9: The human and automation's interaction in the four interaction modes. The sequence of these interaction modes is cooperative-active safety (shaded blue), uncooperative assistive (shaded orange), uncooperative-active safety (shaded yellow), and cooperative-auto pilot mode (shaded green). The outputs of the driver and automation system interaction within non-adaptive and adaptive haptic shared control paradigms are compared. (A) driver intent (red), autonomous system intent (blue) and steering column angle (black) (B) Measured torque (black), human torque (red) and automation torque (blue) (C) Damping coefficients of the agents (D) Stiffness coefficients of the agents. In the proposed adaptive haptic shared paradigm, by recognizing the interaction mode, the appropriate set of weights for the cost function can be determined, and automation can continuously adjust its impedance controller parameters such that not only the safety is ensured, but also the customizability feature of the automation system is improved.
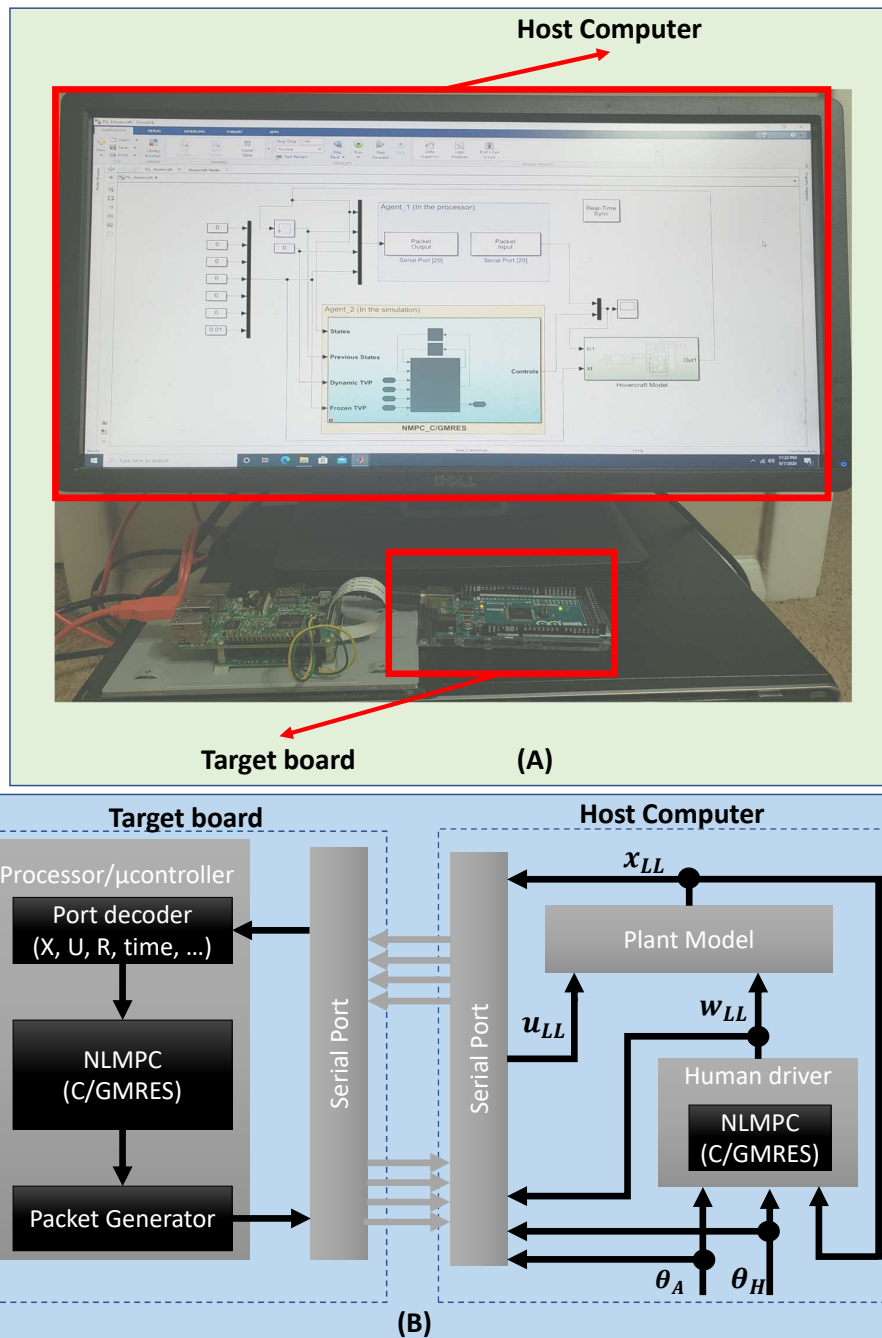
Figure 2.10: (A) The experimental PIL test setup, (B) The block diagram of the PIL setup

has up to 180 MHz operating frequency. Different scenarios are implemented in the PIL test-bed for each of these processors based on the 10, 20, and 30 grid numbers N_p and 10, 15, and 20 maximum iterations C/GMRES solver.

Table 2.2: PIL results for the Low-level controller in active safety and assistive modes

	Grid Num. (N_p)	Arduino Mega2560			STM32F4 Discovery		
		Maximum C/GMRES Iteration					
		10 (Itr)	15 (Itr)	20 (Itr)	10 (Itr)	15 (Itr)	20 (Itr)
Active Safety Mode	10	280	410	570	80	110	150
	20	420	630	910	120	160	230
	30	620	980	1380	170	250	400
Assistive mode	10	210	390	510	70	90	130
	20	370	590	860	100	140	210
	30	580	910	1210	150	230	370

The PIL implementation for low-level controllers is performed for both active safety and assistive modes. The control loop's execution time on a microcontroller depends on the interaction mode (assistive or active-safety modes). For example, On the discover board with grid number 10 and the maximum C/GMRES iteration 15, the execution time for the active-safety and assistive modes are 110 and 90 microseconds, respectively (Table 2.2). The maximum iterations for the continuation method and the horizon view (grid number) are the main effective parameters in the control loop's execution time. The termination condition for convergence in GMRES method is in the range of 10^{-4} for both control signals (Γ_{kA}, Γ_{bA}). For each microcontroller in each mode, nine case studies are performed. Specifically, we considered three values for the maximum C/GMRES iteration and three values of the grid numbers (N_p). Table 2.2 shows the PLI results for both microcontrollers, and the time unit for the recorded execution time is a microsecond. Since the model execution time is equal to 2 milliseconds in the model simulator, the control signals must be computed on the processor before the next sequence. Therefore the loop requirement for the implemented PIL is two milliseconds. Both the Discovery board and Arduino Mega pass the loop requirement, while STM32F407 shows better performance.

REFERENCES

[1] Arvin Agah. Human interactions with intelligent systems: research taxonomy. *Computers & Electrical Engineering*, 27(1):71–107, 2000.

[2] Don Joven Agravante, Andrea Cherubini, Antoine Bussy, Pierre Gergondet, and Abderrahmane Kheddar. Collaborative human-humanoid carrying using vision and haptic sensing. In *2014 IEEE international conference on robotics and automation (ICRA)*, pages 607–612. IEEE, 2014.

[3] A Albu-Schaffer, Antonio Bicchi, G Boccadamo, R Chatila, A De Luca, A De Santis, G Giralt, G Hirzinger, V Lippiello, R Mattone, et al. Physical human-robot interaction in anthropic domains: safety and dependability. In *Proceeding 4th IARP/IEEE-EURON Workshop on Technical Challenges for Dependable Robots in Human Environments*, 2005.

[4] Samuel Au, Max Berniker, and Hugh Herr. Powered ankle-foot prosthesis to assist level-ground and stair-descent gaits. *Neural Networks*, 21(4):654–666, 2008.

[5] Pieter Beyl, K Knaepen, S Duerinck, Michaël Van Damme, Bram Vanderborght, R Meeusen, and Dirk Lefeber. Safe and compliant guidance by a powered knee exoskeleton for robot-assisted rehabilitation of gait. *Advanced Robotics*, 25(5):513–535, 2011.

[6] Akshay Bhardwaj, Amir H Ghasemi, Yingshi Zheng, Huckleberry Febbo, Paramsothy Jayakumar, Tulga Ersal, Jeffrey L Stein, and R Brent Gillespie. Whos the boss? arbitrating control authority between a human driver and automa-

tion system. *Transportation Research Part F: Traffic Psychology and Behaviour*, 68:144–160, 2020.

[7] Akshay Bhardwaj, Brent Gillespie, and James Freudenberg. Estimating rack force due to road slopes for electric power steering systems. In *2019 American Control Conference (ACC)*, pages 328–334. IEEE, 2019.

[8] P. Boehm, A.H. Ghasemi, S. O'Modhrain, P. Jayakumar, and R.B. Gillespie. Architectures for Shared Control of Vehicle Steering. In *IFAC - Human and Machine Symposium*, 2016.

[9] Paul Boehm, Amir H Ghasemi, Sile O'Modhrain, Paramsothy Jayakumar, and R Brent Gillespie. Architectures for shared control of vehicle steering. *IFAC-PapersOnLine*, 49(19):639–644, 2016.

[10] Arthur Earl Bryson. *Applied optimal control: optimization, estimation and control*. CRC Press, 1975.

[11] Ryan Christiansen, Jose Luis Contreras-Vidal, R Brent Gillespie, Patricia A Shewokis, and Marcia K O'Malley. Vibrotactile feedback of pose error enhances myoelectric control of a prosthetic hand. In *2013 World Haptics Conference (WHC)*, pages 531–536. IEEE, 2013.

[12] David J. Cole. Neuromuscular dynamics and steering feel. Technical report, Proc. Steering Tech, 2008.

[13] Lorenzo Fagiano and Mustafa Khammash. Nonlinear stochastic model predictive control via regularized polynomial chaos expansions. In *2012 IEEE 51st IEEE conference on decision and control (CDC)*, pages 142–147. IEEE, 2012.

[14] Roger G Ghanem and Pol D Spanos. *Stochastic finite elements: a spectral approach*. Courier Corporation, 2003.

[15] Amir H. Ghasemi. Game theoretic modeling of a steering operation in a haptic shared control framework. In *Dynamic Systems and Control Conference (DSCC), 2018*. ASME, 2018.

[16] Amir H Ghasemi, Paramsothy Jayakumar, and R Brent Gillespie. Shared control architectures for vehicle steering. *Cognition, Technology & Work*, pages 1–11, 2019.

[17] Amir H Ghasemi, Mishel Johns, Benjamin Garber, Paul Boehm, Paramsothy Jayakumar, Wendy Ju, and R Brent Gillespie. Role negotiation in a haptic shared control framework. In *Adjunct Proceedings of the 8th International Conference on Automotive User Interfaces and Interactive Vehicular Applications*, pages 179–184. ACM, 2016.

[18] Amir H. Ghasemi and Hossein Rastgoftar. Adaptive haptic shared control framework using markov decision process. In *Dynamic Systems and Control Conference (DSCC), 2018*. ASME, 2018.

[19] Amirhossein Ghasemi and Arjun Yeravdekar. Modelling non cooperative human-automation interactions in a haptic shared control framework. Technical report, SAE Technical Paper, 2019.

[20] Christopher J Hasser and Mark R Cutkosky. System identification of the human hand grasping a haptic knob. In *haptics*, page 180. IEEE, 2002.

[21] Vahid Izadi, Akshay Bhardwaj, and Amir H Ghasemi. Impedance modulation for negotiating control authority in a haptic shared control paradigm. In *2020 American Control Conference (ACC)*, pages 2478–2483. IEEE, 2020.

[22] Vahid Izadi, Arjun Yeravdekar, and Amirhossein Ghasemi. Determination of roles and interaction modes in a haptic shared control framework. In *ASME*

2019 Dynamic Systems and Control Conference. American Society of Mechanical Engineers Digital Collection, 2019.

[23] Greg A Jamieson and Kim J Vicente. Designing effective human-automation-plant interfaces: A control-theoretic perspective. *Human Factors*, 47(1):12–34, 2005.

[24] Nathanaël Jarrassé, Themistoklis Charalambous, and Etienne Burdet. A framework to describe, analyze and generate interactive motor behaviors. *PloS one*, 7(11), 2012.

[25] Carl T Kelley. *Iterative methods for linear and nonlinear equations*, volume 16. Siam, 1995.

[26] Keehoon Kim and J Edward Colgate. Haptic feedback enhances grip force control of semg-controlled prosthetic hands in targeted reinnervation amputees. *IEEE Transactions on Neural Systems and Rehabilitation Engineering*, 20(6):798–805, 2012.

[27] Ayse Kucukyilmaz and Illimar Issak. Online identification of interaction behaviors from haptic data during collaborative object transfer. *IEEE Robotics and Automation Letters*, 5(1):96–102, 2019.

[28] Cigil Ece Madan, Ayse Kucukyilmaz, Tevfik Metin Sezgin, and Cagatay Basdogan. Recognition of haptic interaction patterns in dyadic joint object manipulation. *IEEE Transactions on Haptics*, 8(1):54–66, 2014.

[29] Alejandro Melendez-Calderon, V Komisar, G Ganesh, and Etienne Burdet. Classification of strategies for disturbance attenuation in human-human collaborative tasks. In *2011 Annual International Conference of the IEEE Engineering in Medicine and Biology Society*, pages 2364–2367. IEEE, 2011.

[30] Ali Mesbah, Stefan Streif, Rolf Findeisen, and Richard D Braatz. Stochastic non-linear model predictive control with probabilistic constraints. In *2014 American Control Conference*, pages 2413–2419. IEEE, 2014.

[31] Hiroyuki Mori and Kotaro Seki. Continuation newton-gmres power flow with linear and nonlinear predictors. In *2007 Large Engineering Systems Conference on Power Engineering*, pages 171–175. IEEE, 2007.

[32] S Ozgur Oguz, Ayse Kucukyilmaz, Tevfik Metin Sezgin, and Cagatay Basdogan. Haptic negotiation and role exchange for collaboration in virtual environments. In *Haptics Symposium, 2010 IEEE*, pages 371–378. IEEE, 2010.

[33] S Ozgur Oguz, Ayse Kucukyilmaz, Tevfik Metin Sezgin, and Cagatay Basdogan. Supporting negotiation behavior with haptics-enabled human-computer interfaces. *IEEE transactions on haptics*, 5(3):274–284, 2012.

[34] Toshiyuki Ohtsuka. Continuation/gmres method for fast algorithm of nonlinear receding horizon control. In *Proceedings of the 39th IEEE Conference on Decision and Control (Cat. No. 00CH37187)*, volume 1, pages 766–771. IEEE, 2000.

[35] Toshiyuki Ohtsuka. A continuation/gmres method for fast computation of non-linear receding horizon control. *Automatica*, 40(4):563–574, 2004.

[36] Toshiyuki Ohtsuka and Hironori Fujii. Stabilized continuation method for solving optimal control problems. *Journal of Guidance, Control, and Dynamics*, 17(5):950–957, 1994.

[37] Frauke Oldewurtel, David Sturzenegger, Peyman Mohajerin Esfahani, Göran Andersson, Manfred Morari, and John Lygeros. Adaptively constrained stochastic model predictive control for closed-loop constraint satisfaction. In *2013 American Control Conference*, pages 4674–4681. IEEE, 2013.

[38] Joel A Paulson and Ali Mesbah. An efficient method for stochastic optimal control with joint chance constraints for nonlinear systems. *International Journal of Robust and Nonlinear Control*, 29(15):5017–5037, 2019.

[39] Luka Peternel, Nikos Tsagarakis, Darwin Caldwell, and Arash Ajoudani. Robot adaptation to human physical fatigue in human–robot co-manipulation. *Autonomous Robots*, 42(5):1011–1021, 2018.

[40] Oliver C Schrempf, Uwe D Hanebeck, Andreas J Schmid, and Heinz Worn. A novel approach to proactive human-robot cooperation. In *ROMAN 2005. IEEE International Workshop on Robot and Human Interactive Communication, 2005.*, pages 555–560. IEEE, 2005.

[41] Fabrizio Sergi, Dino Accoto, Domenico Campolo, and Eugenio Guglielmelli. Forearm orientation guidance with a vibrotactile feedback bracelet: On the directionality of tactile motor communication. In *2008 2nd IEEE RAS & EMBS International Conference on Biomedical Robotics and Biomechatronics*, pages 433–438. IEEE, 2008.

[42] Ralph C Smith. *Uncertainty quantification: theory, implementation, and applications*, volume 12. Siam, 2013.

[43] Yusuke Soneda and Toshiyuki Ohtsuka. Nonlinear moving horizon state estimation with continuation/generalized minimum residual method. *Journal of Guidance, Control, and Dynamics*, 28(5):878–884, 2005.

[44] Nikolay Stefanov, Angelika Peer, and Martin Buss. Role determination in human-human interaction. In *EuroHaptics conference, 2009 and Symposium on Haptic Interfaces for Virtual Environment and Teleoperator Systems. World Haptics 2009. Third Joint*, pages 51–56. IEEE, 2009.

[45] Nikolay Stefanov, Angelika Peer, and Martin Buss. Online intention recognition for computer-assisted teleoperation. In *Robotics and Automation (ICRA), 2010 IEEE International Conference on*, pages 5334–5339. IEEE, 2010.

[46] Richard A Tapia. Role of slack variables in quasi-newton methods for constrained optimization. Technical report, Rice Univ., Houston, TX (USA). Dept. of Mathematical Sciences, 1979.

[47] Eric C Townsend, Erich A Mielke, David Wingate, and Marc D Killpack. Estimating human intent for physical human-robot co-manipulation. *arXiv preprint arXiv:1705.10851*, 2017.

[48] Nicola Vitiello, Tommaso Lenzi, Stefano Roccella, Stefano Marco Maria De Rossi, Emanuele Cattin, Francesco Giovacchini, Fabrizio Vecchi, and Maria Chiara Carrozza. Neuroexos: A powered elbow exoskeleton for physical rehabilitation. *IEEE Transactions on Robotics*, 29(1):220–235, 2013.

[49] Zheng Wang, Angelika Peer, and Martin Buss. An hmm approach to realistic haptic human-robot interaction. In *World Haptics 2009-Third Joint EuroHaptics conference and Symposium on Haptic Interfaces for Virtual Environment and Teleoperator Systems*, pages 374–379. IEEE, 2009.

[50] Norbert Wiener. The homogeneous chaos. *American Journal of Mathematics*, 60(4):897–936, 1938.

[51] Bo Yu, R Brent Gillespie, James S Freudenberg, and Jeffrey A Cook. Human control strategies in pursuit tracking with a disturbance input. In *Decision and Control (CDC), 2014 IEEE 53rd Annual Conference on*, pages 3795–3800. IEEE, 2014.

[52] Bo Yu, R Brent Gillespie, James S Freudenberg, and Jeffrey A Cook. Identifica-

tion of human feedforward control in grasp and twist tasks. In *American Control Conference (ACC), 2014*, pages 2833–2838. IEEE, 2014.

[53] Yishen Zhao, Philippe Chevrel, Fabien Claveau, and Franck Mars. Continuous identification of driver model parameters via the unscented kalman filter. *IFAC-PapersOnLine*, 52(28):126–133, 2019.

CHAPTER 3: (PAPER 2) Quantifying the Performance of an Adaptive Haptic

Shared Control Paradigm for Steering a Ground-Vehicle

3.1   Introduction

Human-automation teaming (HAT) is gaining importance in commercial and military applications with autonomous vehicles because of its promise to improve performance, reduce the cost of operating and designing platforms, and increase adaptability to new situations [8, 9]. However, adding automation may sometimes have unintended consequences and increase rather than reduce—problems for a human operator, especially when faults occur. Given the fact both human and automation are subject to faults and errors, the fundamental question is how should control be dynamically transitioned between the human and automation to minimize the trade-off between the human partner's preference and the safety and performance of the task in the presence of conflicts between human and automation's goals.

To this end, various schemes have been proposed, differing primarily according to how to control authority is transitioned between the two agents [5, 36, 35, 25]. These schemes can be categorized into two main categories: switch-based control schemes and continuous control schemes [32, 33, 13]. In the switch-based control schemes, the control authority is transferred as a lumped whole from human to automation or back to human. Depending on the scheme, transfers may be initiated by the human driver, by the automation system, or by a separate arbitration algorithm [25, 36, 35]. Switch-based control schemes involve issues such as a protracted-time interval required for full transfer, misinterpretation or misappropriation of responsibility (called mode errors), and incomplete understanding of the environment state (loss of situation awareness) [11, 30, 25]. To address these issues, various schemes have been proposed under

which the control authority is continuously shared between humans and automation to address these shortcomings. Two main groups of these schemes are input-mixing control, and haptic shared control [12, 1, 29, 3, 28, 22, 31, 10]. The main difference between these two paradigms is that haptic shared control paradigms involve a dynamic coupling between a human driver and automation through the steering wheel. In contrast, the input-mixing paradigms do not involve such a coupling. The dynamic coupling allows the driver to remain bodily in the loop, with his/her hands on a motorized steering wheel. A valuable feature of haptic shared control is that the role (e.g., leader/follower) played by each agent and the level of authority held by each agent (how much control an agent exerts) is a dynamic outcome of the interaction between the two agents and the vehicle [24, 16, 17, 6]. The feature of role and level of authority being outcomes of the interaction in haptic shared control is in sharp contrast to the control sharing paradigm of input mixing, where a third party imposes the level of authority (an agent or algorithm that assesses current threat) and potentially make the haptic shared control to be more robust to automation's misses, and faults [12, 3, 1, 19, 5].

Figure 3.1 demonstrates a schematic of a haptic shared control paradigm. Three entities each impose a torque on the steering wheel: τ_H by a driver through his hands, τ_A by automation system through a motor, and τ_V by the road through the steering linkage. Here, we model the driver as a hierarchical two-level controller. The upper-level control represents the cognitive controller, and its output, θ_H represents the driver's intent. The lower-level represents the human's biomechanics which it's parameters z_H can vary in time (e.g., with muscle co-contraction). Similarly, the automation system is modeled as a higher-level controller (AI) coupled with a lower-level impedance controller with the modest gain z_A [18, 14, 14, 21, 20].

In our recent work, comparing HAT performance for steering control across several shared control schemes, we showed that sharing methods like haptic shared control ef-
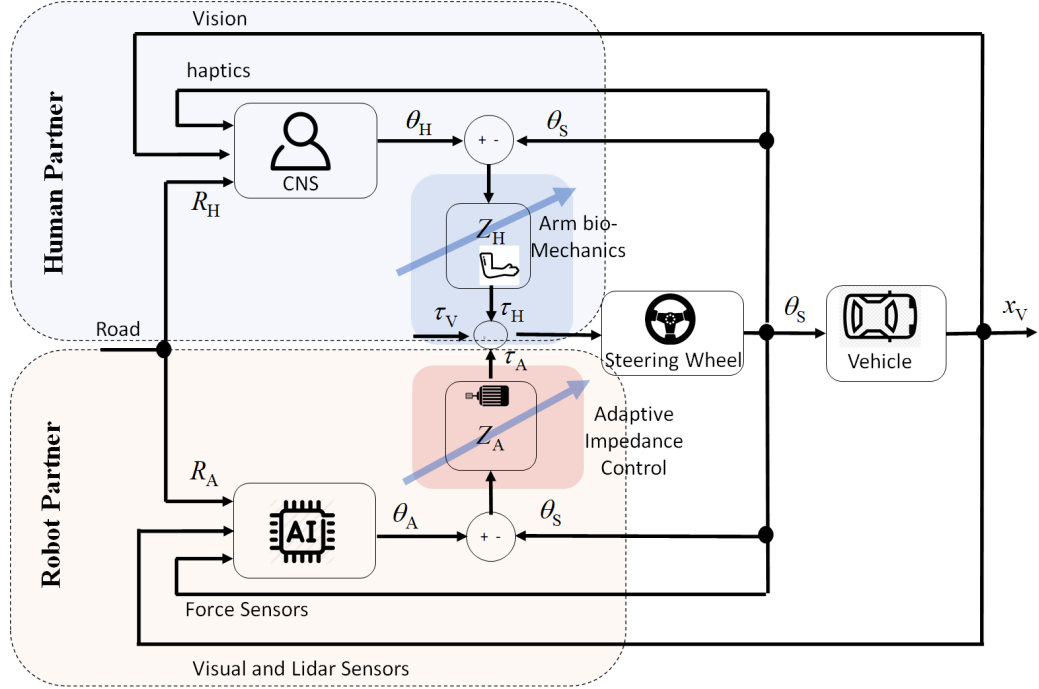
Figure 3.1: A schematic of a haptic shared control where both human and automation collaboratively control the steering of a semi-automated ground vehicle.

fectively support smooth shifts of authority during automation-induced faults [5]. In this study, the automation's impedance z_A - which is an index for automation's level of control - was remained constant; and the human, by modulating its impedance, was responsible for gaining or yielding the control from the automation partner. The invariant impedance resulted in lower driving performance (e.g., longer Safe Approach Distance indicating a lower driver's preparedness) in situations where the automation was subject to faults. We recently addressed this issue by developing algorithms to actively modulate automation's impedance control parameters z_A to improve the quality of human-automation handover [19]. This study employs the algorithm developed in [19] to quantify the performance of the Adaptive Haptic Shared Control in resolving a conflict through a set of human-subject studies. Specifically, we compare the the performance of the Adaptive Haptic Shared Control with two other shared control schemes named ASssistive and Active-safety haptic shared paradigms.

The outline of this paper is as follows. In Section 2, we present our MPC-based

automation system and our driving simulator and elaborate on our implementation of Assistive, Adaptive, and Active-safety shared control paradigms. Next, we describe an experiment in which we asked 27 participants to drive with the assistance of the automation system under these three control sharing schemes. Finally, in Section 3, we present experimental results and follow this with a Discussion and Conclusion in Section 4.

3.2   Method

We conduct a series of human test studies to evaluate the performance of the proposed Adaptive Haptic Shared Control scheme. The details about these studies including the participant characteristics, apparatus, experimental conditions, performance metrics and data analysis method are described in below.

3.2.1   Participants

Twenty-seven test participants (20 male and 7 female) between the ages of 22 and 45 years old recruited for these tests. All participants signed the consent form under the Office of Research Protections and Integrity at the University of North Carolina at Charlotte. All participants were without physical or visual impairments while performing their driving duties and did not receive compensation for participating in the test. Before the test, each participant was given a fifteen to twenty minutes opportunity to become familiar with the test setup and the graphical interface. Participants experienced all three different driving conditions based on the shared control scheme (Assistive Haptic Shared, Adaptive Haptic Shared and Active-safety Haptic Shared). Each participant was asked to complete the three experimental conditions with two repetitions each. The order of conditions was randomized. The vehicle speed was set constant at 13 m/s, and each test run was about 90 s long. The sampling rate of the acquired data, such as the lateral and longitudinal position of the vehicle, features of obstacles (location, avoiding status), steering angle and its first and second deriva-

tives, grip force, differential torque, are 1 kHz. The graphical user interface refresh rate for the road display is set to 20 Hz in the GUI renderer.

Ten obstacles are placed along the route with a randomized locations at each run. When the car approaches these obstacles, as it is demonstrated in Fig. 3.2, two messages are displayed to the driver: recommended direction to avoid the obstacle (left or right) and the suggested level of grip force (high or low). The reference path for each participant is clearly defined graphically, and each participant is asked to avoid the obstacle by turning the steering wheel based on the recommended direction and impedance value. Drivers informed that the autonomous system could employ different trajectories to avoid obstacles, and as a result, they might perceive conflict by experiencing a resistive torque on the steering wheel.

3.2.2 Apparatus

We developed a low-fidelity driving simulator with a motorized steering wheel (see Figure (3.2)). An overview of the track, road trajectory of a subject human driver and automation system with the obstacles from one of the studies is represented in Figure (3.3). The mechanical modules and the sensor/actuator combination was adopted from [5] with some changes, and Table 3.1 represents a part list for the driving simulator setup. The position controller of the DC motor is based on the state-feedback controller, and its input is desired steering angle of the automation system. Therefore, the required tools for the Adaptive Haptic Shared Control scheme are provided to the control algorithm in the Matlab Simulink real-time environment. Unlike [5], in this work, both MPC controller and graphical interface were running on one PCwith Intel-core i7-8700 CPU, 32 GB Ram. The switching frequency of the PWM signal is increased to 3 kHz to remove the torque ripple on the rotor. Furthermore, to increase communication speed between the host board and the Simulink real-time target environments, the rate of the acquired signal is selected to be ten micro-second.
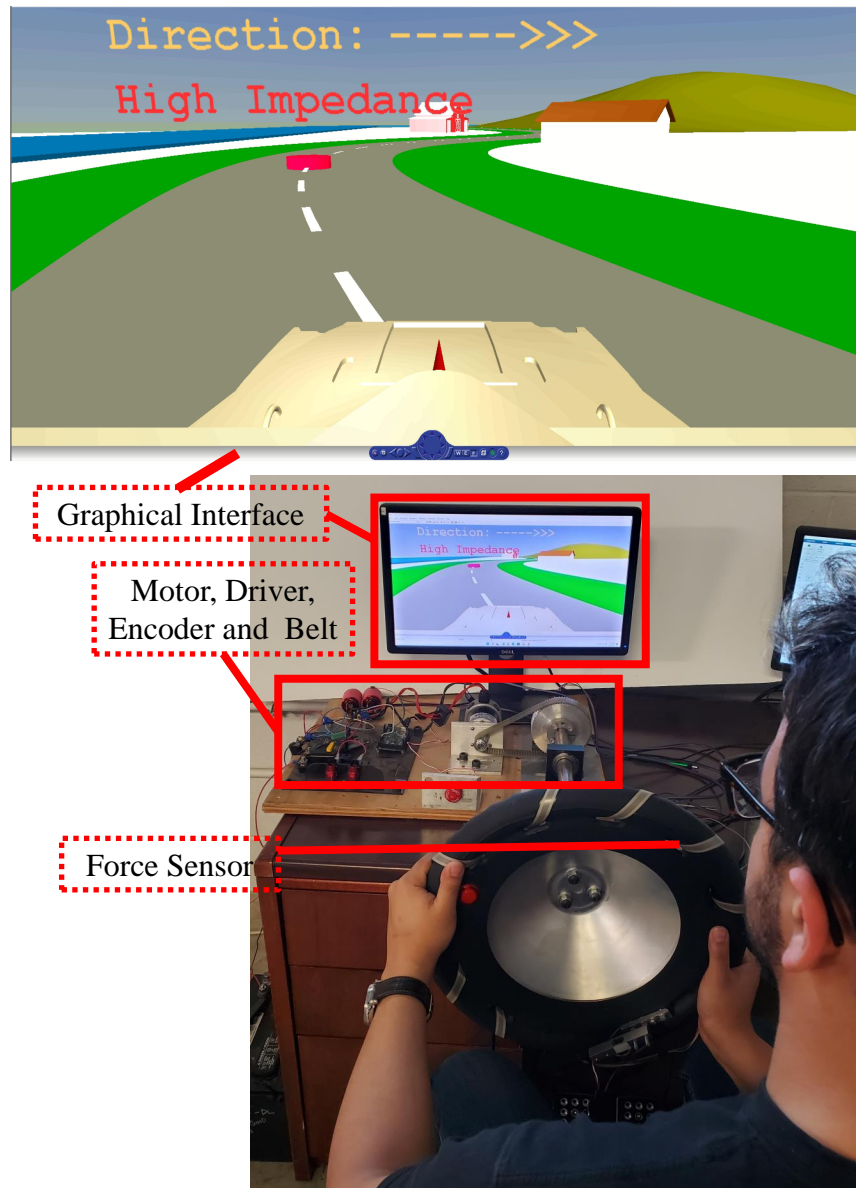
Figure 3.2: Experimental setup of the fixed-base driving simulator with magnified road display on monitor.

Table 3.1: The part list for the driving simulator setup

Component	Model/Producer	Description
DC motor	A28-150/AmpFlow	High performance, 24 volt/ 13.77N.m
Steering Wheel	Speedway	38 cm solid aluminum wheel
Timing Belt	-	72:15 mechanical advantage
Optical Encoder	US Digital HB6M	4096 PPR
Torque Sensor	TAT200/ HT sensor	0 to 50 N.m
Force Sensor	TAL220/Sparkfun	10kg Load Cell
ADC	HX711/Avia Semiconductor	24-Bit/I2C communication
DC motor Driver	BTN7960/dfrobot	Two channel, 15A, 4.8 ~ 35V
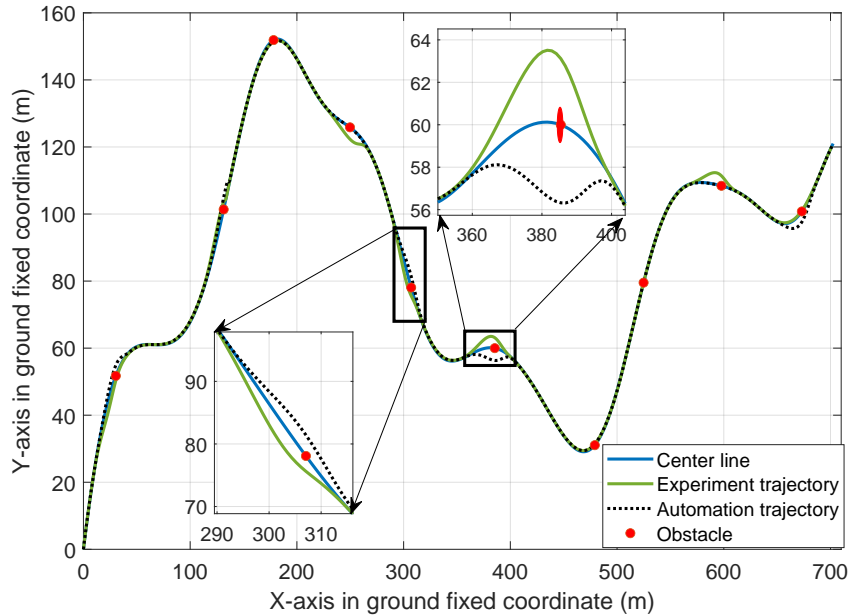
Figure 3.3: An overview of the road trajectory (blue line), automation's intended trajectory (dotted black line), measured experiment (green line) and obstacles (read circles)

The virtual environment was adapted from [5]. It was created using the Matlab-Simulink Virtual Reality Toolbox, and appeared as shown in Fig. 3.2. It contained a notional High Mobility Multipurpose Wheeled Vehicle (HMMWV) and a road with various landmarks that provided motion cues during driving. The vehicle traveled at a constant speed of 13 m/s, and neither the participant nor the automation system had any control over speed. The road (in gray) was 8 m wide with a white dashed centerline. Shoulders of 6 m width (in dark green) were located on either side of the road. The entire track was 850 m long, with 5 left turns and 5 right turns. An overview of the track is shown in Fig. 3.3. Ten cylindrical obstacles with a 2 m diameter and 0.5 m height were distributed along the tracks centerline at intervals that were set randomly between 40 and 50 m.

3.2.3   Control System Design

The automation system consists of three main controllers. At the highest level, to generate the desired steering commands θ_A for the lane-keeping and obstacle evasion,

we employed a pursue tracking controller. A pure pursuit controller generates steering commands such that the path tracking error is minimized using a 'look-ahead' distance away from the vehicle location on the reference path [34]. To ensure that our pursuit tracking is capable of obstacle avoidance, we modified the center-line trajectory considering a concave-arc shape arc around the obstacle. We designed the concave-arc shape to go around the obstacle from either right or left side of the obstacle. Figure 3.3 shows the automation's trajectory with dashed-black lines.

At the mid-level, we used Model Predictive Control (MPC) described in [18] to modulate the impedance parameters of the automation system $z_A = [b_A \ k_A]^T$. Here k_A, b_A represent the gains of the impedance controller. The inputs to this MPC include the vehicle's state x_V, an estimation of the human's steering commands $\hat{\theta}_H$, the automation's steering commands θ_A, an estimation of the parameters of human's impedance $\hat{z}_H = [\hat{b}_H \ \hat{k}_H]^T$, automation impedance parameters $z_A = [b_A \ k_A]^T$, and data describing the track. Here $\hat{k}_H$, $\hat{b}_H$ represent an estimation of the stiffness and damping of the human's biomechanics model presented in [12]. Furthermore, we adopt the kinematic bicycle model to describe the behavior of the vehicle [23].

The MPC's cost function is defined as

$$\min_{\Gamma_A} J(t) = \int_t^{t+t_h} \{\|\hat{\theta}_H - \theta_S\|_{w_{AH}} + \|\theta_A - \theta_S\|_{w_{AA}} + \|\tau_T\|_{w_{A\theta}}\}d\varsigma \qquad (3.1)$$

$$\text{s.t.} \quad \dot{z}_A(t) = \alpha_A z_A(t) + \beta_A \Gamma_A(t) \qquad (3.2)$$

where $\Gamma_A = [\Gamma_{bA}(t) \ \Gamma_{kA}(t)]^T$ is the automations control input for modulating its impedance, t_h is the defined horizon for the model predictive controller, w_{AH}, w_{AA}, $w_{A\theta}$ are weights matrices, and α_A, β_A are the constant matrices. The first term of the cost function over the finite horizon (integration part) aims to minimize the error between the human's desired steering command $\hat{\theta}_H$ and the steering angle. The second term of the cost function over the finite horizon is defined to minimize the tracking

error between the automation's desired steering command θ_{A} (automation's intent) and the steering angle. Since the human's and automation's intent may not necessarily be the same, which is when the negotiation of control authority becomes important, the third term of the cost function over the finite horizon is defined to minimize the disagreement between a driver and the automation system. Here, we defined $\tau_{\mathrm{T}} = k_{\mathrm{T}}(\theta_{\mathrm{H}} - \theta_{\mathrm{A}})$. Additionally, we define two sets of constraints for the nonlinear cost function J to ensure the non-negative values for the impedance controller's parameters b_{A} and k_{A}.

To solve the cost function J, we require to have an estimation of human's steering command $\hat{\theta}_{\mathrm{H}}$ and estimation of the human's impedance parameters $\hat{z}_{\mathrm{H}}$. To estimate θ_{H}, we developed a second pursuit tracking controller similar to the automation pursuit tracking. The only difference between these two pursuit tracking is their reference trajectories. Specifically, the difference between the human reference path and automation's reference trajectory is around six out of ten obstacles, wherein the human's trajectory has an opposite direction with respect to the automation's trajectory (i.e., human is going right but the automation's is going to left or vice versa). It should be noted that the human's actual trajectory r_{H} might be different from the estimated $\hat{r}_{\mathrm{H}}$. Also, to determine an estimation of z_{H}, we used a grip force on the steering wheel (see Figure 3.2). We measured the grip force of each participant in a set of trial tests. Then, the grip force is normalized based on minimum and maximum measured grip force.

$$G_{f,n} = \frac{G_{\mathrm{f,meas}} - G_{\mathrm{f,min}}}{G_{\mathrm{f,max}} - G_{\mathrm{f,min}}} \tag{3.3}$$

where $G_{\mathrm{f,n}}$ is the normalized grip force, $G_{\mathrm{f,meas}}$ is the measured grip force, $G_{\mathrm{f,max}}$ is the maximum measured grip force $G_{\mathrm{f,min}}$ is the minimum measured grip force. We quantitized the normalized grip force $G_{\mathrm{f,n}}$ into five ranges called low when $0 \leq G_{\mathrm{f,n}} \leq$

0.2, medium low ($0.2 \leq G_{f,n} \leq 0.4$), medium ($0.4 \leq G_{f,n} \leq 0.6$), medium high ($0.2 \leq G_{f,n} \leq 0.8$) and high ($0.8 \leq G_{f,n} \leq 1$). For the low $G_{f,n}$, we select the values of the human driver's impedance to be $\hat{z}_H = [0.1\ 0.02]$. For the medium low, $G_{f,n}$, the values of the human driver's impedance to be $\hat{z}_H = [0.25\ 0.04]$. For the medium , $G_{f,n}$, the values of impedance to be $\hat{z}_H = [0.5\ 0.06]$. For the medium high, $G_{f,n}$, the values of the human driver's impedance to be $\hat{z}_H = [0.75\ 0.08]$, and for the high $G_{f,n}$, the values of impedance to be $\hat{z}_H = [1\ 0.1]$. We employed a continuation generalized minimum residual method to solve the cost function J. The detail of these approaches is described in [18]

We also employed a state-feedback controller to generate the motor command torque τ_M as a function of the setpoint trajectory θ_A generated by the automation's pursuit tracking, the automation's impedance z_A generated by the automation MPC controller, and the current steering angle θ_S. In particular, the equations of motion for the motor connected to the steering wheel is considered as

$$J_M\ddot{\theta}_M + b_M\dot{\theta}_M + k_M\theta_M = k_I I_M - M_l \tag{3.4}$$

$$L\dot{I}_M + RI_M + k_b\dot{\theta}_M = v_t \tag{3.5}$$

where (v_t) is the voltage sent to the motor, M_l is the torque applied because of the load connected to the steering motor. Here, this load can be considered as $M_l = (J_S)\left(\frac{r_M}{r_S}\right)^2\ddot{\theta}_M + b_S\left(\frac{r_M}{r_S}\right)^2\dot{\theta}_M + k_S\left(\frac{r_M}{r_S}\right)^2\theta_M$. Here, J_S is the steering inertia, b_S is the steering damping, and k_S is the steering stiffness. Furthermore, I_M, R, L, k_I and k_b are motor's current, resistant, inductance, torque constant, and electromotive force constant, respectively. To determine the voltage sent to the motor, we employ a state-feedback controller. In particular,

$$v_t = k_A(\theta_A - \theta_S) + b_A(\dot{\theta}_A - \dot{\theta}_S) + J_A(\ddot{\theta}_A - \ddot{\theta}_S) \tag{3.6}$$

Here $J_A = 1 \times 10^{-6}$ is a small constant. Finally, the command voltage was converted to the duty cycle of the PWM signal on the HIL board, and it applied the full-bridge motor driver at 3kHz.

3.2.4 Experimental Conditions

Our experiment involved three situations in which control was shared between the human drivers and the automation system: Assistive Haptic Shared Control, Adaptive Haptic Shared Control, and Active-Safety Haptic Shared Control.

Under each situation, participants were requested to follow the road, keeping as close as possible to the centerline but to avoid obstacles. Obstacles were imperceptible until the vehicle was within 40 meters range. Therefore, with a constant velocity of 13 m/s, the participant had three seconds to identify and avoid obstacles.

Ten obstacles were encountered on each run. The automation was designed to maneuver from the left side for 5 of these obstacles and the right side for the other 5. To create a conflict between human and automation, we displayed a sign asking the driver to take to the right or left side of the obstacle (by showing a right-sided or left-sided arrow on the monitor). We randomize these events so that the automation path and the sign displayed to the driver are the reverse directions for six obstacles, and the other four obstacles have the same direction. As it is demonstrated in Figure 3.2, we asked the driver to either adopt a high impedance for 5 of these obstacles or a low impedance for the other five obstacles (i.e., hold the steering wheel tightly or loosely). Below is a table showing the number of obstacles for the four possible interaction modes between the human driver and automation system.

3.2.4.1 Assistive Haptic Shared Control

In the Assistive Haptic Shared Control scheme, we select the weights of the cost function such that automation generates a low impedance in the presence of conflicts. In the Assistive mode, the automation has confidence in the human driver. Its main

Table 3.2: Intent types and the displayed impedance level to participants on the monitor

Intent Type	Impedance Level	repetition	Direction	Sub-repetition
Same Intents (Cooperative)	Human asked for High Impedance	2	Right	1
			Left	1
	Human asked for Low Impedance	2	Right	1
			Left	1
Reverse Intents (Uncooperative)	Human asked for High Impedance	3	Right	1
			Left	2
	Human asked for Low Impedance	3	Right	2
			Left	1

goal is to follow the estimated steering commands of the human driver and not necessarily follow its own steering commands. In the Assistive mode, the automation system employed the MPC algorithm described in Eq.(3.1) with a constant penalty weight value $w_{\text{AA}} = 0.1$ and $w_{\text{AH}} = 0.9$. In the Assistive mode, the automation is confident in the human driver. Its main goal is to follow the estimated steering commands of the human driver and not necessarily follow its steering commands.

3.2.4.2 Active-Safety Haptic Shared Control

In the Active-Safety Haptic Shared Control scheme, we select the weights of the cost function such that automation generates a high impedance in the presence of conflicts. In the Active-safety mode, the automation has low confidence in the human driver. Its main goal is to follow its own estimated steering commands despite a conflict it may arise with a driver. In particular, the automation system employed the MPC algorithm described in Eq.(3.1) with a constant penalty weight value $w_{\text{AA}} = 0.9$ and $w_{\text{AH}} = 0.1$.

3.2.4.3 Adaptive Haptic Shared Control

In the Adaptive Safety Haptic Shared Control scheme, we select the weights of the cost function such that automation can modulate its level of impedance to gain or yield the control from the human driver. To this end, the cost function weights are adaptively modulated based on the human's normalized grip force expressed in Eq.(3.3). We assumed that when a human's grip force is high, automation's confidence

in human actions is also high. Therefore, it yields control to the driver by adopting a lower impedance. When a human's grip force is low, the automation's confidence in human actions is also low; it gains control from the driver by adopting a higher impedance. In Adaptive HSC scheme, for the low $g_{\text{f,n}}$, we select the values of weights to be ($w_{\text{AA}} = 0.99, w_{\text{AH}} = 0.01$). For the medium-low, $G_{\text{f,n}}$, the values of weights to be ($w_{\text{AA}} = 0.75, w_{\text{AH}} = 0.25$). For the medium , $G_{\text{f,n}}$, the values of automation's cost weights to be ($w_{\text{AA}} = 0.5, w_{\text{AH}} = 0.5$). For the medium-high, $G_{\text{f,n}}$, the values of weights to be ($w_{\text{AA}} = 0.25, w_{\text{AH}} = 0.75$), and for the high $G_{\text{f,n}}$, the values of weights to be ($w_{\text{AA}} = 0.01, w_{\text{AH}} = 0.99$).

3.2.5   Performance Metrics

The dependent measures used to characterize the behavior and performance of the driver-automation teams were based on the following two categories: (1) the steering and torque trajectories (2) the excursions around the obstacles.

The time-dependent behavior of the participants is reflected in the vehicle trajectory on the road and the measured differential torque on the steering wheel. The road attached coordinate system is used to specify the vehicle's location. In this coordinate system, the center of the obstacle is considered the same as the origin point. The radius of the cylindrical obstacle is one meter, and it is demonstrated with a red circle in the figures. The absolute value of the differential torque and the lateral vehicle position are employed for demonstration/comparison purposes.

The following four performance metrics were based on the excursions around the obstacles: Obstacle Hits, RMS Lateral Deviation, Approach Distance, and Peak Excursion. Obstacle Hits are simply the number of obstacle collisions within a given run, and its percentage is calculated by considering the total numbers of the obstacle (ten obstacles) in each run. These excursion-related statistics around the obstacles are extracted from the acquired data from each run. For each obstacle, the recorded values from 25 meters before reaching an obstacle and 25 meters after the obstacle

(a)

Reckless

Safe

Threshold Crossing

Vehicle Path

Threshold Crossing

Approach Distance

1m Obstacle Boundary

A

B

Obstacle

Track Centerline

1.5 m Expanded Obstacle Boundary
(including vehicle's dimension)

Peak Excursion

e_1

e_N

A

B

Obstacle

(b)

RMS Lateral Deviation : $e_{rms} = \sqrt{\frac{1}{N}\sum_{i=1}^{N} e_i^2}$
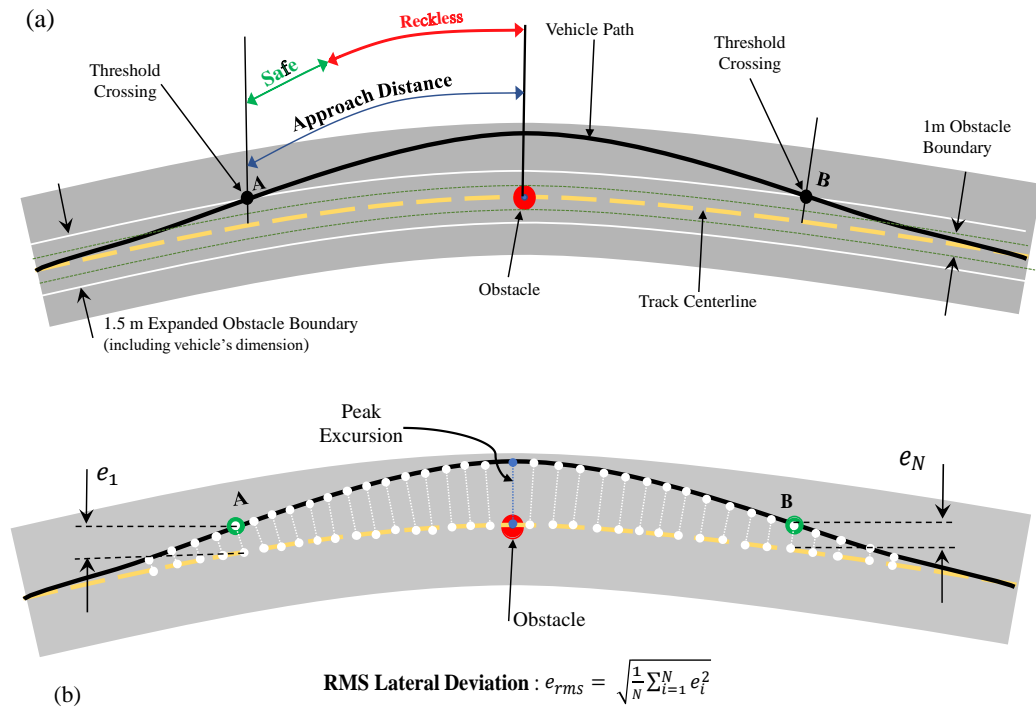
Figure 3.4: The performance metrics Approach Distance, RMS Lateral Deviation, and Excursion Peak are demonstrated in a typical obstacle avoidance trajectory. (a) The intersection of Expanded Obstacle Boundary (white lines) and vehicle path (solid black line) defines points A and B as threshold crossing points. The description of the Approach Distance is the length between point A and obstacle center (O) along the centerline. (b) The RMS value of the Lateral Deviation of the vehicle from the centerline is calculated for the sampled values (starting at point A and ending at point B) denoted by e_1, ..., e_N. The Peak Excursion is defined as the absolute maximum Lateral Deviation of the vehicle around the obstacle.

are utilized to construct the data sets for four excursion-related statistics. The Approach Distance is defined as the distance from the obstacle when the vehicle starts maneuvering one meter away from the road's centerline (see Fig.3.4-a). In order to have a safe driving condition, the Distance Approach must be more than 15 meters. Therefore a Safe Approach Distance can be defined as a difference between raw Approach Distance and 15 meters. Instead of using the raw Approach Distance, the Safe Approach Distance is utilized as a metric in this paper. The Lateral Deviation was then defined as the nearest distance to the centerline for each evenly sampled point on the vehicle trajectory. The RMS Lateral Deviation was the root mean square of the Lateral Deviation between points A and B in Fig.3.4-b). Peak Excursion is defined as the maximum lateral distance from the extended obstacle boundary which is demonstrated on Fig.3.4.

3.2.6   Data Analysis

The present study utilized a three by two by two factorial design, with the three factors being: Control Sharing Condition (Assistive Haptic Shared Active, Adaptive Haptic Shared Control, Active-Safety Haptic Shared Control), similarity of intents (same or reverse intent), and the human's impedance requested from drivers (high, low). The control sharing scheme varies between six trials for each participant (for each human driver, two runs for Assistive, two runs for Adaptive, and two runs for Active-safety schemes), and the obstacle avoiding direction with impedance level is varied within trials.

The experimental data were measured with one thousand hertz. These data are as follow: steering angle and its first and second derivatives (θ_{S}, $\dot{\theta}_{\mathrm{S}}$, $\ddot{\theta}_{\mathrm{S}}$), centerline location ($[X_{\mathrm{cl}},\ Y_{\mathrm{cl}}]$), vehicle location ($[X_{\mathrm{vl}},\ Y_{\mathrm{vl}}]$), obstacles position ($[x_{\mathrm{obs}}^{i},\ y_{\mathrm{obs}}^{i}]$ with $i = 1, 2, ..., 10$), reference trajectory for the autonomous system ($[X_{\mathrm{ref}},\ Y_{\mathrm{ref}}]$), grip force ($F_{\mathrm{grip}}$) and differential torque (τ_{T}). These time series measures are exploited to illustrate the behavior and performance of the driver-automation teams.

The dependent measures are Obstacle Hit percentage, Peak Excursion near each obstacle, Safe Approach Distance from the obstacle, and Maximum Torque. All these measures are extracted from the measured steering and torque behavior of participants. Univariate analysis of variance (ANOVA) is employed to analyze the statistical data of the metrics. The Obstacle Hit metric is investigated using the binary logistic regression approach, whereas Excursion Peak and Safe Approach Distance were analyzed using the linear modeling technique. The control sharing scheme, impedance level, and the preferred direction for avoiding obstacles are selected as independent factors. The ANOVA analysis determines the significant difference between the groups by a p-value less than 0.02. Post-hoc, sequential Bonferroni method is utilized to distinguish significant differences.

3.3   Results

In this paper, we considered twelve interaction modes between the driver and automation system based on the three control schemes (Active-safety, Adaptive and Assistive); similarity of intents (same or reverse intent) and human's adapted impedance (high and low). Below is the detailed Analysis of the performance metrics in each of these modes.

3.3.1   RMS Lateral Deviation

Figure 3.5 demonstrates the vehicle trajectory for these twelve conditions. The first, second and third columns, represent the vehicle trajectory in the Assistive, Adaptive and Active-safety haptic shared control schemes, respectively. The fourth column show the driver's grip force. The first row represent the vehicle trajectory when the human is asked to avoid the obstacle in a direction similar to the automation (cooperative automation) with a high impedance. The second row also represent the same intent scenario but the human is asked to adopt a lower impedance. The third row represent the vehicle trajectory when the human is asked to avoid the obstacle

in a direction opposite to the automation (uncooperative automation) with a high impedance. Finally, the fourth row represent the reverse intent scenario but the human is asked to adopt a lower impedance.
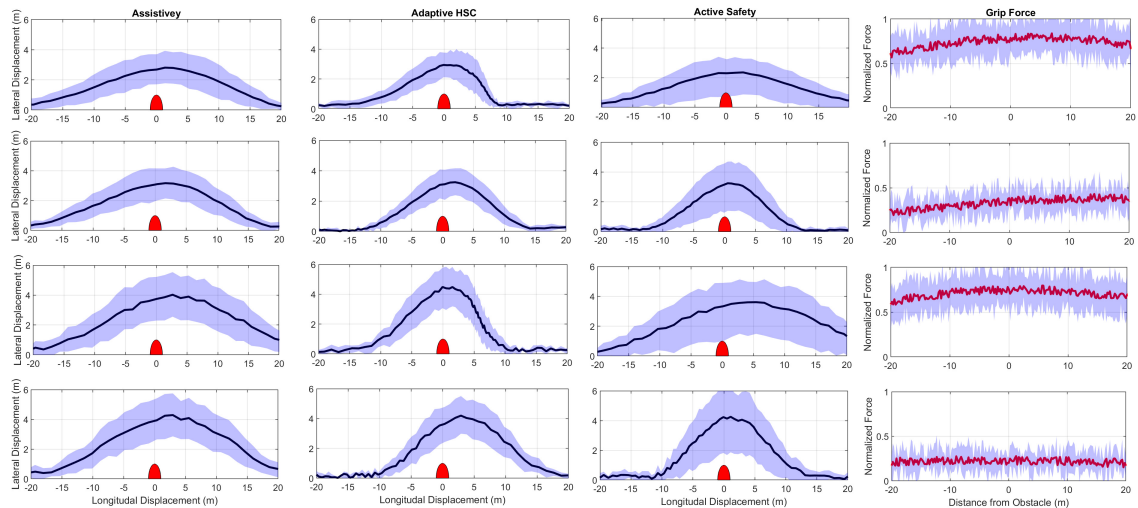
Figure 3.5: The driving trajectories of the vehicle are depicted in the road trajectory coordinate with an obstacle as an origin (a red half-circle). The shaded bands represent the 90% confidence intervals, while the solid line represents the mean value of the measured data from participants. The first three columns are dedicated to a specific shared control scheme (Assistive Adaptive Haptic Shared Control, and Active-Safety,). The last column demonstrates the measured grip force on the steering. Rows are based on the cooperation/impedance status of the automation system and the human driver. The first row illustrates the cooperation between the human driver and the recommended value for the grip force on the steering is high impedance. The second, third and fourth rows are cooperative-Low impedance, uncooperative-high impedance and uncooperative-low impedance interaction modes.

To gauge which shared control scheme resulted in the best maneuver performance around the obstacles, we calculate the RMS Lateral Deviation from the center-line. The RMS Lateral Deviation was only computed for obstacle that were successfully avoided. The means value of RMS Lateral Deviation for all the shared control conditions is presented in Figs.3.6,3.7, 3.8 and Table 3.3. It follows from Fig.3.6 that between all control schemes, the adaptive haptic shared control scheme has a lower RMS Lateral Deviation and consequently better maneuvering performance than Active-

safety ($p = 0.0625$) and assitive ($p = 0.018$).
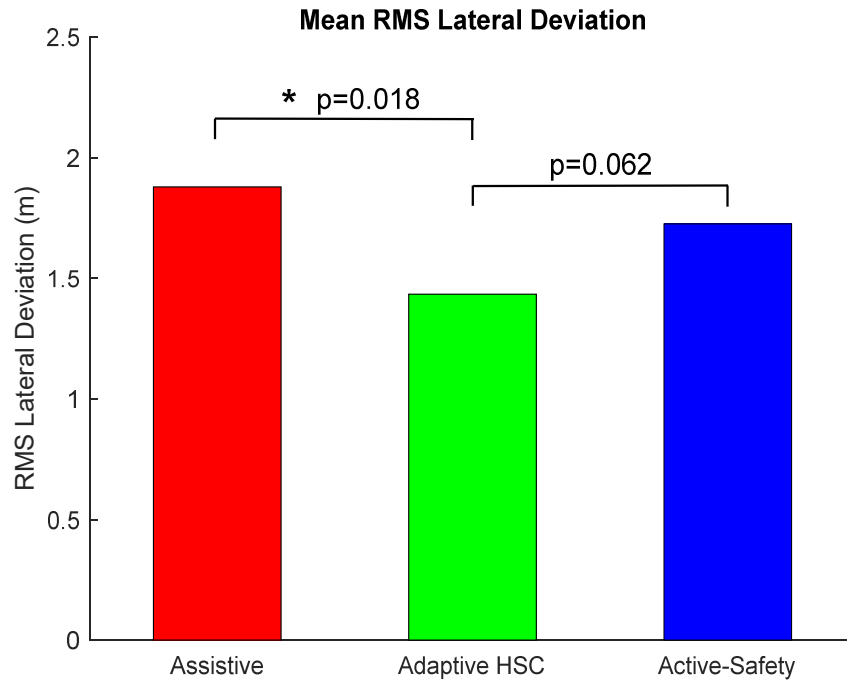
Figure 3.6: RMS value for Lateral Deviation of the vehicle from the centerline for each shared control scheme containing all interaction modes between the human driver and the automation system. The asterisks on the lines linking two bars indicate a significant difference between the two control schemes.

Table 3.3: Mean and Standard Error (S.E.) values of RMS Lateral Deviation

			Assistive	Adaptive HSC	Active-Safety
Cooperative	High Impedance	Mean RMS LD	1.9	1.5	1.7
		S.E. RMS LD	0.4	0.4	0.3
	Low Impedance	Mean RMS LD	1.9	1.5	1.7
		S.E. RMS LD	0.3	0.3	0.3
Uncooperative	High Impedance	Mean RMS LD	1.9	1.5	1.7
		S.E. RMS LD	0.4	0.2	0.2
	Low Impedance	Mean RMS LD	1.8	1.4	1.7
		S.E. RMS LD	0.3	0.2	0.3
Total RMS LD for Each Mode		**Mean RMS LD**	**1.9**	**1.5**	**1.7**
		S.E. RMS LD	**0.3**	**0.2**	**0.2**

It can interfere that a lower value of RMS Lateral Deviation for a specific control scheme indicates that the participant prefers to use that control scheme to maneuver around the obstacle efficiently. Considering the sample trajectory depicted in Fig.3.5, the presented mean and standard error values in Table.3.3 can be more perceptible.

The smaller standard value for the RMS Lateral Deviation has a thinner shaded confidence area in the graphical representation (Figure 3.5).

The mean value of the RMS Lateral Deviation in each control scheme for different interaction modes is approximately the same. There is no significant difference between the interaction modes within the same control scheme, as is demonstrated in the bar chart Fig.3.7. The standard error value in the Assistive control scheme shows a wider variation (S.E. = 0.3), which is bigger even for the cases with high impedance values (S.E. = 0.4). The RMS Lateral Deviation in the Adaptive scheme demonstrates better performance (mean = 1.5m, S.E. = 0.2) compared to Assistive (mean = 1.9m, S.E. = 0.3) and Active-safety (mean = 1.7m, S.E. = 0.2) schemes.
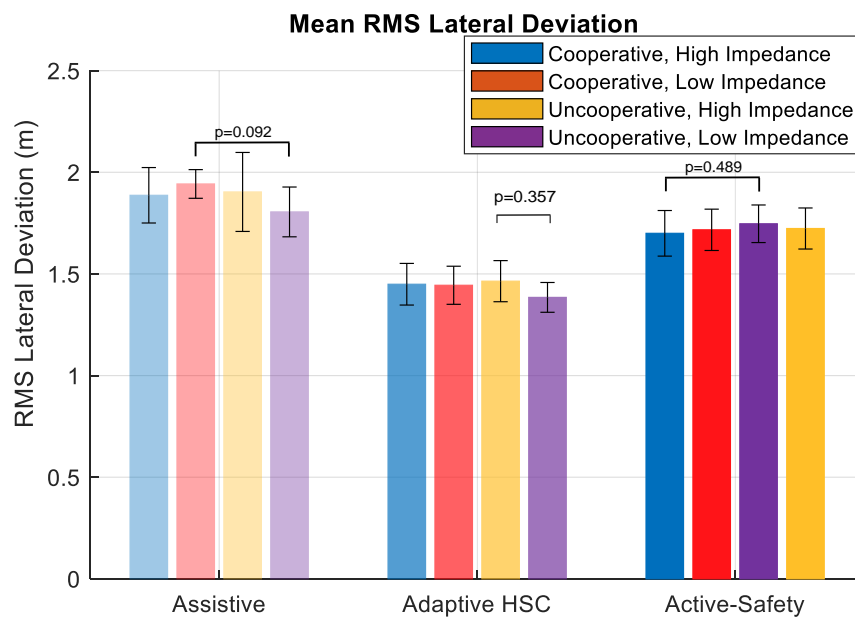
Figure 3.7: RMS value for Lateral Deviation of the vehicle from the centerline for each shared control scheme grouped by interaction mode between the human driver and the automation system.

3.3.2 Differential Torque

Fig.3.9 has the same structure as Figure 3.5 but it represent the the differential torque τ_T between the human driver and automation system around the obstacle. Figure 3.12 represent the maximum differential torque for the three shared control
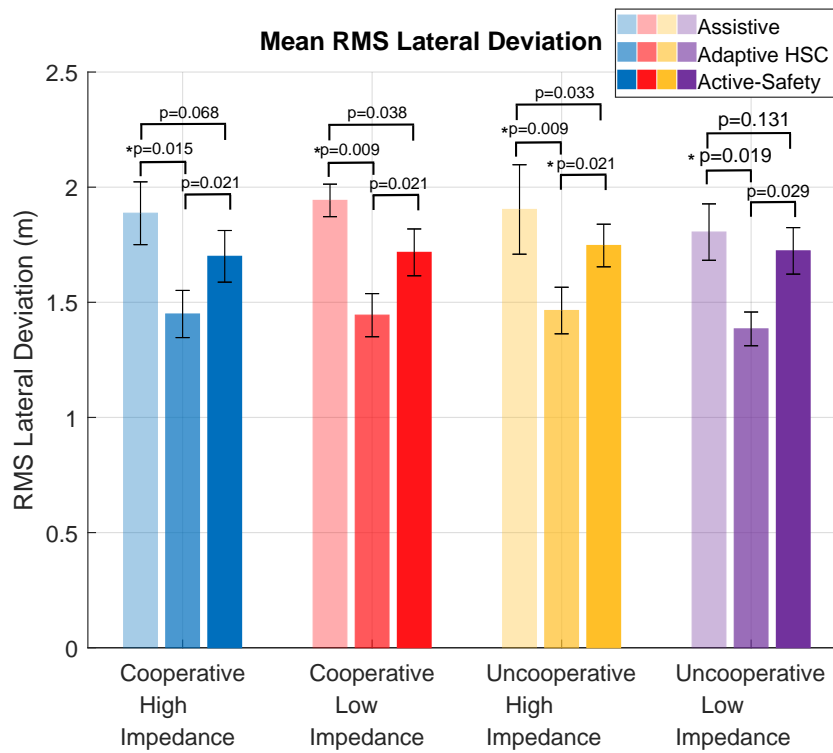
Figure 3.8: RMS value for Lateral Deviation of the vehicle from the centerline for each interaction mode grouped by shared control scheme between the human driver and the automation system.
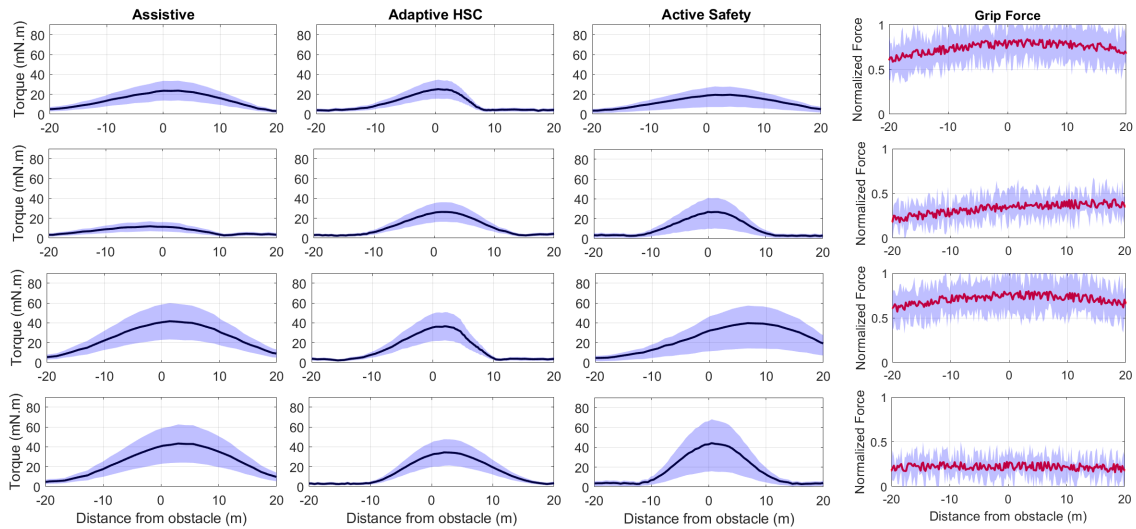
Figure 3.9: The measured differential torque between the human driver and the autonomous system is depicted in the road trajectory coordinate with an obstacle as an origin (a thick red line). The shaded bands represent the 90% confidence intervals, while the solid line represents the mean value of the measured data from participants. The first three columns are dedicated to a specific shared control scheme (Active-Safety, AssiSstive and Adaptive Haptic Shared Control). The last column demonstrates the measured grip force on the steering. Rows are based on the cooperation/impedance status of the automation system and the human driver. The first row illustrates the cooperation between the human driver and the recommended value for the grip force on the steering is high impedance. The second, third and fourth rows are cooperative-Low impedance, uncooperative-high impedance and uncooperative-low impedance interaction modes.

paradigms. Figures 3.10 and 3.11 show the maximum differential torque for the twelve different modes grouped by the shared control scheme and grouped by the interaction mode, respectively.

It follows from Figures 3.11 - 3.12 that, for all three shared control schemes,when the human and automation have reverse intents to avoid the obstacle, they both feel a higher differential torque on the steering wheel. The higher differential torque is an indication of the uncooperativness between the human and automation.

In addition to the intent, differential torque is also a function of the impedance adopted by the driver and automation system. When one agent adopts a lower impedance, the differential torque is expected to be smaller. It follows from Figure 3.11 that in the Assistive and Active safety mode, this assumption is true. Specifically, comparing the torque profile for each of the cases shown in the first row of Figure 3.9 with the torque shown in the second row, it is clear that the differential torque is reduced when the human adopts a lower impedance. Similarly, comparing the torque profile shown in the third row with the torque shown in the fourth row, it is clear that when both human and automation are in the uncooperative mode, if the human adopts a lower impedance, the differential torque between them will be reduced.

By comparing the three shared control schemes (Figure 3.12), it is shown that the differential torque in the Assistive mode is smaller compared to Adaptive haptic shared control and Active-safety control schemes. Considering the gray area in Figure 3.9, the peak measured differential torque is ignorable for the same direction-low impedance case. Because of this case, the overall peak differential torque for the Assistive scheme is smaller than the adaptive haptic shared control. Post-hoc comparisons for the differential torque in different shared control schemes indicated that the possibility of peak torque for the Adaptive HSC condition was significantly lower than the Active-safety ($p = 0.008$) conditions (indicated in Fig.3.12). There
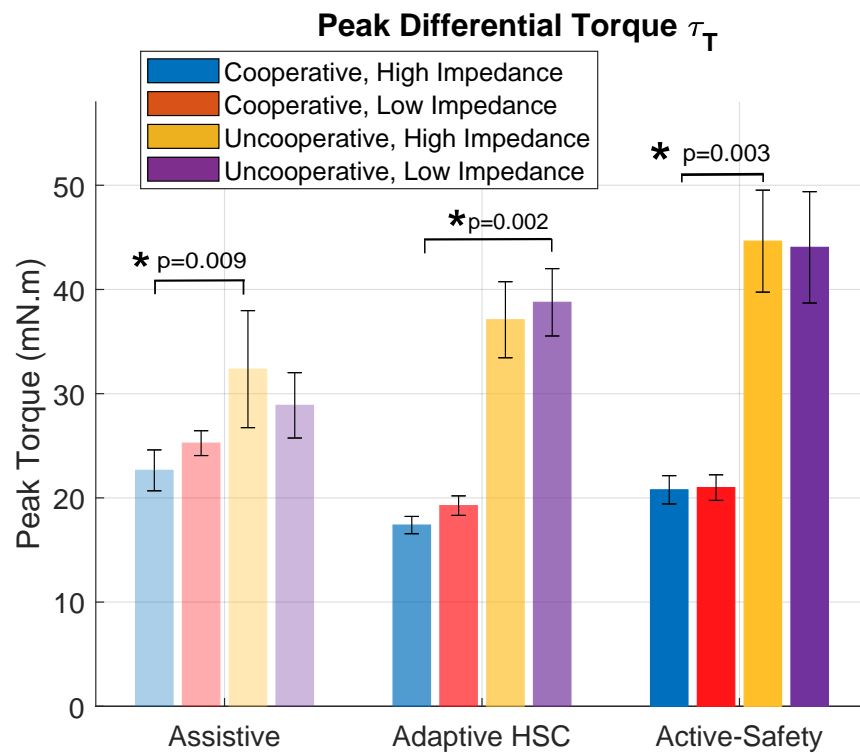
Figure 3.10: Measured differential torque between the human driver and the automation system for each shared control scheme grouped by interaction mode between the human driver and the automation system
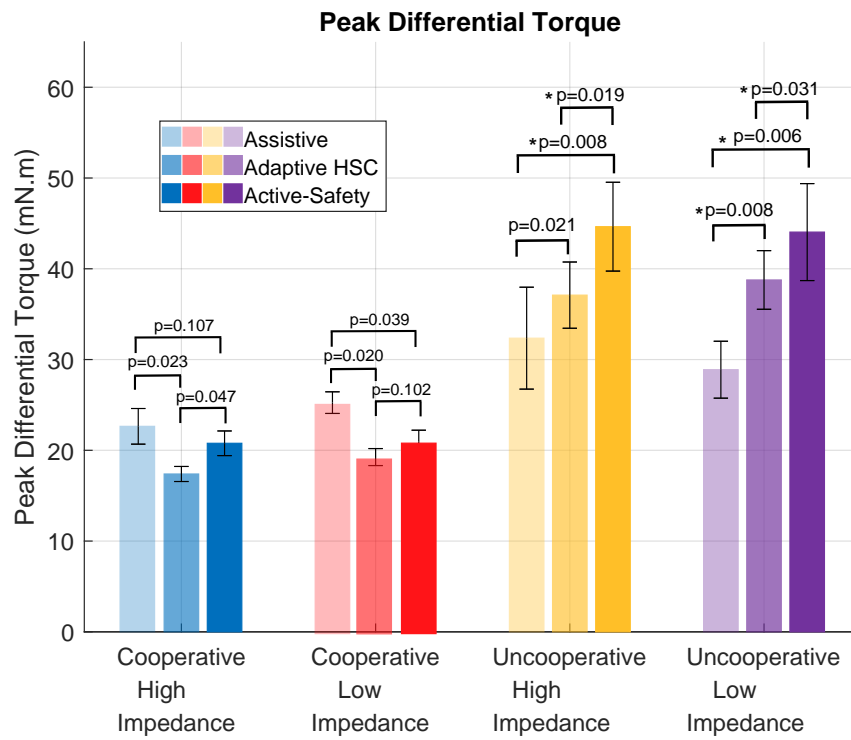
Figure 3.11: Measured differential torque between the human driver and the automation system for each interaction mode grouped by shared control scheme between the human driver and the automation system.

is no significant difference between the Adaptive and Assistive schemes ($p = 0.021$). Considering the RMS value for the Assistive control scheme reveals that the lower peak differential torque in this scheme caused more Lateral Deviation from the road centerline, which is not desired for the driving task.
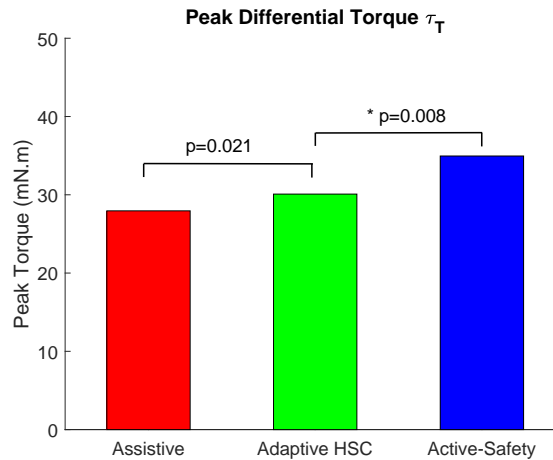
Figure 3.12: Measured differential torque between the human driver and the automation syste for each shared control scheme containing all interaction modes between the human driver and the automation system.

Table 3.4 demonstrates the mean, and the standard error of the peak measured differential torque for different interaction modes and control schemes. As mentioned before, the standard error of the peak differential torque for the cooperative-low impedance case is approximately equal to zero (S.E. $= 0.01$), which caused the smaller peak differential torque for the Assistive scheme with respect to the other control schemes.

3.3.3 Obstacle Hits

Table 3.5 demonstrates the obstacle hit numbers and percentages for each control scheme and the interaction modes. The obstacle hit percentage in each run is calculated based on the number of hits divided by the number of the obstacles (ten obstacles in the road trajectory). As demonstrated in this table, the percentage of obstacles hit in the Adaptive haptic shared conditions is low (0.7%) compared to the

Table 3.4: Mean and Standard Error (S.E.) values of the maximum measured differential torque

			Assistive	Adaptive HSC	Active-Safety
Cooperative	**High Impedance**	Mean PDT	22.64	17.39	20.77
		S.E. PDT	1.04	0.53	0.96
	Low Impedance	Mean PDT	25.25	19.25	20.98
		S.E. PDT	0.01	0.55	0.98
Uncooperative	**High Impedance**	Mean PDT	32.35	37.10	44.64
		S.E. PDT	3.24	3.66	3.21
	Low Impedance	Mean PDT	28.88	38.77	55.04
		S.E. PDT	2.77	2.67	3.20
Total RMS LD for Each Mode		**Mean PDT**	**27.95**	**30.09**	**34.96**
		S.E. PDT	**1.68**	**1.78**	**2.23**

2.2% and 2.7% obstacles hit in the Assistive and Active-safety schemes.

Table 3.5: Mean and Standard Error (S.E.) values of numbers of hits

			Assistive	Adaptive HSC	Active-Safety
Cooperative	**High Impedance**	Obstacles Hit	5/108	0/108	5/108
		%Hit	4.6%	0.0%	4.6%
	Low Impedance	Obstacles Hit	2/108	0/108	1/108
		%Hit	1.9%	0%	0.9%
Uncooperative	**High Impedance**	Obstacles Hit	3/162	1/162	5/162
		%Hit	1.8%	0.6%	3.0%
	Low Impedance	Obstacles Hit	2/162	5/162	4/168
		%Hit	1.2%	3.0%	2.4%
Total Hit for Each Mode		**Obstacles Hit**	**12/540**	**4/540**	**15/540**
		%Hit	**2.2%**	**0.7%**	**2.7%**

By considering only cooperative-high impedance conditions, in the Assistive and Active safety modes, the obstacle hit percentage is 4.6%, whereas there is no obstacle hit in the Adaptive haptic shared control condition. Likewise, in the cooperative-low impedance condition, there is no obstacle hit in the Adaptive haptic shared control condition, while in the Assistive and Active-safety conditions, there are 1.9% and 0.9% obstacles hit. The obstacle hit percentage in the uncooperative-high impedance conditions shows better performance for the Adaptive HSC scheme (only one obstacle out of 162 obstacles has been hit). In contrast, the Assistive and Active-safety schemes have three and five obstacle hits. In Fig.3.13 the bar chart of the percentage of the obstacle hit for different controller structures in four conditions is demonstrated. For each interaction mode, a different color is dedicated to distinguishing them. In the bar chart, the superior performance of the Adaptive HSC scheme for three conditions

is obvious compared to the corresponding conditions in Assistive and Active-safety modes. Only in the uncooperative-low impedance condition the Adaptive HSC scheme has lower performance for obstacle avoidance concerning the other control schemes.
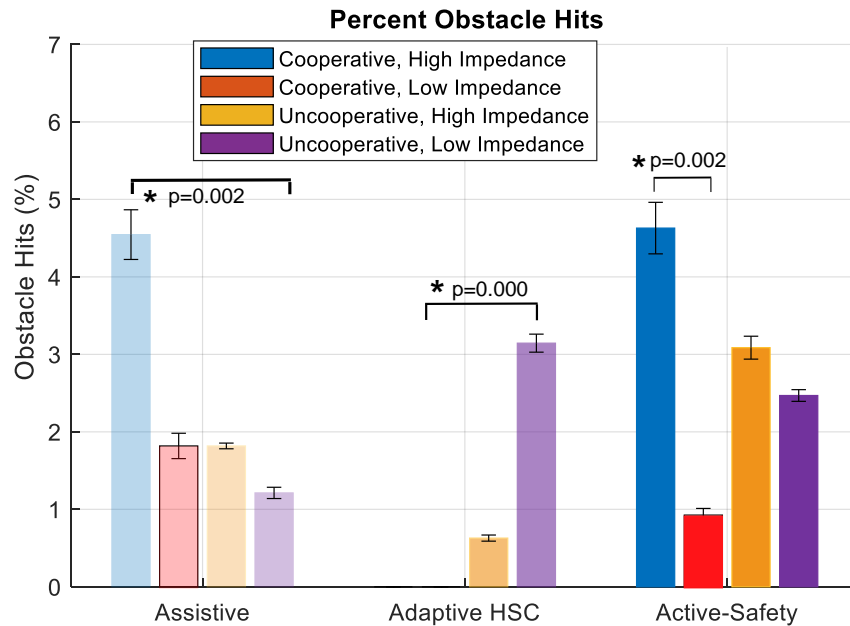
Figure 3.13: Percent Obstacle Hits for each shared control scheme grouped by interaction mode between the human driver and the automation system.

Post-hoc comparisons indicated that the possibility of an obstacle hit for the Adaptive HSC condition was significantly lower than for both the Assistive condition ($p = 0.0005$) and for the Active-safety ($p = 0.0004$) conditions (indicated in Fig.3.15). Analysis of the obstacle hit percentage data for the different interaction modes indicated that the Assistive and Active-safety conditions had a significant main effect ($F(1, 8447) = 0.9231, p = 0.542$) on the likelihood of a hit in their cooperative-high impedance situation. Likewise, the Post-hoc sequential Bonferroni test revealed that in the uncooperative-low impedance mode, Adaptive HSC had a higher likelihood of an obstacle hit than Assistive ($p = 0.0097$) and Active-safety ($p = 0.0097$) conditions. However, since the total hit percentage for the Adaptive HSC is significantly lower than Assistive and Active-safety conditions, the hit percentage in the uncooperative-
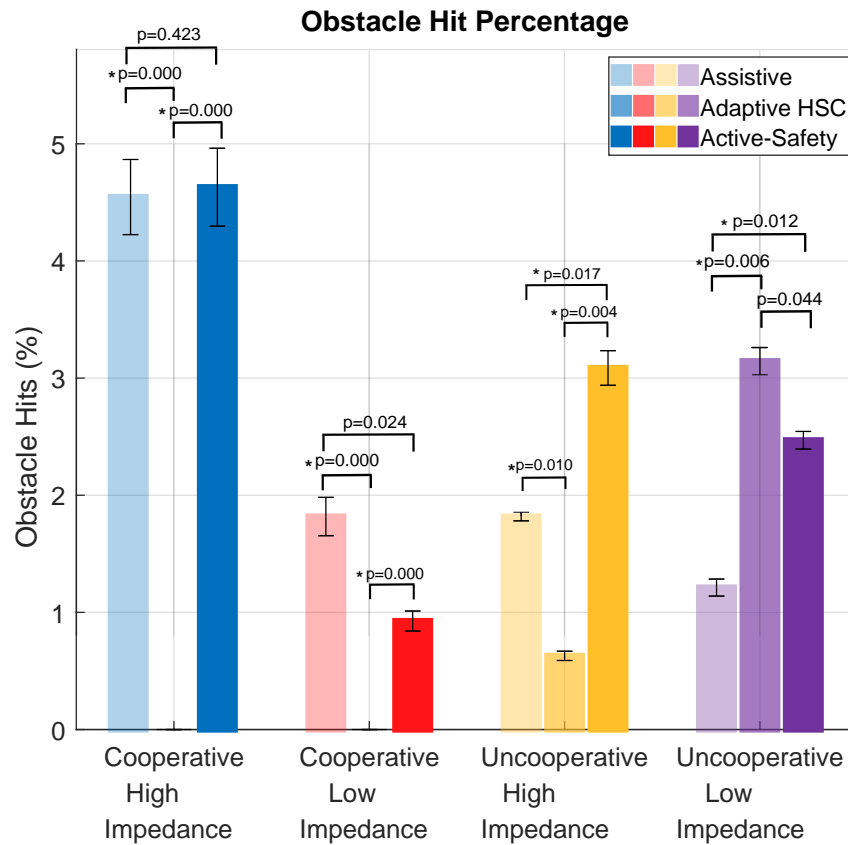
Figure 3.14: Percent Obstacle Hits for each interaction mode grouped by shared control scheme between the human driver and the automation system
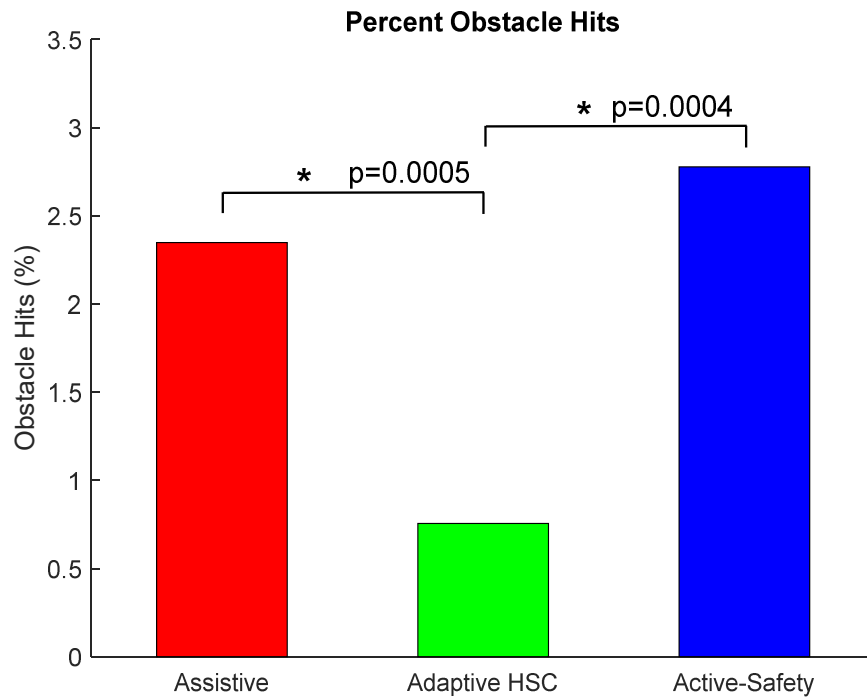
Figure 3.15: Percent Obstacle Hits for each shared control scheme containing all interaction modes between the human driver and the automation system. The asterisks on the lines linking two bars indicate a significant difference between the two control schemes.

low impedance mode of Adaptive HSC could not be generalized to the other groups in Adaptive HSC.

3.3.4   Safe Approach Distance

The Approach Distance is used to gauge the control transfer time between the human and automation system. since the vehicle velocity is constant (13 m/sec), the Approach Distance is presented in meters in this paper. The value of approach distance indicated how early the human-automation team deviated from the center-line track (one meter) to avoid the obstacle. For instance, a lower approach distance implied that the human-automation team took more time to deviate from the track during obstacle avoidance. In this paper, we employed the safe approach distance. The Safe Approach Distance provides a more accurate measure to compare the performance of the different shared control schemes since it removes the reckless distance (15 meters) from the recorded raw Approach Distance values. The means of Safe Approach Distance for all conditions are summarized in Table 3.6.

Table 3.6: Mean and Standard Error (S.E.) values of Safe Approach Distance

			Assistive	Adaptive HSC	Active-Safety
Cooperative	**High Impedance**	Mean AP	1.88	2.59	0.87
		S.E. AP	0.23	0.21	0.20
	Low Impedance	Mean AP	1.98	2.67	0.87
		S.E. AP	0.19	0.20	0.19
Uncooperative	**High Impedance**	Mean AP	1.45	2.94	1.09
		S.E. AP	0.28	0.24	0.20
	Low Impedance	Mean AP	1.28	1.84	1.15
		S.E. AP	0.26	0.19	0.19
Total AP for Each Mode		**Mean AP**	**1.65**	**2.51**	**0.99**
		S.E. AP	**0.24**	**0.21**	**0.20**

Looking at the means of Safe Approach Distance presented in Table 3.6, we see that out of all control schemes, the Adaptive Haptic Shared Control scheme has the highest Safe Approach Distance whereas the Active-Safety Haptic Shared Control has the lowest Safe Approach Distance value.

The mean values for Safe Approach Distance grouped in the different interaction modes (Figure 3.17) and different control schemes (Figure 3.16) reveal that partici-
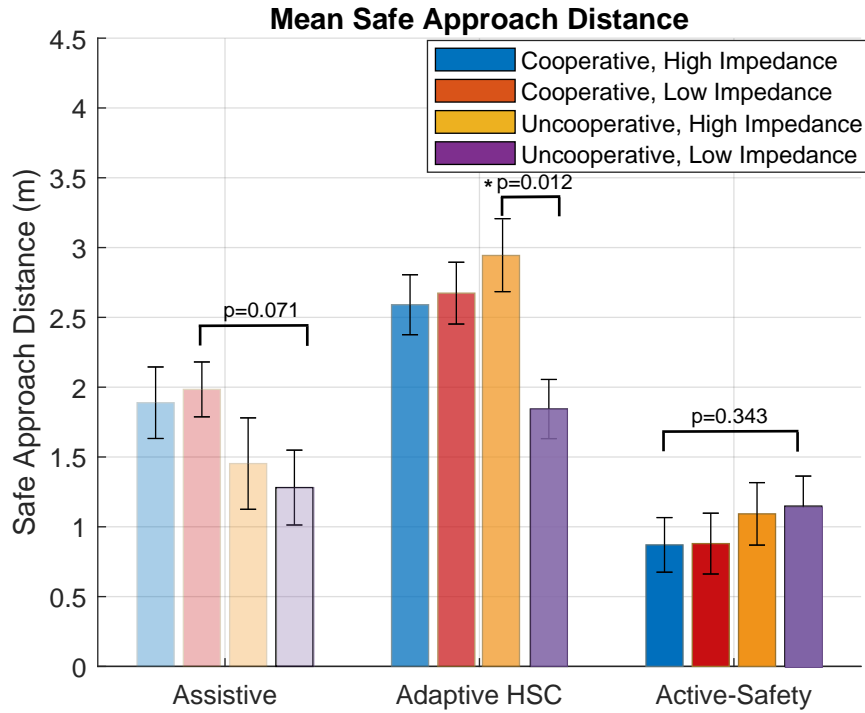
Figure 3.16: Safe approach distance value for each shared control scheme grouped by interaction mode between the human driver and the automation system.
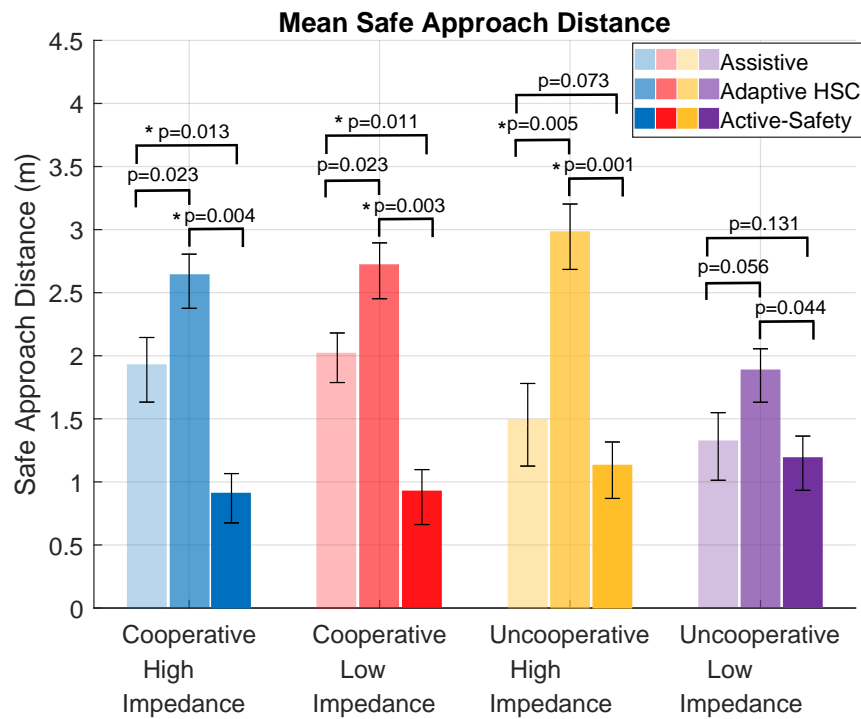

Figure 3.17: Safe approach distance value for each interaction mode grouped by shared control scheme between the human driver and the automation system.

pants have a slower reaction in the Active safety and Assistive control schemes. The results for the analysis of the Safe Approach Distance in different shared control schemes are summarized in Figure 3.18. Through the post hoc tests it was found that the mean value of the Safe Approach Distance for the Adaptive Haptic Shared Control scheme was significantly higher than Assistive ($p = 0.011$) and Active-safety ($p = 0.004$) schemes.
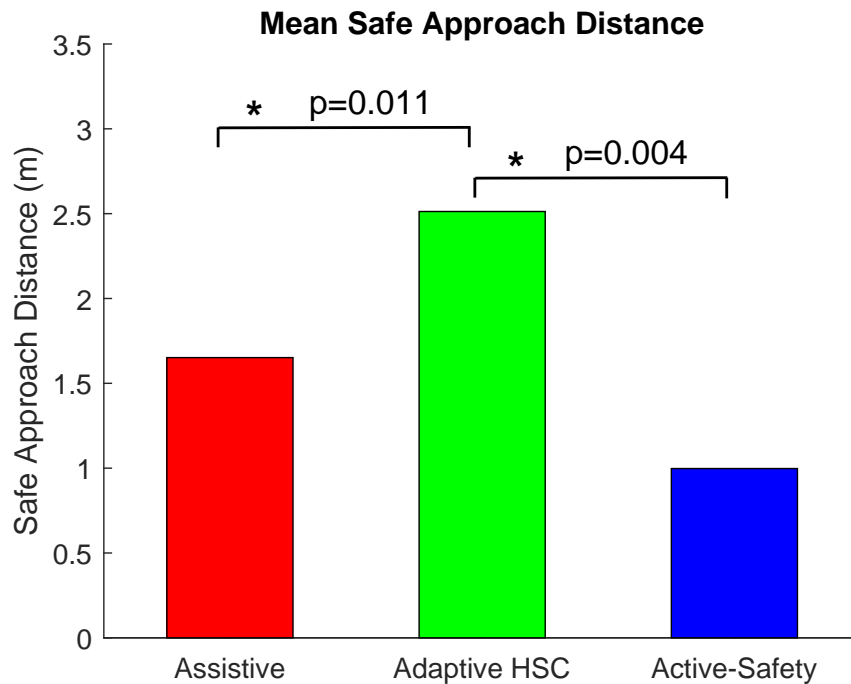
Figure 3.18: Safe Approach Distance value for each shared control scheme containing all interaction modes between the human driver and the automation system.

3.3.5   Peak Excursion

The Peak Excursion is employed to measure the vehicle distance from the obstacle while crossing it. Peak Excursion is calculated as the absolute maximum lateral deviation of the vehicle from the extended obstacle boundary. The mean and standard error values of Peak Excursion for all conditions are summarized in Table 3.6.

Also, the bar chart of the Excursion Peak for the extended obstacle boundary for the different interaction modes (Figure 3.20) and shared control schemes (Figure

Table 3.7: Mean and Standard Error (S.E.) values of Peak Excursion

			Assistive	Adaptive HSC	Active-Safety
Cooperative	**High Impedance**	Mean PE	1.45	1.50	1.45
		S.E. PE	0.25	0.25	0.27
	Low Impedance	Mean PE	1.54	1.48	1.49
		S.E. PE	0.05	0.21	0.27
Uncooperative	**High Impedance**	Mean PE	1.10	1.52	0.47
		S.E. PE	0.60	0.25	0.18
	Low Impedance	Mean PE	1.02	1.43	0.42
		S.E. PE	0.42	0.21	0.18
Total PE for Each Mode		**Mean PE**	**1.27**	**1.48**	**0.96**
		S.E. PE	**0.41**	**0.23**	**0.23**
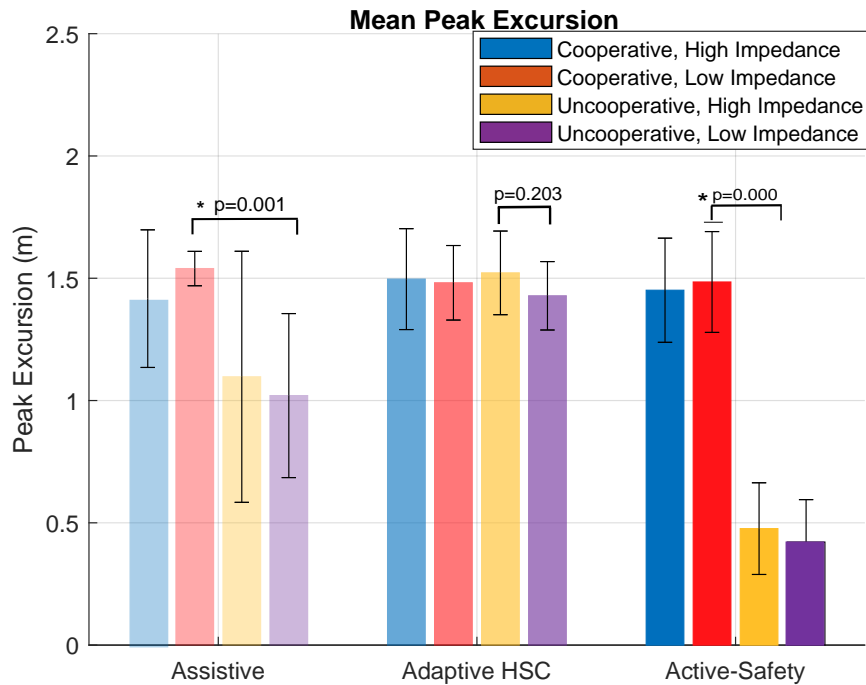
Figure 3.19: Peak excursion value in each shared control scheme grouped by interaction mode between the human driver and the automation system.
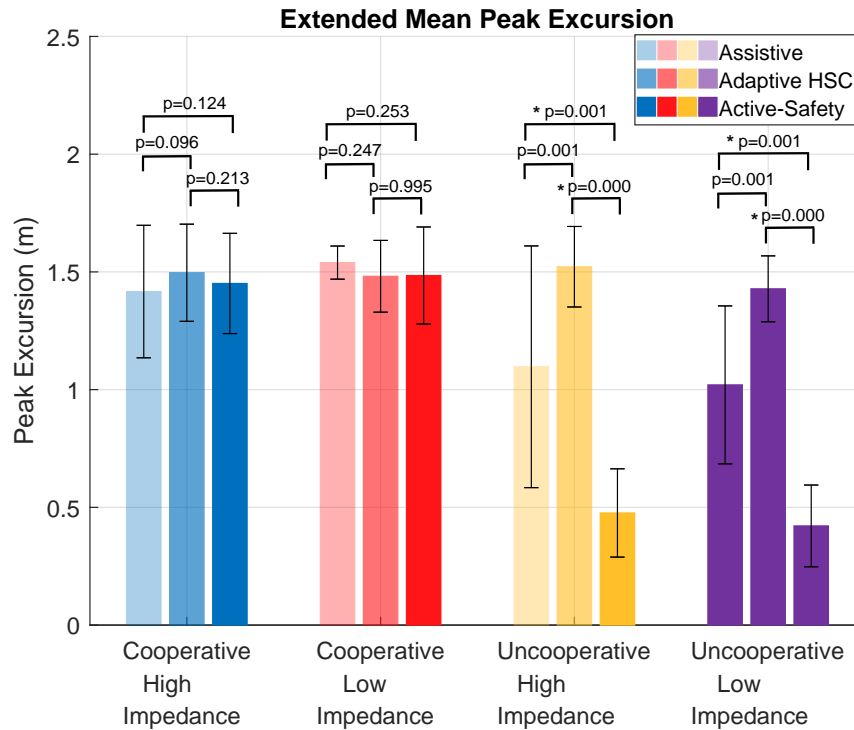
Figure 3.20: Peak excursion value in each interaction mode grouped by shared control scheme between the human driver and the automation system.

3.19) are depicted. In the Adaptive HSC scheme and the cooperative interaction modes, the mean Excursion Peak is about 1.5 meters. It reveals that having an opposite intent for avoiding the obstacles by participants and automation system cause a slower reaction in the driving task. In the Adaptive HSC scheme and the cooperative interaction modes, the mean Excursion Peak is about 1.5 meters (Figure 3.19). In the uncooperative interaction modes of the Active-safety and the Assistive control schemes, the mean value of the Peak Excursion is approximately 1 and 0.5 meters (Figure 3.20), respectively. The post hoc tests found that the mean Peak Excursion for the Adaptive Haptic Shared Control condition was significantly higher than the Active-Safety (p = 0.003) and also higher than the Assistive (p = 0.057) shared control schemes (Figure 3.21).
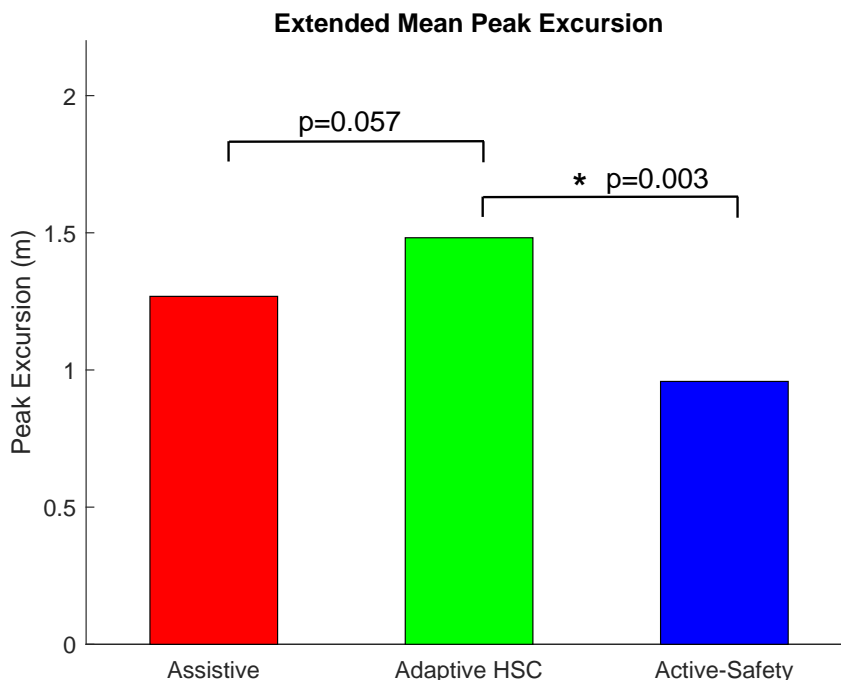
Figure 3.21: Peak excursion value for each shared control scheme containing all interaction modes between the human driver and the automation system.

3.4   Conclusions

In this study, our goal was to compare the performance of shared control schemes in resolving a conflict. To this end, we studied a scenario wherein both human and automation detect an obstacle and try to avoid it. To study the human and automation's interaction outputs, twelves interaction modes were considered. These modes are designed based on the similarity of human and automation intents (same or reverse intent for avoiding the obstacle), the amount of participants' impedance level (high/low) and the share control schemes (Assistive, Active-safety and the Adaptive shared control).

All analyses were undertaken on five performance metrics that focused on distinct aspects of the obstacle avoidance task. The Obstacle Hits and the Peak Excursion metric were used to compare driving safety; higher obstacle hits/lower Peak Excursion corresponded to lower safety. The safe Approach Distance and Peak Differential Torque values were used to gauge the quality of control transfer between the human

and automation. A lower approach distance indicated that around the obstacle, the human driver was either unprepared to take over the driving authority or was unprepared to give away the driving authority to automation. The lower Differential Torque means a higher comfort level for participants for the driving task. Finally, RMS Lateral Deviation was used to compare the driver's maneuvering efficiency around the obstacle; lower RMS lateral deviation indicated that the maneuver was performed more efficiently without excessive lateral deviation from the centerline.

The analyzed results revealed that Adaptive Haptic Shared Control has a better performance based on the Five metrics. The overall Hit percentage of Adaptive HSC scheme in a run was less than 1% which means the numbers of participants who experienced obstacle hit were less that four person (since there were only four-hit over 540). The Adaptive HSC scheme had a significantly lower Peak Differential Torque than the Active-safety HSC scheme and lower Differential Torque than the Assistive HSC scheme. Also, the Adaptive HSC scheme had significantly lower RMS Lateral Deviation than both Assistive and Active Safety schemes and had significantly higher Approach Distance than both Assistive and Active Safety schemes. Moreover, with respect to the five presented metrics, the driving performance with Adaptive HSC was never significantly lower than the Active-Safety and the Assistive HSC schemes. The improvement in driving performance with Adaptive HSC can be attributed to the adaptive structure of collaboration compared to the Assistive and Active-Safety HSC schemes. All three HSC schemes communicated their control efforts to the driver through torque feedback on the steering wheel. In the Adaptive HSC scheme, the automation continuously monitors and estimates the human impedance level to indicate their intention to gain/yield the control authority. Therefore based on human behavior, the Adaptive HSC updates the model of the propagated system in the high-level MPC (Eq. (3.1)).

Based on the presented analysis of our performance metrics, sharing control under

Adaptive HSC promotes safer driving and enhances driving efficiency. Especially, Adaptive HSC improves preparedness to take over or give away the driving authority and fosters more efficient driving maneuvers around obstacles than Assistive and Active-Safety HSC schemes. Complementing previous research [5, 2, 4, 7, 15, 26, 27, 28], this study demonstrates how adaptively adopting the automation intent (updating the system model in the HSC scheme) based on the human driver behavior can help improve driving performance.

There are multiple hyperparameters in the present design of the Adaptive HSC, and the presented results in this paper are dependent on those parameters. Particularly, the dependency of the human impedance determination to the measured grip force, the number of the quantized level for the penalty weights in the cost function (Eq. (3.1)), the designed curvature in the test and the distribution of the interaction types between the obstacles are some of the tunable hyperparameters in the current design. Defining the effect of these parameters in the system design and experimental setup requires sensitivity analysis and an intelligent tuning mechanism. The data-driven approaches can be considered a potential solution to handle these tunable parameters in the current study.

REFERENCES

[1] D.A. Abbink and M. Mulder. Neuromuscular Analysis as a Guideline in designing Shared Control. *Advances in Haptics*, pages 499–517, 2010.

[2] David A Abbink, Mark Mulder, and Erwin R Boer. Haptic shared control: smoothly shifting control authority? *Cognition, Technology & Work*, 14(1):19–28, 2012.

[3] J Anderson, S Walker, and K Iagnemma. Experimental performance analysis of a constraint-based navigation framework. *Transactions on Systems, Man, and Cybernetics–Part A: Systems and Humans*, pages 1–10, 2014.

[4] Mohamed Amir Benloucif, Anh-Tu Nguyen, Chouki Sentouh, and Jean-Christophe Popieul. A new scheme for haptic shared lateral control in highway driving using trajectory planning. *IFAC-PapersOnLine*, 50(1):13834–13840, 2017.

[5] Akshay Bhardwaj, Amir H Ghasemi, Yingshi Zheng, Huckleberry Febbo, Paramsothy Jayakumar, Tulga Ersal, Jeffrey L Stein, and R Brent Gillespie. Whos the boss? arbitrating control authority between a human driver and automation system. *Transportation Research Part F: Traffic Psychology and Behaviour*, 68:144–160, 2020.

[6] Wei Bi, Xiaoyu Wu, Yueyue Liu, and Zhijun Li. Role adaptation and force, impedance learning for physical human-robot interaction. In *2019 IEEE 4th International Conference on Advanced Robotics and Mechatronics (ICARM)*, pages 111–117. IEEE, 2019.

[7] Henri Boessenkool, David A Abbink, Cock JM Heemskerk, Frans CT van der Helm, and Jeroen GW Wildenbeest. A task-specific analysis of the benefit of haptic shared control during telemanipulation. *IEEE Transactions on Haptics*, 6(1):2–12, 2013.

[8] Jon Bornstein. Dod autonomy roadmap: autonomy community of interest. Technical report, Army Research Laboratory Aberdeen Proving Ground United States, 2015.

[9] Ruth A David and Paul Nielsen. Defense science board summer study on autonomy. Technical report, Defense Science Board Washington United States, 2016.

[10] Stephen M Erlien. *Shared vehicle control using safe driving envelopes for obstacle avoidance and stability*. PhD thesis, Stanford University, 2015.

[11] Frank Flemisch, Matthias Heesen, Tobias Hesse, Johann Kelsch, Anna Schieben, and Johannes Beller. Towards a dynamic balance between humans and automation: Authority, ability, responsibility and control in shared and cooperative control situations. *Cognition, Technology and Work*, 14(1):3–18, 2012.

[12] A.H. Ghasemi, Paramsothy Jayakumar, and R. Brent Gillespie. Shared Control Architectures for Vehicle Steering. *Cognition, Technology & Work Special Issue "Shared and cooperative control"*, page submitted., 2017.

[13] Amir H Ghasemi, Paramsothy Jayakumar, and R Brent Gillespie. Shared control architectures for vehicle steering. *Cognition, Technology & Work*, 21(4):699–709, 2019.

[14] Amir H Ghasemi, Mishel Johns, Benjamin Garber, Paul Boehm, Paramsothy Jayakumar, Wendy Ju, and R Brent Gillespie. Role negotiation in a haptic

shared control framework. In *Adjunct Proceedings of the 8th International Conference on Automotive User Interfaces and Interactive Vehicular Applications*, pages 179–184. ACM, 2016.

[15] Paul G. Griffiths and R. Brent Gillespie. Sharing Control Between Humans and Automation Using Haptic Interface: Primary and Secondary Task Performance Benefits. *Human Factors: The Journal of the Human Factors and Ergonomics Society*, 47(3):574–590, oct 2005.

[16] Raphaela Groten, Daniela Feth, Harriet Goshy, Angelika Peer, David A Kenny, and Martin Buss. Experimental analysis of dominance in haptic collaboration. In *Robot and Human Interactive Communication, 2009. RO-MAN 2009. The 18th IEEE International Symposium on*, pages 723–729. IEEE, 2009.

[17] Raphaela Groten, Daniela Feth, Roberta L Klatzky, and Angelika Peer. The role of haptic feedback for the integration of intentions in shared task execution. *IEEE Transactions on Haptics*, 6(1):94–105, 2013.

[18] Vahid Izadi, Akshay Bhardwaj, and Amir H Ghasemi. Impedance modulation for negotiating control authority in a haptic shared control paradigm. In *2020 American Control Conference (ACC)*, pages 2478–2483. IEEE, 2020.

[19] Vahid Izadi and Amir H Ghasemi. Modulation of control authority in adaptive haptic shared control paradigms. *Mechatronics*, 78:102598, 2021.

[20] Vahid Izadi, Amir H Ghasemi, and Pouria Karimi Shahri. Negotiating the steering control authority within haptic shared control framework. Technical report, SAE Technical Paper, 2020.

[21] Vahid Izadi, Arjun Yeravdekar, and Amirhossein Ghasemi. Determination of roles and interaction modes in a haptic shared control framework. In *ASME*

2019 Dynamic Systems and Control Conference. American Society of Mechanical Engineers Digital Collection, 2019.

[22] Justin Storms, Kevin Chen, and Dawn Tilbury. A shared control method for obstacle avoidance with mobile robots and its interaction with communication delay. *The International Journal of Robotics Research*, 36(5-7):820–839, 2017.

[23] Jason Kong, Mark Pfeiffer, Georg Schildbach, and Francesco Borrelli. Kinematic and dynamic vehicle models for autonomous driving control design. In *2015 IEEE intelligent vehicles symposium (IV)*, pages 1094–1099. IEEE, 2015.

[24] Ayse Kucukyilmaz et al. *Haptic role allocation and intention negotiation in human-robot collaboration*. PhD thesis, Koç University, 2013.

[25] Zhenji Lu, Riender Happee, Christopher DD Cabrall, Miltos Kyriakidis, and Joost CF de Winter. Human factors of transitions in automated driving: A general framework and literature survey. *Transportation Research Part F: Traffic Psychology and Behaviour*, 43:183–198, 2016.

[26] F. Mars, D. Mathieu, and Jean-Michel Hoc. Analysis of human-machine co-operation when driving with different degrees of haptic shared control. *IEEE Transactions on Haptics*, 1412(c):1–1, 2014.

[27] Carlo Masone, Paolo Robuffo Giordano, Heinrich H Bülthoff, and Antonio Franchi. Semi-autonomous trajectory generation for mobile robots with integral haptic shared control. In *2014 IEEE International Conference on Robotics and Automation (ICRA)*, pages 6468–6475. IEEE, 2014.

[28] Ryota Nishimura, Takahiro Wada, and Seiji Sugiyama. Haptic Shared Control in Steering Operation Based on Cooperative Status Between a Driver and a Driver Assistance System. *Journal of Human-Robot Interaction*, 4:19–37, 2015.

[29] Marcia K. O'Malley, Abhishek Gupta, Matthew Gen, and Yanfang Li. Shared Control in Haptic Systems for Performance Enhancement and Training. *Journal of Dynamic Systems, Measurement, and Control*, 128(1):75, 2006.

[30] R. Parasuraman and V. Riley. Humans and Automation: Use, Misuse, Disuse, Abuse. *Human Factors*, 39(2):230–253, 1997.

[31] S. M. Petermeijer, D. a. Abbink, and J. C. F. de Winter. Should Drivers be Operating Within an Automation-Free Bandwidth? Evaluating Haptic Steering Support Systems With Different Levels of Authority. *Human Factors: The Journal of the Human Factors and Ergonomics Society*, 57(1):5–20, 2014.

[32] Calder Phillips-Grafflin, Halit Bener Suay, Jim Mainprice, Nicholas Alunni, Daniel Lofaro, Dmitry Berenson, Sonia Chernova, Robert W Lindeman, and Paul Oh. From autonomy to cooperative traded control of humanoid manipulation tasks with unreliable communication. *Journal of Intelligent & Robotic Systems*, 82(3):341–361, 2016.

[33] Thomas B Sheridan and William L Verplank. Human and computer control of undersea teleoperators. Technical report, Massachusetts Inst of Tech Cambridge Man-Machine Systems Lab, 1978.

[34] Jarrod M Snider et al. Automatic steering methods for autonomous automobile path tracking. *Robotics Institute, Pittsburgh, PA, Tech. Rep. CMU-RITR-09-08*, 2009.

[35] Joon Woo Son, Myoung Ouk Park, et al. Situation awareness and transitions in highly automated driving a framework and mini-review. *Journal of Ergonomics*, 2017.

[36] Arie P van den Beukel, Mascha C van der Voort, and Arthur O Eger. Towards a framework for testing drivers' interaction with partially automated driving. In

2015 IEEE 18th International Conference on Intelligent Transportation Systems, pages 1902–1907. IEEE, 2015.

CHAPTER 4: (PAPER 3) Learning and Leveraging Conventions in the Design of Haptic Shared Control Paradigms for Steering a Ground Vehicle

4.1   Introduction

Human-automation teaming (HAT) is gaining importance because it promises to improve performance, reduce the cost of operating, and increase adaptability to new situations [1, 2]. However, the partnership between the human driver and the automation system can potentially present some challenges because the two types of intelligence are not symmetrical (a gap between the world as a human sees it vs. the world as modeled by the automation) [3, 4, 5]. For instance, given that both humans and automation systems are subject to faults, the hand-off problem how to exchange control between a driver and automation plays a critical role in ensuring HAT's performance [6, 7, 8, 9]. To this end, various schemes have been proposed, differing primarily according to how to control authority is transitioned between the two agents [10, 11, 12, 7]. These schemes can be categorized into two main categories: switch-based control schemes and continuous control schemes [13, 14, 15]. In the switch-based control schemes, the control authority is transferred as a lumped whole from human to automation or back to human. Depending on the scheme, transfers may be initiated by the human driver, by the automation system, or by a separate arbitration, algorithm [7, 11, 12]. Switch-based control schemes involve issues such as a protracted-time interval required for full transfer, misinterpretation or misappropriation of responsibility (called mode errors), and incomplete understanding of the environment state (loss of situation awareness) [16, 17, 7]. Researchers have proposed various schemes under which the control authority is continuously shared between humans and automation to address these shortcomings. Two main groups of these schemes are

input-mixing control and haptic shared control [15, 18, 19, 20, 21, 22, 23, 24, 25]. The main difference between these two paradigms is that haptic shared control paradigms involve a dynamic coupling between a human driver and automation through the steering wheel. In contrast, the input-mixing paradigms do not involve such a coupling. The dynamic coupling allows the driver to remain bodily in the loop, with his/her hands on a motorized steering wheel. A valuable feature of haptic shared control is that the role (e.g., leader/follower) played by each agent and the level of authority held by each agent (how much control an agent exerts) is a dynamic outcome of the interaction between the two agents and the vehicle [26, 27, 28, 29]. The feature of role and level of authority being outcomes of the interaction in haptic shared control is in sharp contrast to the control sharing paradigm of input mixing, where a third party imposes the level of authority (an agent or algorithm that assesses current threat) and potentially make the haptic shared control to be more robust to automation's misses, and faults [15, 20, 18, 30, 10].

Balancing between the driver's preference and the joint task's safety in a haptic shared control may result in several possible handover strategies that differ mainly in human's and automation's shared conventions. Here, we define conventions as the shared knowledge that emerges from repeated interactions [31]. Consider a scenario when the human and automation see an obstacle but decide to maneuver around different sides of the obstacle (see Figure 4.2). If both human and automation applies the same torque, but in the opposite direction on the steering wheel, they cancel out each other's input, and the vehicle would hit the obstacle. Three possible solutions to resolve such a conflict are, the automation can apply a lower torque and yield the control to the human-driver. On the other hand, the automation can apply a higher torque and gain control from the human driver. Also, the automation can adapt its desired path and select a path similar to the human driver. Since the human driver is a non-stationary partner meaning different humans may prefer different forms of

handover policy, it is important to study the principles of convention formation so that we can design an adaptable automation system that can (to some extent) personalize its behavior to the human partner.

To study convention, a wide range of approaches such as the theory of mind, game theory, and pragmatic reasoning are focused on modeling the human reasoning over the partner's states and strategies based on observations of their actions and unfolding events [32, 33, 34, 35]. The main drawback of these approaches is that they become easily computationally intractable and therefore can not be used to adapt robot's behavior in real-time [31]. The other group of studies employ multi-agent reinforcement learning techniques to qualitatively detect emergent conventions through post-hoc assessment of the learned strategies [36]. But, these studies do not provide a platform that separates partner-specific conventions from task-dependent representations, making it challenging to leverage learned conventions [31]. Recently, a few studies have proposed a platform to separate partner-specific conventions from task-dependent representations [31, 37] using a two-player Markov Decision Process (MDPs) framework.

In this paper, we follow the same idea but instead of employing MDP framework, we propose a framework wherein the human and automation actions are defined based on optimization of a set of cost functions. Here, we model the human and automation cost function for driving a semi-automated vehicle (e.g., obstacle avoidance) as a weighted linear combination of a set of features that a human and automation care about (e.g., collision avoidance, staying on the road, or distance to the final goal). While these features can represent the task, we argue that the distribution of the weights associated with these features and how they may evolve in time can be used as a proxy to learn and leverage the conventions formed between the human driver and automation system. Additionally, defining the concept of cooperative and competitive cost functions, we create a map to characterize the outputs of human-automation

interaction under different conventions. Using such a map, an adaptable automation system can be designed to change its behavior adaptive and form a desirable convention with a human driver.

To adaptively form conventions, an automation system should automatically learn complex policies and adjust its behavior accordingly. While model-predictive-base approaches are powerful tools to deal with the uncertainty and complexity of human-automation interaction, they lack the learning capability [38, 39, 40, 41, 42]. On the other hand, conventional end-to-end learning algorithms require significant amounts of data (hundreds or even thousands of experiments) to achieve a desired level of performance that may not be feasible. To merge the strengths of these approaches, recent efforts have been focused on combining data-driven techniques learning with the model-based controller [39]. For instance, several approaches have used reinforcement learning (RL) based methods to update the hyper-parameters of the model-predictive controller (MPC) [43, 44, 45, 38]. Although there have been few works combining MPC with learning-based techniques, there seems to be no such work done for the problem in the context of convention formation to the best of our knowledge. To this end, we implement a DDPG based RL method to select appropriate weights for the automation's cost function such that the automation can adapt its desired steering policy if needed. We test the performance of our convention formation framework in the context of resolving a conflict between a human-driver and automation.

In summary, the main contributions of this paper are (i) creating and testing a method that can be used for extracting modular structure which separates partner-specific conventions from task-dependent representations; (ii) characterizing a map that can connect the space of conventions to outcomes of a human-automation interaction for resolving the reverse intent conflict, (iii) development of an adaptable automation system that can form a convention with a human driver.

The outline of this paper is as follows. Section II presents the model of the adaptive

haptic shared control paradigm. Section III presents the principles of the convention formation in a haptic shared control paradigm. In this section, we propose the basics of a modular structure that can be used for separating partner-specific conventions from task-dependent representations. Using this structure, we create a map to connect different forms of the conventions with the outputs of the human-automation interaction. We further develop an RL-based MPC-controller for the automation system to enable it to form conventions adaptively. Section IV presents numerical results, followed by Section V, which presents the conclusions and plan.

4.2 Adaptive Haptic Shared Control Framework

Figure 4.1 shows a schematic of an adaptive haptic shared control paradigm. Three entities each impose a torque on the steering wheel: a driver through his hands, an automation system through a motor, and the road through the steering linkage.

We model the human and automation system with a similar structure. We model the driver as a hierarchical two-level controller. The upper-level control represents the cognitive controller, and its output, θ_H, represents the driver's intent. The lower-level represent the human's biomechanics, z_H, and is considered back-drivable [46]. To indicate that driver's biomechanic parameters vary with changes in grip on the steering wheel, use of one hand or two, muscle co-contraction, or posture changes, we have drawn an arrow through human z_H. Similarly, the automation system is modeled as a higher-level artificial intelligence (AI) coupled with a lower-level impedance controller. The automation system is also considered to be back-drivable, and the gains of the impedance controller, z_A, are designed to be modest rather than infinite. In other words, the automation is not intended to behave as an ideal torque source; instead, the automation imposes its command torque τ_A through an impedance z_A that is approximately matched to the human impedance z_H.

Modeling the driver as a spring-mass-damper with a proximal motion source $\theta_H(t)$,
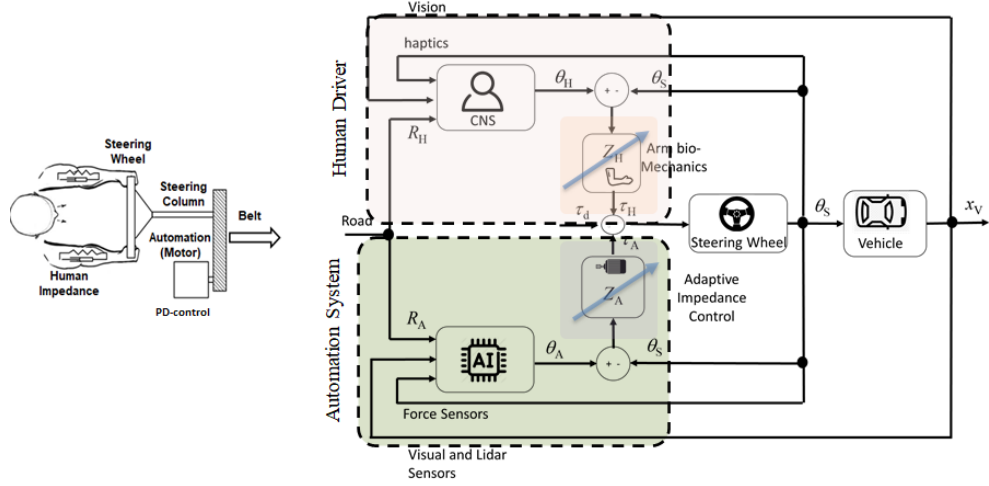
Figure 4.1: A schematic of a haptic shared control paradigm. The human and automation are modeled as two-level controller that their dynamics are coupled through the steering wheel.

the torque applied by the human on the steering wheel is [47]

$$\tau_{\mathrm{H}} = -J_{\mathrm{H}}\ddot{\theta}_{\mathrm{SW}} + b_{\mathrm{H}}(\dot{\theta}_{\mathrm{H}} - \dot{\theta}_{\mathrm{SW}}) + k_{\mathrm{H}}(\theta_{\mathrm{H}} - \theta_{\mathrm{SW}}) \tag{4.1}$$

where J_{H}, b_{H}, and k_{H} are the inertia, damping and stiffness of the driver's arm. Similarly, considering an impedance controller in the lower-level of the automation system, the torque generated by the motor can be presented as

$$\tau_{\mathrm{A}} = b_{\mathrm{A}}(\dot{\theta}_{\mathrm{A}} - \frac{r_{\mathrm{S}}}{r_{\mathrm{M}}}\dot{\theta}_{\mathrm{S}}) + k_{\mathrm{A}}(\theta_{\mathrm{A}} - \frac{r_{\mathrm{S}}}{r_{\mathrm{M}}}\theta_{\mathrm{S}}) \tag{4.2}$$

where k_{A}, b_{A} represent the gains of the impedance controller and $r_{\mathrm{S}}/r_{\mathrm{M}}$ is the mechanical advantages of a timing belt connecting the motor to the steering wheel. Human and automation system can modulate their gains $z_{\mathrm{H}} = [b_{\mathrm{H}} \ k_{\mathrm{H}}]^{\mathrm{T}}$, $z_{\mathrm{A}} = [b_{\mathrm{A}} \ k_{\mathrm{A}}]^{\mathrm{T}}$ to gain or yield the control [47].

We use a differential torque sensor between the steering wheel and steering shaft to measure the differential torque between humans and automation. The magnitude of the differential torque can be used as a metric for identifying the level of cooper-

ativeness between humans and automation [47]. We model the torque measured by the torque sensor as

$$\tau_\text{T} = K_\text{T}(\theta_\text{SW} - \theta_\text{S}) \tag{4.3}$$

Furthermore, we adopt the bicycle model to describe the vehicle dynamics [48]. In particular,

$$\dot{x}_\text{V} = A_\text{V} x_\text{V} + B_\text{V} \theta_\text{S} \tag{4.4}$$

where θ_S is the steering column angle and $x_\text{V} = [v_y \quad \omega \quad y_\text{V} \quad \psi]^\text{T}$ are states of the vehicle, and

$$A_\text{V} = \begin{bmatrix} -\frac{C_{\alpha f} + C_{\alpha r}}{m v_x} & \frac{-l_f C_{\alpha f} + l_r C_{\alpha r} - m v_x^2}{m v_x} & 0 & 0 \\ \frac{l_f C_{\alpha f} - l_r C_{\alpha r}}{I_z v_x} & \frac{-l_f^2 C_{\alpha f} + l_r^2 C_{\alpha r}}{I_z v_x} & 0 & 0 \\ 1 & 0 & 0 & v_x \\ 0 & 1 & 0 & 0 \end{bmatrix}, \tag{4.5}$$

$$B_\text{V} = \begin{bmatrix} \frac{C_{\alpha f}}{m r_{sw}} & \frac{l_f C_{\alpha f}}{I_z r_{sw}} & 0 & 0 \end{bmatrix}^\text{T} \tag{4.6}$$

Here, $v_y(t)$ is the lateral velocity, $\omega(t)$ is the yaw velocity ,$\psi(t)$ is the yaw angle of vehicle , $y_\text{V}(t)$ is the lateral displacement and $C_{\alpha f}, C_{\alpha r}, m, I_z, I_r, l_f, l_r$ and r_{sw} are vehicle parameters.

By combining the vehicle dynamics and the dynamics of the human-machine interaction on the steering wheel, the equation of motion for a haptic shared control can be expressed as

$$\dot{x}(t) = f(x(t), p(t), w(t)) + B_A(p(t))u_A(t) + B_H(p(t))u_H(t) \qquad (4.7a)$$

$$y = h(x(t)); \qquad (4.7b)$$

where $x = [\theta_{SW}\ \dot{\theta}_{SW}\ \theta_S\ \dot{\theta}_S\ x_V^T]^T$, are the state of the integrated system, $u_A = [\theta_A\ \dot{\theta}_A]^T$, and $u_H = [\theta_H\ \dot{\theta}_H]^T$ are the automation system and the human driver's control commands, $p(t) = [z_H^T\ z_A^T]^T$ are the time-varying parameters of the system, and $w(t) = \tau_V$ is exogenous signals, and

$$f(x(t), p(t), w(t)) = \begin{bmatrix} \dot{\theta}_{SW} \\ \dfrac{-b_H\dot{\theta}_{SW} - k_H - \theta_{SW} - K_T(\theta_{SW} - \theta_S)}{J_{SW} + J_H} \\ \dot{\theta}_S \\ \dfrac{-\left(\frac{r_S}{r_M}\right)^2 b_A\dot{\theta}_S - \left(\frac{r_S}{r_M}\right)^2 k_A\theta_S + K_T(\theta_{SW} - \theta_S) + \tau_v)}{J_S + \left(\frac{r_S}{r_M}\right)^2 J_M} \end{bmatrix} \qquad (4.8a)$$

$$B_H(p(t)) = \frac{1}{J_{SW} + J_H} \begin{bmatrix} 0 & 0 & 0 & 0 \\ k_H & b_H & 0 & 0 \\ 0 & 0 & 0 & 0 \\ 0 & 0 & 0 & 0 \end{bmatrix} \qquad (4.8b)$$

$$B_A(p(t)) = \frac{\frac{r_S}{r_M}}{J_S + \left(\frac{r_S}{r_M}\right)^2 J_M} \begin{bmatrix} 0 & 0 & 0 & 0 \\ 0 & 0 & 0 & 0 \\ 0 & 0 & k_A & b_A \\ 0 & 0 & 0 & 0 \end{bmatrix} \qquad (4.8c)$$

It should be noted that in this paper, we assume all the measured variables y are accessible. In practice, θ_S can be measured using the encoder attached to the steering column, τ_T can be measured using the differential torques indicating the
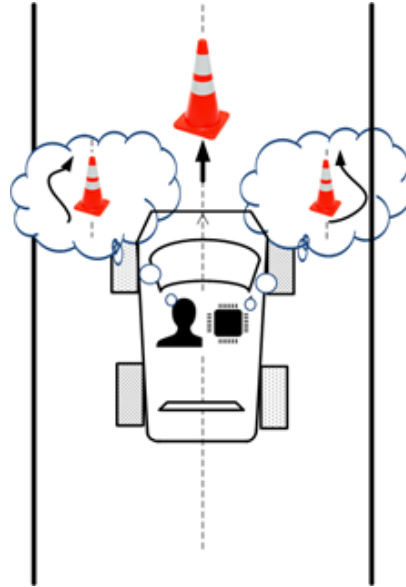
Figure 4.2: Demonstration of a scenario when both human and automation systems select a different path for avoiding obstacle

difference between θ_{SW} and θ_{S}. Additionally, k_{H} and b_{H} can be estimated using various techniques such as identification techniques discussed in [49, 50] and k_{A} and b_{A} are design parameters and directly can be calculated.

4.3   Convention Formation through Intention Negotiation

In a haptic shared control paradigm, there are can be scenarios where a human and automation face a conflict. For instance, Figure 4.2 shows a scenario when both human and automation systems see an obstacle and select a different path for avoiding it. In such a scenario, if both the human and automation select the same impedance ($z_{\text{H}} = z_{\text{A}}$), their control commands cancel out each other, and the vehicle hits an obstacle. In addition, to reverse intents, the other forms of conflicts can be considered when (i) one agent does not provide any control inputs (e.g., one agent does not detect an obstacle), (ii) too much or too little inputs (e.g., two agents have different perceptions from the size/position of an obstacle), (iii) control inputs arrive too early or too late, and (iv) additional inputs cause conflict (e.g., disturbance feedback from the road).

To potentially resolve a conflict such as having a reverse intent, the human and automation can adapt their control strategies by modulating their impedance parameters [47] and also by updating their steering commands θ_H and θ_A. While there might be multiple strategies for resolving a conflict (e.g., updating their steering commands or modulating their impedance parameters), some of these strategies may be more preferable than others to the human-driver. The idea behind the convention formation is to narrow the possible strategies for collaboration into a subset of these strategies to which the human partner might naturally be more gravitated.

To achieve this goal, three technical challenges must be met. First, we need to create a modular structure that separates partner-specific conventions from task-dependent representations. Second, using this structure, a map shall be developed to connect conventions to the outputs of human-automation interaction. Third, an adaptable automation system shall be designed to learn complex policies and adapt its behavior so that a desirable shared convention can be reached. Below, we discuss our approach for addressing these three challenges.

4.3.1 Distinguishing Partner-specific Conventions from Task-dependent Representations

To be able to learn and leverage conventions, we need to create a modular structure that separates partner-specific conventions from task-dependent representations. To this end, in this paper, we consider a structure where in the human and automation's steering commands at the higher-level can be determined by optimizing cost functions J_H, and J_A, respectively. These cost functions are defined as a combination of a set of hand-coded features $\phi_H = [\phi_{H,1} \ \cdots \ \phi_{H,n_H}]^T$ and $\phi_A = [\phi_{A,1} \ \cdots \ \phi_{A,n_A}]^T$ and vectors of the weights $w_H = [w_{H,1} \ \cdots \ w_{H,n_H}]$ and $w_A = [w_{A,1} \ \cdots \ w_{A,n_A}]$. In particular, $J_H = \phi_H w_H$ and $J_A = \phi_A w_A$. The hand coded features can be defined as possible maneuvering paths and the control effort for each agent.

The focus of this paper is to develop a platform wherein the concept of conven-

tions can be utilized for resolving a conflict between a human driver and automation system. To this end, we select an example of conflict as shown in Figure 4.2. In this scenario, both human and automation may see an obstacle and they have two possible maneuvering trajectories r_R from the right side and r_L from the left side of the obstacle. To determine their steering commands, they both solve an optimization problem as follow:

$$\min_{\theta_\mathrm{H}} J_\mathrm{H}(x,u) = \sum_{k=1}^{N_p} \left(\|y_\mathrm{V}(k) - r_\mathrm{R}(k)\|_{w_\mathrm{HR}} + \|y_\mathrm{V}(k) - r_\mathrm{L}(k)\|_{w_\mathrm{HL}} + \|\theta_\mathrm{H}(k)\|_{w_\mathrm{H\theta}} \right)$$
(4.9a)

$$\min_{\theta_\mathrm{A}} J_\mathrm{A}(x,w) = \sum_{k=1}^{N_p} \left(\|y_\mathrm{V}(k) - r_\mathrm{R}(k)\|_{w_\mathrm{AR}} + \|y_\mathrm{V}(k) - r_\mathrm{L}(k)\|_{w_\mathrm{AL}} + \|\theta_\mathrm{A}(k)\|_{w_\mathrm{A\theta}} \right)$$
(4.9b)

$$\text{s.t.} \quad x_\mathrm{d}(k+1) = f_\mathrm{d}(x_\mathrm{d}(k), p(k), d(k)) + B_\mathrm{d,H}(p(k)_\mathrm{d})u_\mathrm{H}(k) + B_\mathrm{d,A}(p(k))u_\mathrm{A}(k)$$
(4.9c)

Here, Eq. (4.9c) describes the discrete dynamics of the haptic shared control framework. In this paper, we derived the discrete dynamics using zero-order hold on the inputs and a sample time of T_s and N_p is a horizon time. Here $\phi_{\mathrm{H},1} = \phi_{\mathrm{A},1} = \|y_\mathrm{V} - r_\mathrm{R}\|$ and $\phi_{\mathrm{H},2} = \phi_{\mathrm{A},2} = \|y_\mathrm{V} - r_\mathrm{L}\|$ represent possible strategies for maneuvering the vehicle from the right or left of the obstacles. The last term (i.e., $\phi_{\mathrm{H},3} = \|\theta_\mathrm{H}\|$ and $\phi_{\mathrm{A},3} = \|\theta_\mathrm{A}\|$) represent the control effort value. The weight distribution over these features determines the interaction behavior between the human and automation. Three examples of these behaviors are discussed below.

First, let define ϵ_comp, ϵ_coop, and $\epsilon_\mathrm{undecided}$ to be three design parameters. Also, let assume $w_\mathrm{H\theta} = w_\mathrm{A\theta} = const$. Furthermore, assume $w_\mathrm{AR} = 1 - w_\mathrm{AL}$ and $w_\mathrm{HR} = 1 - w_\mathrm{HL}$. Then, for a fixed $w_\mathrm{H} = [w_\mathrm{HR} \ w_\mathrm{HL} w_\mathrm{H\theta}]$, the automation system's can adopt different

levels of cooperativeness by assigning how weight vectors $w_A = [w_{AR} \ w_{AL} w_{A\theta}]$ shall be distributed. If the driver selects one of the two paths ($|w_{HR} - w_{HL}| > \epsilon_{undecided}$), then, three human-automation interaction behavior at the higher-level can be defined as

- Uncooperative Automation: When automation selects a different path than the human driver. This behavior can be described when $|w_{HR} - w_{AL}| \leq \epsilon_{comp}$. Similarly, it can be described when $|w_{HL} - w_{AR}| \leq \epsilon_{comp}$.

- Undecided Automation: The automation's assign similar weights to the two paths around the obstacle. This behavior can be described when $|w_{AR} - w_{AL}| \leq \epsilon_{undecided}$.

- Cooperative Automation: When automation selects a path similar to the human driver. This behavior can be described when $|w_{HR} - w_{AR}| \leq \epsilon_{coop}$. Similarly, $|w_{HL} - w_{AL}| \leq \epsilon_{coop}$.

Note, the driver can be also undeceives meaning $|w_{HR} - w_{HL}| \leq \epsilon_{undecided}$ but for the sake of brevity, we don't consider such a case in this paper.

4.3.2 Characterization of Convention Maps

To be able to adapt automation system so that a desired convention can be reached, a map should be created to connect the space of convention to the outcomes of human-automation interaction. To create such a map, the first step is to determine driver and automation's intents. To this end, we employ an open-loop Nash solution [51] wherein it is assumed that each agent minimize its own cost function considering the optimal input of the other agent. In particular, the steering angle pair θ_H and θ_A is a Nash solution if the following holds.

1. The control θ_H^* provides a solution to the optimal control problem of the human

driver's cost function. Specifically,

$$\theta_{\text{H}}^* = \underset{\theta_{\text{H}}}{\text{argmax}}\left(J_{\text{H}}(x, \theta_{\text{H}}, \theta_{\text{A}}^*)\right) \tag{4.10}$$

where θ_{A}^* is the optimal solution of automation's cost function.

2. The control θ_{A}^* provides a solution to the optimal control problem of the automation's cost . The control θ_{H}^* provides a solution to the optimal control problem of the human driver's cost function. Specifically,

$$\theta_{\text{A}}^* = \underset{\theta_{\text{A}}}{\text{argmax}}\left(J_{\text{A}}(x, \theta_{\text{H}}^*, \theta_{\text{A}})\right) \tag{4.11}$$

where θ_{H}^* is the optimal solution of automation's cost function.

The two optimization problem will be solved iteratively until the Nash optimal solution $(\theta_{\text{H}}^*, \theta_{\text{A}}^*)$ is reached. Specifically,

$$J_{\text{H}}(\theta_{\text{H}}^*, \theta_{\text{A}}^*) \leq J_{\text{H}}(\theta_{\text{H}}^*, \theta_{\text{A}}) \tag{4.12}$$

$$J_{\text{A}}(\theta_{\text{H}}^*, \theta_{\text{A}}^*) \leq J_{\text{A}}(\theta_{\text{H}}, \theta_{\text{A}}^*) \tag{4.13}$$

We solve the two optimization problem using C-GMRES technique [52]. The details of the C-GMRES is described in the [47].

It should be noted that the sufficient conditions for having a unique Nash solution is given in [53]. In the context of haptic shared control, these conditions are (i) the domains of $\theta_{\text{A}}(t)$ and $\theta_{\text{H}}(t)$ are closed and convex subsets of $\mathbb{R}^2$; (ii) two matrices B_{A}, $B_{\text{H}}(t)$ continuously depend on time t and the states of the integrated system $x(t)$; (iii) the Lagrangian of the cost functions be strictly convex; and (iv) the Lagrangian is have superlinear growth [53]. It follows from Eq. (4.9) that all these conditions are satisfied and therefore there is a unique Nash solution to the optimization problem described by Eq. (4.9).

The main goal behind leveraging conventions is to determine a behavior for the automation system such that the overall cost functions of the human and automation system is minimized. In particular,

$$J_{\mathrm{H}}(\theta_{\mathrm{H}}^*, \theta_{\mathrm{A}}^*) + J_{\mathrm{A}}(\theta_{\mathrm{H}}^*, \theta_{\mathrm{A}}^*) = \min_{\theta_{\mathrm{H}}, \theta_{\mathrm{A}}} \left(J_{\mathrm{H}}(\theta_{\mathrm{H}}, \theta_{\mathrm{A}}) + J_{\mathrm{A}}(\theta_{\mathrm{H}}, \theta_{\mathrm{A}}) \right) \tag{4.14}$$

However, this choice may favor one agent much more that the other. For example, $J_{\mathrm{A}}(\theta_{\mathrm{H}}^*, \theta_{\mathrm{A}}^*) \ll J_{\mathrm{H}}(\theta_{\mathrm{H}}^*, \theta_{\mathrm{A}}^*)$. Such an outcome which may not be agreeable to one agent (i.e., human driver in this case). To resolve this problem, the concept of co-operative and competitive (co-co) game theory has been established [54]. This co-co concept models a situation where one agent pays/receives an incentive to implement a strategy that minimizes the combined cost function. Specifically, employing a co-co game, the original game can be split as the sum of a purely cooperative game, where both players have the same cost function, and a purely competitive (i.e., zero-sum) game, where the players have opposite cost functions [55]. An issue regarding the cooperative-competitive game is that the incentive amount shall be known.

In this paper, instead of solving the co-co game, we split the combined cost function of the human and automation systems into two competitive J_{comp} and cooperative J_{coop} cost functions and calculate their values at the Nash solution (i.e., θ_{H}^* and θ_{A}^*). In particular

$$J_{\mathrm{coop}}(\theta_{\mathrm{H}}^*, \theta_{\mathrm{A}}^*) = \frac{J_{\mathrm{H}}(\theta_{\mathrm{H}}^*, \theta_{\mathrm{A}}^*) + J_{\mathrm{A}}(\theta_{\mathrm{H}}^*, \theta_{\mathrm{A}}^*)}{2}, \tag{4.15a}$$

$$J_{\mathrm{comp}}(\theta_{\mathrm{H}}^*, \theta_{\mathrm{A}}^*) = \frac{J_{\mathrm{H}}(\theta_{\mathrm{H}}^*, \theta_{\mathrm{A}}^*) - J_{\mathrm{A}}(\theta_{\mathrm{H}}^*, \theta_{\mathrm{A}}^*)}{2} \tag{4.15b}$$

It follows from Eq. (4.15) that $J_{\mathrm{H}} = J_{\mathrm{coop}} + J_{\mathrm{comp}}$ and $J_{\mathrm{A}} = J_{\mathrm{coop}} - J_{\mathrm{comp}}$.

To create the convention map, we evaluate the values of J_{coop} and J_{comp} for a range of weights w_{H} and w_{A} (see Figure 4.4). To form a desirable conventions, it is desirable to minimize J_{coop} and also keep J_{comp} as close as possible to zero (i.e.,

cooperation is maximum and competition is minimum). To this end, we developed an adaptable automation system that for a given w_H, determines an appropriate w_A such the conflict is resolved while the safety of the vehicle is guaranteed.

4.3.3   Design an Adaptable Automation System

To adaptively form conventions, an automation system should be able to automatically learn and perform complex decision-making policies. In the context of the intent negotiation with the human driver this means that the automation system should be able to adjust the weights of its higher-level cost function and produce a desired steering behavior. To this end, we develop an episode-based policy search using Deep Deterministic Policy Gradients (DDPG) technique to determine automation's optimal policies (i.e., automation's model-predictive weights vector w_A– See Figure 4.3). We select DDPG since it is deemed particularly powerful in handling continuous action spaces and its relative simplicity. Our action space is naturally continuous, as the choice of the automation's weight vector can take any real value in a constrained range.

Figure 4.3 shows the structure of the DDPG approach that includes two neural networks named critic and actor networks. At each time-step k, the DDPG algorithm receives a system states feedback $S_k = [x^T(k)\, p^T(k)]^T$ as its observation, and generates action $A_k = \{\omega_{AR,i},\ \omega_{AL,k}\}$ from the action set $\mathbb{A}$ according to a policy $\pi(S_k)$. The undertaken action A_k (penalty weights) results in a scalar reward r_k and the updated system states S_{k+1}.

A DDPG algorithm aims to determine an optimal policy such that the aggregated discounted future reward defined as $\mathcal{R}_i = \sum_{i=0}^{\infty} \gamma^i\, r_{k+i}$ is maximized. Here, $\gamma = (0,\ 1]$ is the discount factor. To this end, the DDPG algorithm use the Q-value function $Q(S, A)$ and the deterministic policy $\pi(S)$. Here, S and A are state and action spaces, respectively. In the learning phase, at each time step, the DDPG algorithm updates the actor and critic networks properties and stores the experiences in the previous
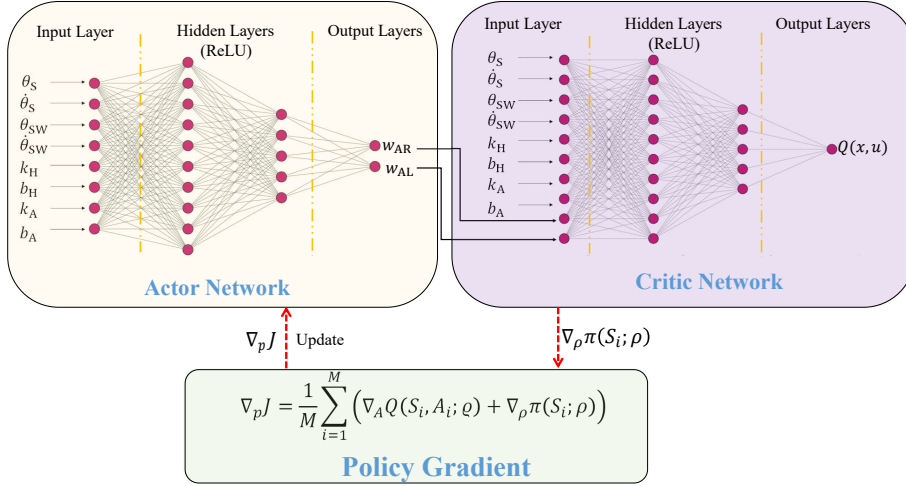
Figure 4.3: Schematic diagram of the DDPG with the system states as the input for actor and critic networks.

time-steps by a circular buffer. A mini-batch of randomly sampled experiences from the circular buffer updates the actor and critic [56]. The DDPG algorithm at each training step perturbs the action selected by the policy using stochastic noise.

The DDPG agent contains four function approximators name: actor $\pi\left(S;\rho\right)$, target actor $\pi_{\text{trg}}\left(S;\rho_{\text{trg}}\right)$, critic $Q(S,A;\varrho)$, and target critic $Q_{\text{trg}}(S,A;\varrho_{\text{trg}})$ to estimate the value function and policy. Here $\{\rho,\ \rho_{\text{trg}},\ \varrho,\ \varrho_{\text{trg}}\}$ are the parameters of the networks. At the actor network, the policy $\pi\left(S;\rho\right)$ generates action A to maximize the long-term reward based on the states S. At the critic network, the $Q(S,A;\varrho)$ function generates the long-term reward expectation based on the states S and action A. The target actor and target critics with the same structure and parameterization as the actor and critics, respectively, are employed to improve the stability of the optimization. During the training phase, the DDPG agent adjusts the parameter values in $\{\rho,\ \rho_{\text{trg}},\ \varrho,\ \varrho_{\text{trg}}\}$ and these parameters remain at their tunned value after the training phase. Algorithm 1 described the training of the DDPG network at each time step [56]. The DDPG algorithm updates the critics' network parameters ϱ by minimizing the following loss

function:

$$L = \frac{1}{M} \sum_{k=1}^{M} \left(Q\left(S_k, A_k; \varrho\right) - \ell_k \right)^2 \tag{4.16}$$

where M is the number of DDPG's training episode.

$$\ell_k = r(S_k, A_k) + \gamma Q\left(S_{k+1}, \kappa\left(S_{k+1}\right); \varrho\right)$$

$$\kappa\left(S_{k+1}\right) = \operatorname*{argmax}_{A} Q(S, A) \tag{4.17}$$

Here, $\kappa(S)$ is a greedy policy from the Q-learning algorithm. The sampled policy gradient $\nabla_p J$ for maximizing the discounted reward $\mathcal{R}$ is:

$$\nabla_p J = \frac{1}{M} \sum_{i=1}^{M} \left(\nabla_A Q\left(S_i, A; \varrho\right) + \nabla_\rho \pi\left(S_i; \rho\right) \right) \tag{4.18}$$

Here, $\nabla_A Q$ and $\nabla_\rho \pi$ are gradients of the critic and actor, respectively, with respect to the action computed by the actor A and the actor parameters ρ. These gradients are evaluated for states S_k. The sampled policy gradient $\nabla_p J$ updates the actors' network parameters ρ. The target actor ρ_{trg} and critic ϱ_{trg} parameters in the DDPG agent are updated based on the smoothing method at every time sample with a smoothing factor $\mathcal{K}$.

$$\varrho_{\text{trg}} = \mathcal{K} \varrho + (1 - \mathcal{K}) \varrho_{\text{trg}} \tag{4.19}$$

$$\rho_{\text{trg}} = \mathcal{K} \rho + (1 - \mathcal{K}) \rho_{\text{trg}} \tag{4.20}$$

The aggregated reward and the state errors are stored in their dedicated buffer in each episode. These buffers supply the observation and the reward value to the DDPG algorithm. The update rate of the automation systems' penalty weights in the training phase on the DDPG agent is the same as the episode length. In this paper, for each

set of weights, the nonlinear MPC of the automation system is executed 100 times, and in each execution time, the model propagated to cover the view horizon.

Algorithm 3: DDPG agents training algorithm

- Initialization of actor $\pi(S; \rho)$ and critic $Q(S, A; \varrho)$ networks with random weights ρ and ϱ
- Initializing target networks $\pi_{trg}(S; \rho_{trg})$ and critic $Q_{trg}(S, A; \varrho_{trg})$ with weights $\rho_{trg} = \rho$ and $\varrho_{trg} = \varrho$
- Set up an empty experience buffer R

for episode = 1 to M **do**

  1: Begin with an Ornstein-Uhelnbeck (OU) noise $\mathcal{N}$ for exploration

  2: Receive initial observation state

  3: Apply action A, Observe the reward R and next observation S'.

  4: Store transitions (S_i, A_i, R_i, S_{i+1}) into experience buffer R.

  5: Sample a random mini-batch of M experiences from the experience buffer.

  6: value function target $y_i = R_i + \gamma Q_{trg}\big(S_i', \pi_{trg}(S_i'; \rho_{trg}), ; \varrho_{trg}\big)$

  7: Update the critic parameters by minimizing the loss L across all sampled experiences.

  8: Update the actor policy using the sampled policy gradient $\nabla_\rho J$.

  9: Update the target networks by smoothing factor k.

end

4.4 Numerical Simulations and Discussion

In this section, we present a series of simulation studies demonstrating the effectiveness of the convention formation for resolving a conflict between a human driver and automation system. The following simulations consider a scenario where the human driver and the automation system detect an obstacle and negotiate on controlling the steering wheel to safely avoid the obstacle. We consider the two cost functions in Eqs. (4.9) for the human-driver and automation system. Table 4.1 shows the numerical values that are used in the simulation. Here, we select different values for the parameters of the human driver and automation's impedance controllers to demonstrate

different lower-level interaction modes. (e.g., active-safety vs. assistive mode.)

Figure 4.4 shows the competitive-cooperative cost functions values for a range of w_A and w_H in three lower-level interaction modes named active safety, neutral and assistive modes. Specifically, we define active safety mode when the parameters of the automation's impedance controller is larger than the parameters of the human driver's bio-mechanics ($z_A - z_H > \epsilon_1$). The assistive mode is when the parameters of the automation's impedance controller is smaller than the parameters of the human driver's bio-mechanics ($z_H - z_A > \epsilon_1$). Finally, the neutral is when the human and automation's impedance parameters are almost the same ($|z_H - z_A| < \epsilon_1$). Here, we considered $z_A = 0.1z_H$ in the assisitve mode, $z_A = z_H$ in the neutral and $z_A = 10z_H$ in the active-safety mode. To create the conventions map, we considered $w_{HR} = 1 - w_{HL}$ and $w_{H\theta} = 1$. Similarly, we considered $w_{AR} = 1 - w_{AL}$ and $w_{A\theta} = 1$.

It follows from Figure 4.4 that the convention maps for the cooperative surfaces have two maximum points. These two maximum points are when $[w_{HR} \ w_{AR}] = [0 \ 0]$ representing a scenario when both agents choose the left path to avoid the obstacle or when $[w_{HR} \ w_{AR}] = [1 \ 1]$ representing a scenario when both agents choose the left path to avoid the obstacle. The competitive cost surfaces have also two maximum points. Specifically, the competitive cost value is maximum when $[w_{HR} \ w_{AR}] = [0 \ 1]$ representing a scenario when human driver choose the left path but automation choose the right path to avoid the obstacle or when $[w_{HR} \ w_{AR}] = [1 \ 0]$ representing a scenario when human driver choose the right path but automation choose the left path to avoid the obstacle.

Comparing the shape of cooperative and competitive surfaces for the three lower-level interaction modes, it can be seen that by changing the lower-level interaction mode the flatness of the convention map for the cooperative/competitive value surfaces and the direction of curvature of the competitive value surface varies. It should be noted that since the competitive surface defines the payoff of one agent to the

Table 4.1: Numerical values for the system parameters in the simulation

Parameters	Description	Haptic Interaction mode		Units
		Active-Safety	Assistive	
k_{H}	Driver arms stiffness	0.5	3	N.m/rad
b_{H}	Driver arms damping	0.2	0.5	N.m.s/rad
k_{A}	Automation's initial value of the arms stiffness	0.5	3	N.m/rad
b_{A}	Automation's initial value of the arms damping	0.2	0.5	N.m.s/rad
$\beta_{\mathrm{k_A}}$	Activation coefficient of k_{A}	1		-
$\beta_{\mathrm{b_A}}$	Activation coefficient of b_{A}	1		-
$\alpha_{\mathrm{k_A}}$	Memory coefficient of k_{A}	-1		-
$\alpha_{\mathrm{b_A}}$	Memory coefficient of b_{A}	-1		-
J_{H}	Driver arms inertia	1×10^{-3}		kg.m^2
J_{SW}	Steering wheel inertia	1×10^{-2}		kg.m^2
J_{S}	Steering column inertia	1×10^{-2}		kg.m^2
J_{M}	Motors inertia	1×10^{-3}		kg.m^2
K_{T}	Torque sensor stiffness	1000		N.m/rad
$r_{\mathrm{S}}/r_{\mathrm{M}}$	Timing belt mechanical advantage	1		-
m	Total mass of vehicle	1385		kg
I_{z}	Vehicle yaw moment of inertia	2065		kg.m^2
l_{f}	Distance from CG to front axle	1.114		m
l_{r}	Distance from CG to rear axle	1.436		m
r_{sw}	Steering ratio	15		
C_{f}	Front cornering stiffness	85,000		N/rad
C_{t}	Rear cornering stiffness	123,000		N/rad
v_{x}	Vehicle longitudinal velocity	20		m/sec
$N_{\mathrm{P_{Imp}}}$	Prediction horizon for Impedance Control	10		-
$N_{\mathrm{P_{H\_L}}}$	Prediction horizon for Higher-level Controller	100		-
$N_{\mathrm{C_{Imp}}}$	Control horizon for Impedance Control	2		-
$N_{\mathrm{C_{H\_L}}}$	Control horizon for Higher-level Controller	20		-
T_{s}	Simulation time step	0.002		sec
$\mathcal{I}_{\mathrm{max\_out}}$	Maximum index for outer iteration C/GMRES algorithm	5		-
$\mathcal{I}_{\mathrm{max\_in}}$	Maximum index for inner iteration C/GMRES algorithm	10		-
δ	KKT vector norm range	1×10^{-2}		-
λ_{rate}	Learning rate	0.001		-
γ	Discount Factor	0.9		-
-	Mini-Batch size	128		-
-	Reply buffer size	1×10^{5}		-
-	Reply start size	300		-
$\mathfrak{k}$	Target update smoothing factor	0.01		-
M_{sub}	Time steps for fixe weights	200		-
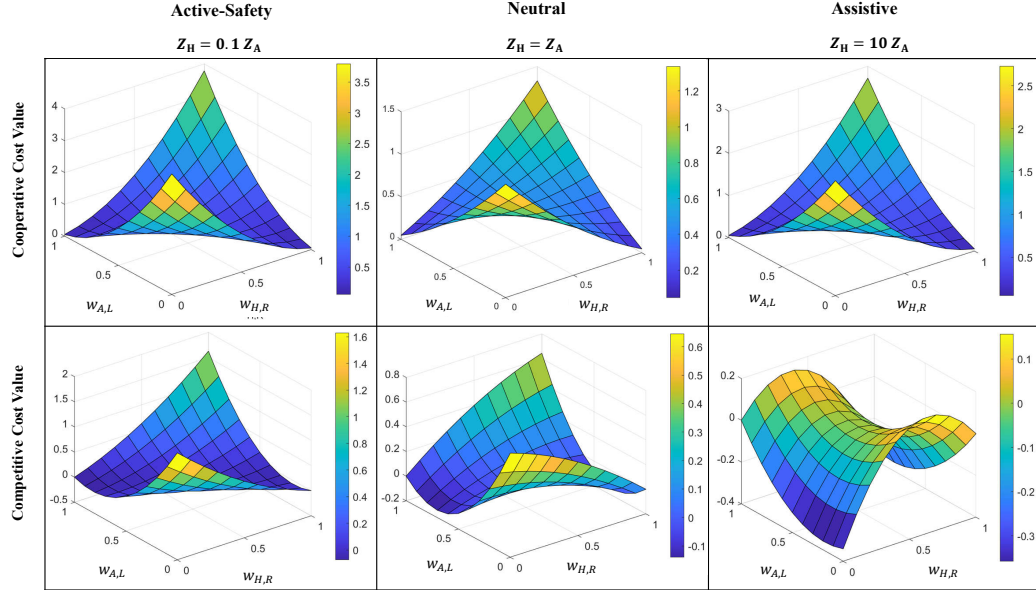
Figure 4.4: Competitive-Cooperative cost functions values for lower-level interaction modes. The columns represent the interaction mode, and the rows depict the cooperative/competitive cost values from the Nash solution. In each surface has w_H, w_H and V_{Coop}/V_{Comp} coordinates axis. The color-bars demonstrate the range for each surface based on its minimum and maximum value.

other one (zero-game part), having zero competition is desirable in the interaction between two agents. Therefore, in defining the reward function for the RL agent (Eq. (4.21)), the second norm of the aggregated competitive value is employed in addition to the differential torque and the cooperative value.

Figure 4.4 can be used as a map to connect conventions to the output of human-automation interaction. For instance, Figure 4.5 shows the outputs of the human and automation interaction associated with the three points shown with red, blue and orange circles in Figure 4.4 when both human and automation has similar impedance parameters. These three circles demonstrate three interaction modes where in the automation is cooperative (red circle), undecided (orange circle) and uncooperative (blue circle) as discussed in section 3.1. For all these three cases the human's desired path for maneuvering the obstacle is from the right of the obstacle (i.e., $w_{HR} = 1$). Therefore, the red circle represent a case where automation's desired path is from the

left side (i.e., $w_{AL} = 1$). Orange circle represent a case where the automation's wights both right and left paths the same (i.e., $w_{AR} = w_{AL} = 0.5$). Blue circle represent a case where the automation's desired path is also from the right side (i.e., $w_{AR} = 1$).
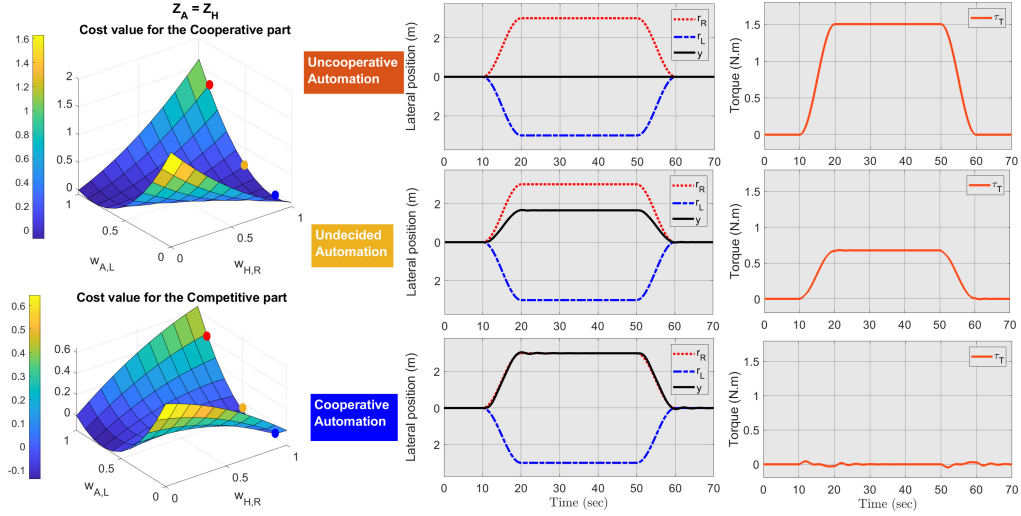
Figure 4.5: The outputs of the human and automation interaction associated with the three points shown with red, blue and orange circles in the neutral interaction mode ($Z_H = Z_A$). The surfaces represent the convention map's cooperative (right-top) and competitive (right-bottom) surfaces. The plots on the second column represent the lateral deviation of the vehicle from the centerline of the road. The last column is for the differential torque between the human driver and the automation system. The human drivers' behavior identifies each row based on his/her weight for the right direction w_{HR}.

The first column of Figure 4.5 shows the two possible path for avoiding the obstacles and the vehicle's r_R and r_L and the vehicle's lateral position y_V. The second column shows the differential torque measured by the torque sensor τ_T. It is demonstrated that when human and automation's have opposite different path since their impedance is the same, their control commands cancel out and the vehicle hit the obstacle. To avoid such a conflict, two possible solutions can be presented. First, we can modulate the automation's impedance controller's parameters to yield or gain the control as studied in our previous work [47]. Also, the automation's intent can be adapted to the select a path similar to the human driver as demonstrated in Figure 4.5. In this paper, we focus on the latter approach.

When the human driver and the automation system have the same intent ($w_{AR} = w_{HR} = 1$ shown in the third row of Figure 4.5), the differential torque is much smaller compared to the other two cases (the uncooperative automation shown and undecided automation). It should be noted that even though the competitive value for the blue and orange points are approximately the same, since the cooperative value is different, the differential torque for the undecided automation is not zero. Also, the vehicle's lateral position is not the same as the right reference path for the undecided automation system.
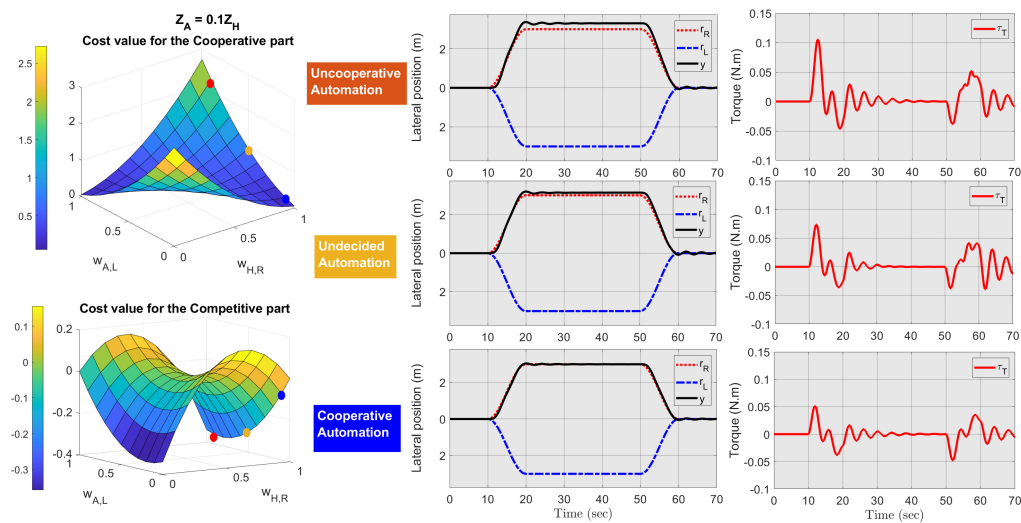

Figure 4.6: The outputs of the human and automation interaction associated with the three points shown with red, blue and orange circles in the assistive interaction mode ($Z_H = 10Z_A$). The surfaces represent the convention map's cooperative (right-top) and competitive (right-bottom) surfaces. The plots on the second column represent the lateral deviation of the vehicle from the centerline of the road. The last column is for the differential torque between the human driver and the automation system. The human drivers' behavior identifies each row based on his/her weight for the right directionw_{HR}.

Figure 4.6 shows the outputs of the human and automation interaction in the assisitive mode ($z_A = 0.1z_H$). It follows from Figure 4.6 that for the three cases of uncooperative automation, undecided automation and cooperative automation, the vehicle path is close to the human's desired path. Also, the differential torque is relatively small for all the three cases. This is because automation's impedance is

relatively small meaning it only applies a low torque on the steering wheel. In this scenario, the human driver is mainly in control of the vehicle.
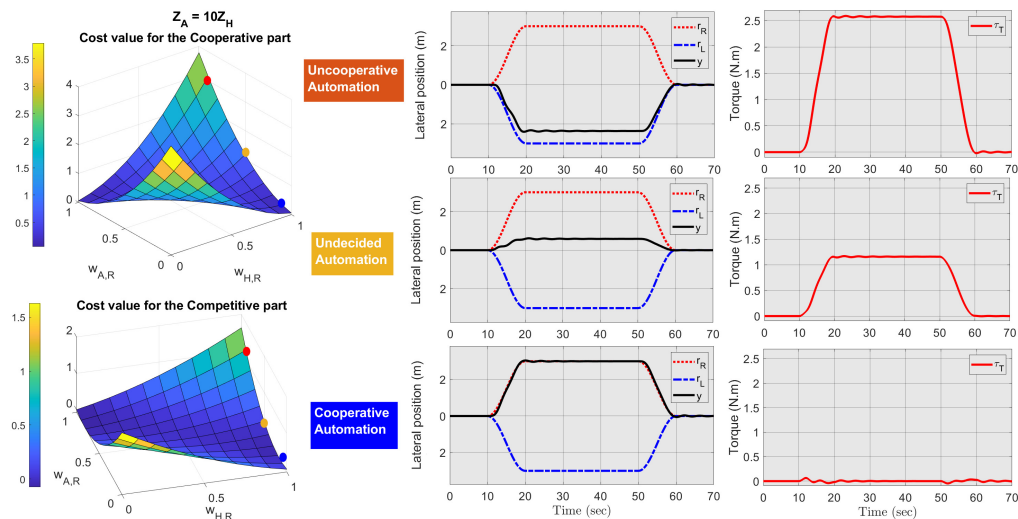

Figure 4.7: The outputs of the human and automation interaction associated with the three points shown with red, blue and orange circles in the active-safety interaction mode ($Z_H = 0.1Z_A$). The surfaces represent the convention map's cooperative (right-top) and competitive (right-bottom) surfaces. The plots on the second column represent the lateral deviation of the vehicle from the centerline of the road. The last column is for the differential torque between the human driver and the automation system. The human drivers' behavior identifies each row based on his/her weight for the right directionw_{HR}.

Figure 4.7 shows the outputs of the human and automation interaction in the assisitive mode ($z_A = 10z_H$). It follows from Figure 4.7 that for the three cases of uncooperative automation, undecided automation and cooperative automation, the vehicle path is close to the automation's desired path. When the human and automation has a reverse intent the differential torque is relatively high in the active safety mode. This is because automation's impedance is relatively high meaning it applies a high torque in an opposite direction as the human driver which can cause a discomfort to the driver but it ensure the safety of the vehicle.

As demonstrated in Figures 4.5-4.7 the interaction between the human driver and automation system depends on the weights of the nonlinear MPC for each of them. A point in the convention maps demonstrates the agent's decision to choose the pre-

ferred path in the obstacle avoidance task. Based on human behavior, the automation system can adapt w_{AR} and w_{AL} to minimize the conflict in the interaction. To resolve a conflict between the automation system and the human driver, impedance modulation in the lower-level controller or intent adaption of the automation system in the higher-level controller can be used as a solution. The impedance modulation was studied in detail in [47]. In this paper, we discuss intent adaptation for resolving a conflict.

Figure 4.8 shows how the weights of the nonlinear model predictive controller in the automation system are adjusted dynamically with the DDPG agent to minimize the conflict. For the DDPG agent, each actor and critic network has an input layer, an
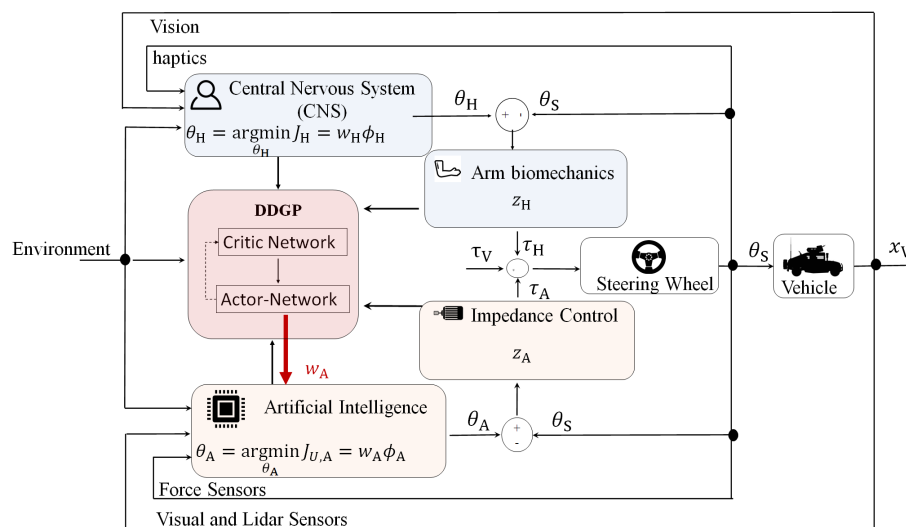
Figure 4.8: Schematic diagram of the DDPG-based intent adaptation approach. The DDPG agents receive the observations from the model, lower-level and higher-level controller and generate updated w_A.

output layer, and three hidden layers of 100 units. In the hidden layer, the rectified linear unit (ReLU) is employed as the activation function which projects the input to the output signal. The reward function in the DDPG algorithm is defined to minimize the integrated differential torque and cooperative value while maintaining

the competitive value to zero:

$$r_{\text{k}} = \frac{1}{M_{\text{sub}}} \left(\sum_{k=1}^{M_{\text{sub}}} \left(-100 \left\| V_{\text{coop}} \right\| - 100 \left\| V_{\text{comp}} \right\| - \left\| \tau_{\text{T}} \right\| \right) \right) \quad\quad (4.21)$$

which M_{sub} is the number of time steps with fixed weights in the cost function of the automation system. In a training phase of the DDPG agent, the number of the time step in each episode includes $100M_{\text{sub}}$. V_{coop} and V_{comp} are the cooperative and competitive cost values in the equilibrium point. The hyperparameters of the DDPG agent are presented in Table 4.1.
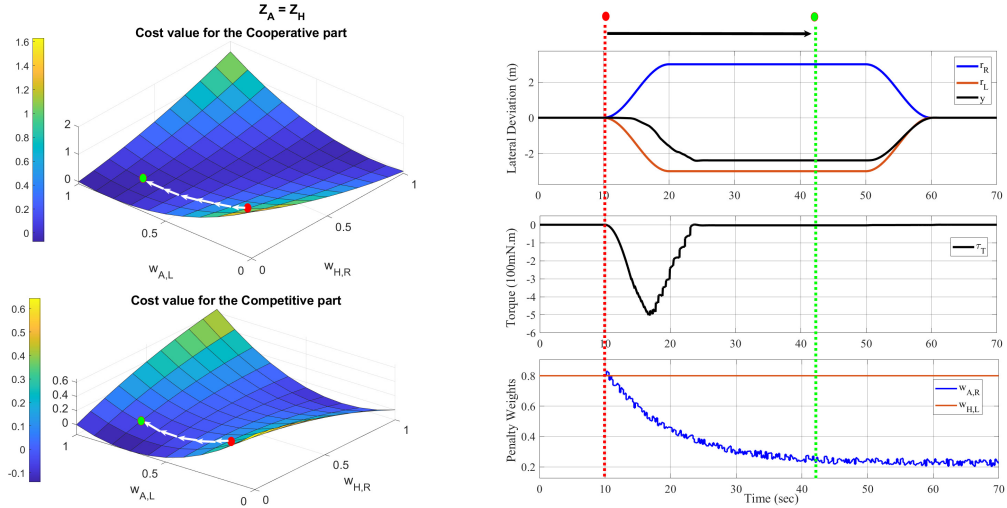
Figure 4.9: RL-based intent adaptation for the case that the human and automation system have the same impedance. The first column demonstrates the convention map with the cooperative and competitive cost values. The second column shows the lateral deviation, differential torque and the cost weights ωAR and ωHL. The red circle on the convention map is the initial weight value, and the green circle is the adapted weight value.

Figure 4.9 demonstrates the performance of the RL-based intent adaptation approach when the human driver wants to go more in the left direction for avoiding the obstacle with weight $[w_{\text{HR}}\ w_{\text{HL}}] = [0.2\ 0.8]$ and they have equal impedance. On the contrary, the automation system preferred the right direction for avoiding the obstacle ($[w_{\text{AR}}\ w_{\text{AL}}] = [0.8\ 0.2]$). The initial weight value of the human driver and

the automation system is depicted by a red circle on the cooperative and competitive surfaces of the convention map (the first column). The lateral deviation of the vehicle (y_V) and the reference paths for right (r_R) and left (r_L) sides are depicted in the first row of the second column. The measured differential torque is depicted in the second row of the second column, and the units of the y-axis are 100 mN.m. The weight value of the human driver and the automation system is demonstrated in the second column of the last row. By approaching the obstacle, the trained DDPG agent adopts the weight in the cost function of the automation system to minimize conflict between the automation and the human driver. The red dashed line demonstrate the start of the intent adaptation, and the green dashed line depicts the green circle on the convention map as the terminal weight of the automation system, and after this line, the conflict is minimized. The value of the differential torque retained approximately to the zero value after the intent adaption, which shows zero fight. Also, the competitive value is zero, so there is no side payment from the automation system to the human driver or vice versa. Therefore, the DDPG agent handled the intent adaptation for minimizing the conflict while the vehicle avoided the obstacle.

4.5   Conclusions

This project aims to study the principles of convention formation in a haptic shared control framework wherein both humans and automation collaboratively control the steering of a semi-automated ground vehicle to determine optimal handover strategies in uncertain circumstances. Here, we focused on a specific type of conflict between the driver and automation, named reverse intent. We introduced a modular structure that can be used for separations of partner-specific conventions and task-dependent representations. Using this structure, we created a map to connect conventions with the outputs of the human-automation interaction. Finally, we designed an RL-based model predictive controller to search for automation's optimal strategy such that conventions can be reached.

To validate the performance of the proposed platform, the first step is to integrate the proposed platform with an inverse reinforcement learning approach to capture the distribution of the human weight vector. By capturing the human's weight vector, we can realize whether the weight vector distribution can be used as a proxy for identifying the partner-specific conventions. We further plan to improve the automation system capability by employing Bayesian optimization (BO) to determine automation's optimal policies. We select BO since it is deemed particularly powerful in handling multi-objective optimization problems with a mixture of continuous and discrete decision variables and accommodating the system's uncertainties and constraints (i.e., adversarially robust BO [39]). Finally, we plan to develop a framework that allows transferring the knowledge of learned conventions into interacting with new users or on new tasks.

REFERENCES

[1] Jon Bornstein. Dod autonomy roadmap: autonomy community of interest. Technical report, Army Research Laboratory Aberdeen Proving Ground United States, 2015.

[2] Ruth A David and Paul Nielsen. Defense science board summer study on autonomy. Technical report, Defense Science Board Washington United States, 2016.

[3] Jessie YC Chen and Michael J Barnes. Human–agent teaming for multirobot control: A review of human factors issues. *IEEE Transactions on Human-Machine Systems*, 44(1):13–29, 2014.

[4] Michael Barnes, Linda R Elliott, Julia Wright, Angelique Scharine, and Jessie Chen. Human-robot interaction design research: From teleoperations to human-agent teaming. Technical report, CCDC Army Research Laboratory Aberdeen Proving Ground United States, 2019.

[5] Maya Indira Ganesh. The ironies of autonomy. *Humanities and Social Sciences Communications*, 7(1):1–10, 2020.

[6] Frank Flemisch, Matthias Heesen, Tobias Hesse, Johann Kelsch, Anna Schieben, and Johannes Beller. Towards a dynamic balance between humans and automation: Authority, ability, responsibility and control in shared and cooperative control situations. *Cognition, Technology and Work*, 14(1):3–18, 2012.

[7] Zhenji Lu, Riender Happee, Christopher DD Cabrall, Miltos Kyriakidis, and Joost CF de Winter. Human factors of transitions in automated driving: A

general framework and literature survey. *Transportation Research Part F: Traffic Psychology and Behaviour*, 43:183–198, 2016.

[8] J. C F De Winter and D. Dodou. Preparing drivers for dangerous situations: A critical reflection on continuous shared control. *Conference Proceedings - IEEE International Conference on Systems, Man and Cybernetics*, pages 1050–1056, 2011.

[9] Raja Parasuraman and Victor Riley. Humans and automation: Use, misuse, disuse, abuse. *Human factors*, 39(2):230–253, 1997.

[10] Akshay Bhardwaj, Amir H Ghasemi, Yingshi Zheng, Huckleberry Febbo, Paramsothy Jayakumar, Tulga Ersal, Jeffrey L Stein, and R Brent Gillespie. Whos the boss? arbitrating control authority between a human driver and automation system. *Transportation Research Part F: Traffic Psychology and Behaviour*, 68:144–160, 2020.

[11] Arie P van den Beukel, Mascha C van der Voort, and Arthur O Eger. Towards a framework for testing drivers' interaction with partially automated driving. In *2015 IEEE 18th International Conference on Intelligent Transportation Systems*, pages 1902–1907. IEEE, 2015.

[12] Joon Woo Son, Myoung Ouk Park, et al. Situation awareness and transitions in highly automated driving a framework and mini-review. *Journal of Ergonomics*, 2017.

[13] Calder Phillips-Grafflin, Halit Bener Suay, Jim Mainprice, Nicholas Alunni, Daniel Lofaro, Dmitry Berenson, Sonia Chernova, Robert W Lindeman, and Paul Oh. From autonomy to cooperative traded control of humanoid manipulation tasks with unreliable communication. *Journal of Intelligent & Robotic Systems*, 82(3):341–361, 2016.

[14] Thomas B Sheridan and W Verplank. *Human and Computer Control of Undersea Teleoperators (Man-Machine Systems Lab Report).* 1978.

[15] Amir H Ghasemi, Paramsothy Jayakumar, and R Brent Gillespie. Shared control architectures for vehicle steering. *Cognition, Technology & Work*, pages 1–11, 2017.

[16] Frank Flemisch, Matthias Heesen, Tobias Hesse, Johann Kelsch, Anna Schieben, and Johannes Beller. Towards a dynamic balance between humans and automation: authority, ability, responsibility and control in shared and cooperative control situations. *Cognition, Technology & Work*, 14(1):3–18, 2012.

[17] Raja Parasuraman and Victor Riley. Humans and automation: Use, misuse, disuse, abuse. *Human factors*, 39(2):230–253, 1997.

[18] D.A. Abbink and M. Mulder. Neuromuscular analysis as a guideline in designing shared control. *Advances in Haptics*, pages 499–517, 2010.

[19] Marcia K. O'Malley, Abhishek Gupta, Matthew Gen, and Yanfang Li. Shared Control in Haptic Systems for Performance Enhancement and Training. *Journal of Dynamic Systems, Measurement, and Control*, 128(1):75, 2006.

[20] J Anderson, S Walker, and K Iagnemma. Experimental performance analysis of a constraint-based navigation framework. *Transactions on Systems, Man, and Cybernetics–Part A: Systems and Humans*, pages 1–10, 2014.

[21] Ryota Nishimura, Takahiro Wada, and Seiji Sugiyama. Haptic shared control in steering operation based on cooperative status between a driver and a driver assistance system. *Journal of Human-Robot Interaction*, 4(3):19–37, 2015.

[22] Justin Storms, Kevin Chen, and Dawn Tilbury. A shared control method for

obstacle avoidance with mobile robots and its interaction with communication delay. *The International Journal of Robotics Research*, 36(5-7):820–839, 2017.

[23] S. M. Petermeijer, D. a. Abbink, and J. C. F. de Winter. Should Drivers be Operating Within an Automation-Free Bandwidth? Evaluating Haptic Steering Support Systems With Different Levels of Authority. *Human Factors: The Journal of the Human Factors and Ergonomics Society*, 57(1):5–20, 2014.

[24] Stephen M Erlien. *Shared vehicle control using safe driving envelopes for obstacle avoidance and stability*. PhD thesis, Stanford University, 2015.

[25] Stephen M Erlien, Susumu Fujita, and Joseph Christian Gerdes. Shared steering control using safe envelopes for obstacle avoidance and vehicle stability. *IEEE Transactions on Intelligent Transportation Systems*, 17(2):441–451, 2016.

[26] Ayse Kucukyilmaz et al. *Haptic role allocation and intention negotiation in human-robot collaboration*. PhD thesis, Koç University, 2013.

[27] Raphaela Groten, Daniela Feth, Harriet Goshy, Angelika Peer, David A Kenny, and Martin Buss. Experimental analysis of dominance in haptic collaboration. In *Robot and Human Interactive Communication, 2009. RO-MAN 2009. The 18th IEEE International Symposium on*, pages 723–729. IEEE, 2009.

[28] Raphaela Groten, Daniela Feth, Roberta L Klatzky, and Angelika Peer. The role of haptic feedback for the integration of intentions in shared task execution. *IEEE Transactions on Haptics*, 6(1):94–105, 2013.

[29] Wei Bi, Xiaoyu Wu, Yueyue Liu, and Zhijun Li. Role adaptation and force, impedance learning for physical human-robot interaction. In *2019 IEEE 4th International Conference on Advanced Robotics and Mechatronics (ICARM)*, pages 111–117. IEEE, 2019.

[30] Vahid Izadi and Amir H Ghasemi. Modulation of control authority in adaptive hapticshared control paradigms. *arXiv preprint arXiv:2007.07436*, 2020.

[31] Andy Shih, Arjun Sawhney, Jovana Kondic, Stefano Ermon, and Dorsa Sadigh. On the critical role of conventions in adaptive human-ai collaboration. *arXiv preprint arXiv:2104.02871*, 2021.

[32] Emmanouil Gkeredakis. The constitutive role of conventions in accomplishing coordination: insights from a complex contract award project. *Organization Studies*, 35(10):1473–1505, 2014.

[33] Dietrich Meutsch and Siegfried J Schmidt. On the role of conventions in understanding literary texts. *Poetics*, 14(6):551–574, 1985.

[34] Chris L Baker, Julian Jara-Ettinger, Rebecca Saxe, and Joshua B Tenenbaum. Rational quantitative attribution of beliefs, desires and percepts in human mentalizing. *Nature Human Behaviour*, 1(4):1–10, 2017.

[35] Connor Brooks and Daniel Szafir. Building second-order mental models for human-robot interaction. *arXiv preprint arXiv:1909.06508*, 2019.

[36] Hengyuan Hu and Jakob N Foerster. Simplified action decoder for deep multi-agent reinforcement learning. *arXiv preprint arXiv:1912.02288*, 2019.

[37] Robert D Hawkins, Minae Kwon, Dorsa Sadigh, and Noah D Goodman. Continual adaptation for efficient machine communication. *arXiv preprint arXiv:1911.09896*, 2019.

[38] Yunlong Song and Davide Scaramuzza. Learning high-level policies for model predictive control. In *2020 IEEE/RSJ International Conference on Intelligent Robots and Systems (IROS)*, pages 7629–7636. IEEE, 2020.

[39] Joel A Paulson, Georgios Makrygiorgos, and Ali Mesbah. Adversarially robust bayesian optimization for efficient auto-tuning of generic control structures under uncertainty. *AIChE Journal*, page e17591, 2021.

[40] Joel A Paulson, Ketong Shao, and Ali Mesbah. Probabilistically robust bayesian optimization for data-driven design of arbitrary controllers with gaussian process emulators. In *Proceedings of the IEEE Conference on Decision and Control*, 2021.

[41] Qiugang Lu, Ranjeet Kumar, and Victor M Zavala. Mpc controller tuning using bayesian optimization techniques. *arXiv preprint arXiv:2009.14175*, 2020.

[42] Qiugang Lu, Leonardo D González, Ranjeet Kumar, and Victor M Zavala. Bayesian optimization with reference models: A case study in mpc for hvac central plants. *Computers & Chemical Engineering*, 154:107491, 2021.

[43] P Travis Jardine, Michael Kogan, Sidney N Givigi, and Shahram Yousefi. Adaptive predictive control of a differential drive robot tuned with reinforcement learning. *International Journal of Adaptive Control and Signal Processing*, 33(2):410–423, 2019.

[44] Guillaume Bellegarda and Katie Byl. An online training method for augmenting mpc with deep reinforcement learning. In *2020 IEEE/RSJ International Conference on Intelligent Robots and Systems (IROS)*, pages 5453–5459. IEEE, 2020.

[45] Karnchanachari Napat, Miguel I Valls, David Hoeller, and Marco Hutter. Practical reinforcement learning for mpc: Learning from sparse objectives in under an hour on a real robot. In *2nd Annual Conference on Learning for Dynamics and Control (L4DC 2020)(online)*. OpenReview, 2020.

[46] Paul Boehm, Amir H Ghasemi, Sile O'Modhrain, Paramsothy Jayakumar, and

R Brent Gillespie. Architectures for shared control of vehicle steering. *IFAC-PapersOnLine*, 49(19):639–644, 2016.

[47] Vahid Izadi and Amir H Ghasemi. Modulation of control authority in adaptive haptic shared control paradigms. *Mechatronics*, 78:102598, 2021.

[48] Eunhyek Joa, Kyongsu Yi, and Kilsoo Kim. A lateral driver model for vehicle–driver closed-loop simulation at the limits of handling. *Vehicle system dynamics*, 53(9):1247–1268, 2015.

[49] Yishen Zhao, Philippe Chevrel, Fabien Claveau, and Franck Mars. Continuous identification of driver model parameters via the unscented kalman filter. *IFAC-PapersOnLine*, 52(28):126–133, 2019.

[50] Bo Yu, R Brent Gillespie, James S Freudenberg, and Jeffrey A Cook. Human control strategies in pursuit tracking with a disturbance input. In *Decision and Control (CDC), 2014 IEEE 53rd Annual Conference on*, pages 3795–3800. IEEE, 2014.

[51] T Basar and GJ Olsder. Dynamic noncooperative game theory, vol. 23 (siam, philadelphia). 1999.

[52] Toshiyuki Ohtsuka. A continuation/gmres method for fast computation of nonlinear receding horizon control. *Automatica*, 40(4):563–574, 2004.

[53] Alberto Bressan. Noncooperative differential games. *Milan Journal of Mathematics*, 79(2):357–427, 2011.

[54] Alberto Bressan. Noncooperative differential games. a tutorial. *Department of Mathematics, Penn State University*, page 81, 2010.

[55] Marcin Stryszowski, Stefano Longo, Dario DAlessandro, Efstathios Velenis, Gregory Forostovsky, and Sabato Manfredi. A framework for self-enforced optimal

interaction between connected vehicles. *IEEE Transactions on Intelligent Transportation Systems*, 22(10):6152–6161, 2020.

[56] Timothy P Lillicrap, Jonathan J Hunt, Alexander Pritzel, Nicolas Heess, Tom Erez, Yuval Tassa, David Silver, and Daan Wierstra. Continuous control with deep reinforcement learning. *arXiv preprint arXiv:1509.02971*, 2015.

CHAPTER 5: CONCLUSIONS

This dissertation focused on designing and validating an adaptive haptic shared control paradigm to shorten the control transfer time, improve interpretation and appropriation of responsibility, produce a more accurate understanding of the vehicle and/or environment, and reduce the driver's cognitive load. This dissertation was presented in a three-article format. Chapter 2 (Paper1) presented a design of an adaptive haptic shared control framework wherein both humans and automation are physically connected through a steering angle. To shorten the control transition time in the present conflict, we designed a modulation algorithm to vary the automation's impedance controller parameter in different interaction modes. This work was published in the Mechatronics journal in 2021. This paper considered a cost function to determine an optimal modulation policy. Its terms were defined to minimize performance error and reduce the disagreement between the human and automation system. We employed a nonlinear stochastic model predictive approach to solving the cost function subjected to probabilistic uncertainties in human biomechanics. The polynomial chaos expansions were employed to obtain a computationally tractable form of the cost function. The continuation generalized minimum residual method was utilized to solve the tractable nonlinear cost function. To demonstrate the effectiveness of the proposed approach, we considered a scenario where the human and the automation system both detect an obstacle and negotiate on controlling the steering wheel so that the obstacle can be avoided safely. For this scenario, four interaction modes were defined based on the cooperation status (cooperative and uncooperative) and the control transfer's desired direction (human to automation or automation to human). The numerical results demonstrated that when the human control command

is sufficient for avoiding the obstacle, the disagreement between the human and automation systems can be reduced by modulating and adopting smaller values for the impedance controller. On the other hand, when the human's control command is insufficient, by modulating and adopting larger values for the impedance controller parameters, the automation system gains the control authority and ensures the safety of the obstacle avoidance task. Additionally, we performed tests with processors in the loop (PIL) to show the proposed predictive controller can compute the optimal modulation policy in real-time. The PIL results showed high computational speed and numerical accuracy for the proposed method using two low-cost micro-controllers.

In Chapter 3 (Paper2), we quantified the performance of an adaptive haptic shared control paradigm through a set of human-subject test studies. We invited 27 participants to drive a vehicle in a fixed-based driving simulator. The drivers are asked to follow a road and avoid the static obstacles on the road. To study the performance of the proposed controller in resolving a conflict, for sixty percent of these obstacles, the human driver is instructed to avoid the obstacles in the opposite direction as the automation system. For the other forty percent of the obstacles, the human driver is instructed to take a similar direction as the automation system to avoid the obstacle. To determine the optimal impedance modulation policy, we employed a predictive model controller which its cost function contains three terms. These terms are the error between the steering angle and the human's desired steering command, the error between the steering angle and the automation's desired steering command, and the differential torque on the steering wheel. We compared the adaptive haptic shared control with two other shared control paradigms: named assistive haptic shared and active-safety haptic shared control. The automation system weighs the error term between the steering angle and the driver's desired steering command in the assistive paradigm. This mode represents a case where the automation has relatively high

confidence in the driver's actions. In the active-safety paradigm, the automation system weighs the error term between the steering angle and the automation's desired steering command. This mode represents a case where the automation has relatively low confidence in the driver's action. In the adaptive haptic shared control, the automation adaptively assigns different weights to the error terms based on the human's adopted impedance. When the human's adopted impedance is high, the automation in the adaptive paradigms acts more like the assistive paradigm, and when the human's impedance is low, the automation in the adaptive paradigms acts more like the active-safety paradigm. Here, we used the human grip force as a proxy to estimate the human impedance on the steering wheel. Specifically, we quantized the human grip force into five ranges: low, medium-low, medium, medium-high, and high. Based on the recorded grip force, the automation policy of an adaptive haptic shared control paradigm is adapted to determine optimal impedance control parameters. We compared the performance of these three shared control schemes by analyzing five metrics, including obstacle hits and metrics related to driving maneuvers around the avoided obstacles. Our statistical analysis indicated that the adaptive haptic shared control paradigm supports the best overall team performance in resolving a conflict between the driver and automation system while keeping the vehicle safe.

Chapter 4 (Paper3) established a platform to study the principles of convention formation in a haptic shared control framework wherein both humans and automation collaboratively control the steering of a semi-automated ground vehicle. We then applied these principles to determine optimal strategies for exchanging the control authority between human drivers and an automation system. In the first step, we proposed a modular structure to separate partner-specific conventions from task-dependent representations and use this structure to learn and leverage different forms of conventions. In this structure, we assumed the human and automation steering commands could be determined by optimizing a set of cost functions. For each agent,

the cost function was defined as a combination of hand-coded features and vectors of weights. We argued that the hand-coded features could be selected to describe task-dependent representations. On the other hand, the weight distributions over these features can be used to determine the partner-specific conventions. Next, to leverage the learned conventions, we developed a map that connects different forms of conventions to the outputs of human-automation interaction. Finally, an adaptable automation system was designed using the convention map to reach a desirable shared convention. In particular, we developed a reinforcement-learning-based model predictive controller to enable the automation system to learn complex policies and adapt its behavior accordingly. Specifically, we designed an episode-based policy search using the Deep Deterministic Policy Gradients technique to determine automation's cost function's optimal weights vector distribution. Next, we applied the proposed platform to the problem of intent negotiation for resolving a conflict. Specifically, we considered a scenario where both humans and automation detect an obstacle but choose different paths to maneuver around the obstacle. The simulation results demonstrate that the convention-based handover strategies can successfully resolve a conflict and improve the performance of the human-automation teaming.

5.1   Recommendations for Future Works

A set of challenges needs to be addressed before implementing the proposed shared control paradigm in real-world applications. These challenges are the subjects of our future studies.

The proposed adaptive haptic shared control design and test assumed that the human partner's impedance and his/her preferred path are known. Therefore, developing a set of learning and identification approaches to estimate the intent and impedance adopted by the human driver and track them as they vary will allow us to design a more effective controller. Furthermore, it is crucial to create a method that allows recognizing the current interaction mode in real-time using the data ac-

quired by onboard sensors. An appropriate cost function can be defined by knowing the interaction mode, and the automation system can adjust its behavior based on this cost function. Additionally, the proposed nonlinear model predictive control method in paper 1 assumed that the uncertainty in the human-automation interaction is characterized. In future work, we will address these shortcomings by developing a learning-and-scenario-based optimal controller that (1) learns the (intrinsically state- and control-dependent) uncertainties in the system and updates the human-automation dynamics online; and (2)given the uncertainty in the system, calculates an optimal modulation policy within the required sampling time scales. Also, while the main focus of paper 1 was on modulating the impedance controller parameters, knowing how and when to attempt transitions is another challenge. It is essential to test various transition schemes, including discrete and slow or fast continuous transitions, to determine an optimal speed for exchanging the control authority. Finally, a user-adaptive path planner can be designed and integrated into the shared steering control problem, thereby reducing steering conflicts and overall cognitive load on the operator while improving mission performance.

In our human-subject tests discussed in paper 2, the human driver was engaged in driving the vehicle and interacting with the automation system. However, a driver's attention might be occupied with other tasks during driving. Therefore, it is necessary to test the performance of the adaptive haptic shared control in more sophisticated driving situations, including a case where the driver is also responsible for a secondary task. In addition, instead of the low-fidelity Matlab Simulink real-time environment presented in paper 2, we plan to use CarSim software and a Unity-based Virtual Reality driving simulation setup so that participants will have greater immersion and a wider field of view. Furthermore, the proposed shared control algorithm shall be tested on a physical ground vehicle platform to discover the potential challenges that might not be present in the controlled simulation environment.

While paper 3 discussed the principles of convention formation in a haptic shared control paradigm, many steps still need to be taken to enable collaborative partnerships between teams of humans and semi-automated ground vehicles based on the formed conventions. For instance, the problem of convention formation shall be studied considering the interaction at both intent and body levels. By such analysis, we can determine the best approach for negotiating intent and transitioning control authority between the driver and automation system. We also need to consider the role of uncertainty in how the automation's policy search will be designed or modified. Furthermore, it is necessary to discuss the transfer of conventions knowledge so that it can be used to exploit the structural similarity among a distribution of partner-specific conventions and task-dependent representations. The capability of transferring convention knowledge will allow us to optimize automation's behavior for rapid adaptation to new partners and new tasks.

Appendix: C/GMRES Solver

To solve the nonlinear cost function described in Eq. 4.9, we discretize the equations of motion using the forward Euler method. It should be noted that higher order discretizations can be employed at the expense of the computational complexity. Similarly, the cost function J_i and the set of constraints will be transformed in the discrete form on time axis as:

$$\min_{u_i} J_i^{(k)} = \varphi_i^{k+N_p}(x, w) + \sum_{j=0}^{N_{\mathrm{p}}-1} T_{\mathrm{s}}\{\widetilde{\mathcal{L}}_i^{k+j}(x, w, u)\}$$

$$\text{s.t. :} \quad \begin{cases} x^{(k+1)} = x^{(k)} + T_{\mathrm{s}} f\left(x^{(k)}, w^{(k)}\right) + T_{\mathrm{s}} B u^{(k)} \\ \\ C_{i,\mathrm{eq}}^{(k)} = 0 \end{cases} \quad (6.1)$$

where T_{s} is the size of the time-step, k is the number of time-step (considered as the current time-step), $x^{(k)}$, $w^{(k)}$ and $u^{(k)}$ are equal to $x(t = T_{\mathrm{s}}k)$, $w(t = T_{\mathrm{s}}k)$ and $u(t = T_{\mathrm{s}}k)$, respectively. We discretize the necessary optimality conditions by dividing the horizon into N_{p} steps. The discretized KarushKuhnTucker (KKT) necessary conditions with the boundary conditions are given as follows:

$$x^{*(k+1)} = x^{*(k)} + T_{\mathrm{s}} f\left(x^{*(k)}, w^{(k)}\right) + T_{\mathrm{s}} B u^{*(k)} \tag{6.2}$$

$$x^{*(0)} = x^{(0)} \tag{6.3}$$

$$\lambda_i^{*(k)} = \lambda_i^{*(k+1)} + T_{\mathrm{s}} \frac{\partial H_i}{\partial x} \tag{6.4}$$

$$\lambda_i^{*(k+N_{\mathrm{p}})} = \varphi_i^{k+N_p}(x, w) \tag{6.5}$$

$$\frac{\partial H_i}{\partial u} = 0 \tag{6.6}$$

$$C_{i,\mathrm{eq}}^{(k)} = 0 \tag{6.7}$$

By employing forward recursion, for $j = 1, \cdots, N_{\mathrm{p}}$, the state variables $x^{*(k+j)}$, can be defined using equations (6.2) and (6.3). Furthermore, by employing back recursion from the terminal cost to the present time-step ($j = N_{\mathrm{p}}, N_{\mathrm{p}} - 1, \cdots, 1$) the co-states $\lambda^{*(k+j)}$ can be determined using (6.4) and (6.5). Therefore, the state and co-state variables $x^{k+j}|_{j=0}^{N_p}$ and $\lambda^{k+j}|_{j=0}^{N_p}$ sequences formed in terms of control input $u^{k+j}|_{j=0}^{N_p}$ and Lagrange multiplier $\mu^{k+j}|_{j=0}^{N_p}$ sequences which are unknown. Finally, by plugging $x^{*(k+j)}$ and $\lambda^{*(k+j)}$ into equations (6.6) and (6.7), a KKT vector $F(X, U, t)$ for N_p horizon can be defined, where

$$F_i\left(X,U,t\right) = \begin{bmatrix} \dfrac{\partial H_i^{(k)}(x^*,w,u^*,\lambda^*,\mu^*)}{\partial u} \\[2ex] C_{i,\mathrm{eq}}^{(k)} \\[2ex] \vdots \\[1ex] \dfrac{\partial H_i^{(k+N_\mathrm{c})}(x^*,w,u^*,\lambda^*,\mu^*)}{\partial u} \\[2ex] C_{i,\mathrm{eq}}^{(k+N_\mathrm{c})} \\[2ex] \vdots \\[1ex] \dfrac{\partial H_i^{(k+N_\mathrm{p}-1)}(x^*,w,u^*,\lambda^*,\mu^*)}{\partial u} \\[2ex] C_{i,\mathrm{eq}}^{(k+N_\mathrm{p}-1)} \end{bmatrix} \tag{6.8}$$

where

$$X = [x^{(k)}, w^{(k)}, x^{(k+1)}, w^{(k+1)}, ..., x^{(k+N_\mathrm{p})}, w^{(k+N_\mathrm{p})}]^{\mathrm{T}} \tag{6.9}$$

where N_c is the number of the control horizon steps. Note that for $N_\mathrm{c} \le j \le N_\mathrm{p}$, $u^{k+j} = u^{k+N_\mathrm{c}}$.

Continuation/GMRES method

To solve $F\left(X,U,t\right) = 0$ with respect to the unknown vector U, for each time-step, the C/GMRES method is employed [?]. In C/GMRES method, instead of solving $F(X,U,t) = 0$, we select the proper initial value $U(0)$ and take the time derivative of

Eq. (6.8) into account. Specifically, we define

$$\dot{F}(X, U, t) = A_\mathrm{s} F(X, U, t) \tag{6.10}$$

where A_s is a stable matrix (i.e. with negative eigenvalues). Differentiating the left side of Eq. (6.10) yields:

$$F_U(X, U, T)\dot{U} = A_\mathrm{s} F(X, \ U, \ t) - F_X(X, U, T)\dot{X} - \dot{F}(X, U, T) \tag{6.11}$$

Since F_U is non-singular, we can obtain the differential equation for $\dot{U}$ as:

$$\dot{U} = F_U^{-1}\left(A_\mathrm{s} F(X, \ U, \ t) - F_X(X, U, T)\dot{X} - \dot{F}(X, U, T)\right) \tag{6.12}$$

The calculation of Jacobians F_X and F_U are computationally expensive. Instead to solve Eq. (6.12), we employed the forward-difference approximation to eliminate the calculation of the Jacobians. To this end, using the concept of forward difference, we approximate the products of Jacobians and some $\bar{X}$, $\bar{U}$, and $\bar{t}$ and replaced it to Eq. (6.12) which results in:

$$D_\mathrm{h} F\left(X, U, t : 0, \dot{U}, 0\right) = b\left(X, \dot{X}, U, t\right) \tag{6.13}$$

$$\tag{6.14}$$

where

$$b\left(X, \dot{X}, U, t\right) = A_\mathrm{s} F(X, U, t) - D_\mathrm{h} F\left(X, U, t : \dot{X}, 0, 1\right) \tag{6.15}$$

$$D_\mathrm{h} F|_{X,U,t}^{\bar{X},\bar{U},\bar{t}} = \frac{F\left(X + h\bar{X}, U + h\bar{U}, t + h\bar{t}\right) - F(X, U, t)}{h} \tag{6.16}$$

where h is a positive real number, $D_\mathrm{h} F\left(X, U, t : \bar{X}, \bar{U}, \bar{t}\right)$ stands for the concept of forward difference for F. It should be noted that there is the main difference between

forward-difference approximation and finite-difference approximation with regards to computational expenses. The forward difference approximation of the Jacobians and vectors' products can be calculated with only an additional evaluation of the function, which requires notably less computational burden than an approximation of the Jacobians themselves. Since Eq. (6.13) is a linear equation with respect to $\dot{U}$ and $\dot{U}_{\text{Hap}}$, we applied the forward difference GMRES method to solve it [?].

$\dot{U}$ is the outputs of the forward-difference GMRES algorithm and integration of this value results in U for the current time step. It should be noted that the C/GMRES is an iterative method that solves Eq.(6.8) concerning $\dot{U}$ only once at each sampling time and, therefore, requires much less computational expenses than other iterative methods such as Newtons method. Moreover, C/GMRES involves no line search, which is also a significant difference from standard optimization methods [?].